The Effect of Metal Solution Contaminants on the Electro-catalyst Activities of Direct Methanol Fuel Cell

Soghra Jalil Pour Kivi

Thesis submitted to the University of Ottawa
in partial fulfillment of the requirements for the
Doctor of Philosophy

Department of Chemistry and Biomolecular Sciences
Faculty of Science
University of Ottawa

Table of Contents

Abstract

Direct methanol fuel cells (DMFCs) are considered a clean source of electrical power for future energy demand, creating a potential to reduce our dependency on fossil fuels. Despite their advantages, including high energy density, efficiency and easy handling and distribution of fuel, the commercialization of DMFCs has suffered from some drawbacks, including methanol crossover and contamination of the system. Metal cation contaminants (such as Ni, Co, etc) introduced through the degradation of fuel cell components (bipolar plate and electro-catalyst layer) can significantly affect the Nafion-membrane properties and overall fuel cell performance. In the current study, a systematic approach is taken to characterize and identify the mechanism of the effect of metal solution contaminants on the activities of electro-catalysts of DMFCs.

Cyclic voltammetry and rotating disk electrode (RDE) techniques were utilized in order to characterize the effect of various concentrations (i.e., $2x10^{-x}$ M (x=1-7)) of six metal solution contaminants (i.e., Co, Ni and Zn with sulfate and nitrate as counter-anions) on the voltammetric properties and electro-catalytic activity of polycrystalline Pt during methanol oxidation reaction (MOR) and oxygen reduction reaction (ORR). The results showed a decrease in the MOR and ORR activities of Pt as the concentration of metal solution increased. The effect of counter-anion on the Pt activity was further investigated. The results showed that a combined effect of counter-anions and metal cations may be responsible for the decrease in the electro-catalytic activity of Pt.

The effect of metal solution contaminants on the Nafion-ionomer of anode

electro-catalysts was investigated using Nafion-coated Pt electrode. Voltammetric properties and MOR activities of Nafion-coated and bare Pt electrodes in the presence of Ni solution contaminants were characterized using cyclic voltammetry and electrochemical impedance spectroscopy (EIS). The overall results showed a significant negative effect of Ni solution contaminants on the electro-catalytic activity of bare Pt electrode as compared to the Nafion-coated Pt electrode. Based on the results, it appears that Nafion-ionomer film may interact with metal cations (through its sulfonate groups) and repel them away from the Pt active sites, partially inhibiting the negative effect of metal cations on the Pt activity of Nafion-coated Pt electrode.

The effect of metal solution contaminants on the carbon-supported platinum nanoparticle (Pt/C) with various Nafion-ionomer distributions and contents (i.e., Nafion-incorporated Pt/C and Nafion-coated Pt/C electrodes) was further investigated. Cyclic voltammetry and EIS techniques were employed to characterize the effect of Ni solution contaminants on the voltammetric properties and MOR activities of Nafion-incorporated and Nafion-coated Pt/C electrodes. The overall results showed a stronger negative effect of Ni solution contaminants on the electro-catalytic activity of Nafion-incorporated Pt/C electrodes as compared to the Nafion-coated Pt/C electrodes. This further confirms previous observations showing the sulfonate groups of Nafion-ionomer film may attract the Ni metal cations, localize them away from the Pt active sites, and subsequently suppress the negative effect of cations on the activity of Nafion-coated Pt/C electrodes.

List of Figures

List of Table

List of Abbreviations

- CE — Counter Electrode
- CPE — Constant Phase Element
- CV — Cyclic Voltammogram
- DMFC — Direct Methanol Fuel Cell
- ECSA — Electrochemical Active Surface Area
- EIS — Electrochemical Impedance Spectroscopy
- MEA — Membrane Electrode Assembly
- MOR — Methanol Oxidation Reaction
- ORR — Oxygen Reduction Reaction
- PEMFC — Polymer Electrolyte Membrane Fuel Cell
- R_{ct} — Charge Transfer Resistance
- RDE — Rotating Disk Electrode
- RE — Reference Electrode
- RHE — Reversible Hydrogen Electrode
- RRDE — Rotating Ring Disk Electrode
- R_s — Solution Resistance
- SCE — Saturated Calomel Electrode
- UPD — Underpotential Deposition
- WE — Working Electrode

Acknowledgments

First and foremost, I would like to thank my supervisor, Dr. Barry MacDougall for giving me the opportunity to work under his guidance. I am always grateful for his continuous support through my Ph.D. study. Without his understanding and kind support, this journey wouldn't have been as enjoyable as it was. I would also like to thank Dr. Christina Bock for her guidance and mentorship during the time I conducted my experiments at the National Research Council (NRC). I am grateful to my examining committee members, Dr. Daniel Guy, Dr. Maria DeRosa, Dr. Elena Baranova, and Dr. Darrin Richeson who helped me through their constructive reviews.

I have been fortunate to be surrounded by many incredible people at the NRC and chemistry department of University of Ottawa, and I am grateful for their encouragement and support. I would like to thank JingPeng Wang, David Hall, Daniela Marquez, Mohammad Zein Aghaji, Olga Naboka and Nuha Salem who helped me through this journey.

I would like to acknowledge the contribution of Oltion Kodra who performed the XPS measurements for this work and assisted with the interpretation of the results.

I would like to acknowledge the financial support from Dr. Yu scholarship, the Institute of Energy and Climate Research (IEK), Jülich and NRC. Without their support this research wouldn't have been possible.

I am deeply thankful to my family, especially my mother and Firoozeh, who

always supported me and encouraged me during this time. Thanks for always being there for me.

To my husband, Reza, you know it was impossible to accomplish this without your help, patience and support. Thanks for standing besides me for every single step of this journey. Looking forward to spend the rest of our journey together with you and our baby girl, Isla.

1 Introduction

1.1 Overview

Rapid depletion of non-renewable fossil fuels and increasing environmental concerns associated with the consumption of such resources have led to an increased desire for the development of alternative sources of energy (e.g., solar and wind power) [1]. As these energy sources are intermittent, the development of reliable and cost efficient energy storage systems such as fuel cells and batteries is essential. Fuel cell is a promising technology that has been developed as a clean and efficient source of energy as part of efforts to meet future energy needs. Fuel cells are electrochemical devices, which convert the chemical energy in the fuel to electrical energy through electrochemical reactions. In fuel cells, the externally stored fuel and oxidant are continuously supplied to the system, enabling the fuel cell to operate indefinitely [2].

Proton exchange membrane fuel cell (PEMFC) is a type of fuel cell that utilizes hydrogen as fuel and oxygen as oxidant. However, hydrogen has a low energy density and is a difficult fuel to produce, store and transport, which has caused a major obstruction in the commercialization of PEMFCs. These issues have led to the development of liquid fuels such as methanol for fuel cell systems. Owing to the distinctive properties of methanol such as high energy density, fast refueling potential, facile distribution and low cost [3], direct methanol fuel cells (DMFCs) have the potential to become a reliable portable power source for future applications.

Ongoing research studies in recent years have focused on evaluating the

performance and durability of DMFCs affected by methanol crossover and system contaminants. Contaminants such as air impurities (e.g., CO, NO_x, SO_2, and H_2S) and metal cation contaminants (e.g., Fe^{3+}, Cr^{3+}, and Ni^{2+}) can be introduced to the fuel cell system through the air stream and the degradation of fuel cell components (e.g., bipolar plates and electro-catalyst layer), respectively. It has been shown that even at very low concentrations, air impurities can result in a significant degradation in the fuel cell performance [4]. In addition to the air impurities, the presence of metal cation contaminants (e.g., Fe^{3+}, Ni^{2+} and Cu^{2+}) can result in a significant change in Nafion membrane properties, as well as degradation in the overall fuel cell performance [5–11]. It is known that multivalent cations can easily displace the protons of Nafion membrane due to their higher affinities toward the sulfonate sites of Nafion, thus affecting its water management properties and ionic conductivity [12–16].

Although durability and performance of fuel cells in the presence of metal cation contaminants have been extensively investigated, the effect of metal cation contaminants on the electro-catalyst activities of fuel cells is not well documented. This understanding is essential in improving the design and long-term performance of fuel cell systems.

1.2 Research Objectives

The research in this thesis is intended to expand the available literature on the effect of metal solution contaminants on the anode and cathode activities of DMFCs. The specific objectives of this study are presented below:

1. To understand the effect of various concentrations of metal solution contaminants on the activity of polycrystalline Pt. In particular:
    - To understand the effect of various concentrations of metal solutions (i.e., Co, Ni and Zn) on the voltammetric properties of polycrystalline Pt, utilizing cyclic voltammetry technique.
    - To understand the effect of various concentrations of metal solutions (i.e., Co, Ni and Zn) on the methanol oxidation reaction (MOR) activity of polycrystalline Pt and Pt_xRu_y electro-catalysts, utilizing cyclic voltammetry technique.
    - To understand the effect of various concentrations of metal solutions (i.e., Co, Ni and Zn) on the oxygen reduction reaction (ORR) activity of polycrystalline Pt, utilizing rotating disk electrode (RDE) technique.
2. To understand the role of Nafion-ionomer of the anode electro-catalyst in the presence of metal solution contaminant. In particular:
    - To understand the effect of Ni solution contaminants on the voltammetric properties of Nafion-coated and bare Pt electrodes, utilizing cyclic voltammetry technique.
    - To understand the effect of Ni solution contaminants on the activity and mechanism of MOR on the Nafion-coated and bare Pt electrodes, utilizing MOR voltammetry and electrochemical impedance spectroscopy (EIS) techniques.
3. To provide an enhanced understanding of the role of Nafion-ionomer distribution

and content in the carbon-supported platinum nanoparticle (Pt/C) electro-catalysts in the presence of metal solution contaminants. In particular:

- To understand the effect of Ni solution contaminants on the voltammetric properties of Nafion-incorporated and Nafion-coated Pt/C electrodes with different Nafion contents, utilizing cyclic voltammetry technique.
- To understand the effect of Ni solution contaminants on the activity and mechanism of MOR on the Nafion-incorporated and Nafion-coated Pt/C electrodes with different Nafion contents, utilizing MOR voltammetry and EIS techniques.

1.3 Outline of Thesis

This thesis contains six chapters. Chapters three to five are presented as independent journal papers based on the experimental studies conducted in this thesis. A summary of each chapter is presented below:

Chapter one presents an overview of the research, the objectives and the outline of this work.

Chapter two presents an overview of the fuel cell components. The available literature and electro-chemical techniques pertinent to the scope of this research are discussed.

Chapter three reports the effect of various concentrations of metal solution

contaminants (i.e., Co, Ni and Zn with sulfate and nitrate as counter-anions) on the voltammetric properties and MOR activities of polycrystalline Pt and Pt_xRu_y using cyclic voltammetry technique. Furthermore, the effect of these metal solution contaminants on the electro-catalytic activities of polycrystalline Pt during ORR is investigated using rotating disk electrode (RDE) technique.

Chapter four reports the effect of nickel solution contaminants on voltammetric properties of Nafion-coated and bare polycrystalline Pt electrodes. Further, the activity and mechanism of MOR on these electrodes are evaluated after Ni solution exposure using cyclic voltammetry and EIS techniques.

Chapter five reports the effect of nickel solution contaminants on voltammetric properties of Nafion-incorporated and Nafion-coated Pt/C catalysts with different Nafion contents. Further, the activity and mechanism of MOR on these electrodes are evaluated after Ni solution exposure using cyclic voltammetry and EIS techniques.

Chapter six provides the summery and conclusions of the thesis. Recommendations for future studies in this area are also presented in this chapter.

2 Background

2.1 Direct Methanol Fuel Cells Working Principle

The working principle of a DMFC is schematically shown in Figure 2.1. The DMFC primarily consists of a polymer electrolyte membrane (PEM), two electrodes (i.e., anode and cathode), and two bipolar plates. The PEM is used as a proton conductor and a separator between the anode and cathode. Each electrode consists of a catalyst layer and a diffusion layer. The catalyst layer is typically made of nanoparticle platinum-based catalysts coated on the diffusion layer. The PEM sandwiched between anode and cathode electrodes is known as membrane electrode assembly (MEA). The MEA is clamped by two electronically conductive bipolar plates, which contain grooved flow field channels. The components of fuel cell will be discussed in detail in the following sections.

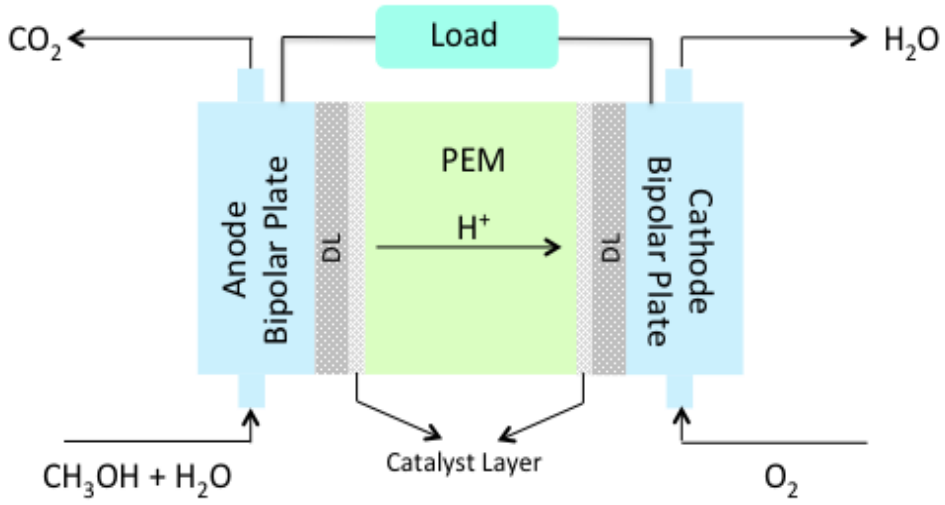

Figure 2-1: Components and working principle of a DMFC.

In a DMFC, the methanol solution (as fuel) is directly fed with water to the anode side of cell to flow through the flow field channel and arrive at the diffusion layer. Methanol can subsequently penetrate into the anode electro-catalyst, where it is oxidized to the carbon dioxide (CO_2), protons (H^+) and electrons (e^-). The formed CO_2 is removed from the catalyst layer through the diffusion layer and flow field channel. The formed protons (H^+) are transported through the polymer electrolyte membrane (PEM) to the cathode catalyst layer. At the cathode, oxygen (as oxidant) combines with protons (H^+) and electrons transferred through external electrical circuit to form water (H_2O). The overall half-cell electrochemical reactions taking place at the anode and cathode are presented below:

Anode: $CH_3OH + H_2O \rightarrow CO_2 + 6H^+ + 6e^-$ Equation 2-1

Cathode: $6H^+ + 6e^- + \frac{3}{2} O_2 \rightarrow 3H_2O$ Equation 2-2

The overall electrochemical reaction of a DMFC is summarized below:

$CH_3OH + \frac{3}{2} O_2 \rightarrow CO_2 + 2\ H_2O$ Equation 2-3

2.2 DMFC Components

2.2.1 Bipolar Plate

Bipolar plate or current collector is a multifunctional component of DMFC. Its main functions are to direct the flow of the methanol and oxygen through the flow field channel to the diffusion layer of anode and cathode, respectively, and to further remove the reaction products (i.e., CO_2 and H_2O) from the cell [17]. It also provides a conductive

pathway for the electrons produced through methanol oxidation reaction (MOR) at the anode to flow through the external circuit to reach the cathode for the oxygen reduction reaction (ORR). It also plays an important role in the cell's mechanical structure support.

Bipolar plates are made of electrically conductive materials to conduct the current through the system. Graphite is the commonly used material for the bipolar plate owing to its high electrical conductivity, chemical resistance to the corrosion in fuel cell environment, and low density (as compared to metal plates). However, graphite plates have low mechanical stability (brittleness) and porous structure, preventing them to be machined [18]. The high material and processing cost for the large-scale production of graphite plate have led to the consideration of alternative materials such as metallic and composite materials as bipolar plates [19–21].

2.2.2 Diffusion Layer

Diffusion layers enhance effective and uniform distribution of reactants from the flow field channel of bipolar plates to the surface of catalyst layer and also manage the transport of reaction products from the catalyst layers. These layers are electrically conductive to allow the current to flow between the catalyst layer and the bipolar plate. Porous materials (e.g., porous carbon paper and porous carbon cloth) are typically used in diffusion layers due to their high water and gas permeability and electrical conductivity [22,23]. Diffusion layers also contain polytetrafluoroethylene (Teflon), in order to enhance the hydrophobic properties necessary to manage the water transport and to prevent the flooding phenomena [23]. Low water diffusion through the diffusion layer may result in flooding in the catalyst layer, which may impede oxygen supply to the

cathode side [24]. On the other hand, high water diffusion through diffusion layer may result in catalyst layer dry-out.

2.2.3 Catalyst Layer

The anode and cathode catalyst layers are the main parts of fuel cell where the electrochemical reactions take place. The electrodes are designed to enhance the transport of electrons, protons and reactants to the catalyst sites. Therefore, Nafion-ionomer is used in the catalyst layer as the proton conductive materials to transport protons to or from cathode and anode, respectively. As electrons are also involved during electrochemical reactions, carbon support nanoparticles are used to provide the electrical conductivity in the catalyst layer and to further increase the catalyst surface area. Carbon supported platinum-ruthenium (PtRu) and platinum (Pt) nanoparticles are the most commonly used anode and cathode catalysts, respectively, in the DMFC. The properties of these catalysts and their corresponding electrochemical reactions are discussed later in detail.

2.2.4 Polymer Electrolyte Membrane

Nafion membrane, discovered by DuPont in 1960, is the most commonly used electrolyte membrane for the PEMFCs and DMFCs owing to its high proton conductivity, chemical stability and mechanical strength [25]. Nafion membrane is used to conduct protons from anode to cathode sides of PEM fuel cell. It is also used as a separator between the anode and cathode side to inhibit the mixing of the fuel and oxidant [26,27]. The chemical structure of Nafion is presented in Figure 2-2. As shown, Nafion is composed of a hydrophobic backbone (polytetrafluoroethylene (PTFE)) with hydrophilic

perfluorinated ether pendant side chains terminated by sulfonic acid (-SO_3H) groups [28]. While the PTFE backbone of Nafion provides high chemical and thermal stability, the sulfonic acid groups provide hydrophilic region for facile proton transport.

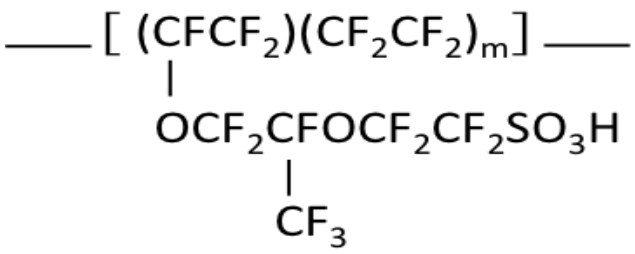

Figure 2-2: Chemical structure of Nafion. Adapted with permission from ref [28].

Water uptake of Nafion has a critical role for its proton transport properties. In the hydrated Nafion, an interconnected proton conducting network can be formed by the sulfonic acid groups of Nafion and water. The protons are transported through hydrated Nafion membrane by either the Grotthus (proton-hopping) mechanism or the vehicle (electro-osmotic drag) mechanism. In the Grotthus mechanism, the proton transfer can occur through the proton hopping, in which protons hop from one water molecule to the adjacent one across the membrane followed by the reorientation of water dipoles [29]. In the vehicle mechanism, the protons diffuse through aqueous medium of membrane along with water molecule as “vehicle” (as the result of electro-osmotic drag) [30].

Despite numerous advantages of Nafion membrane, its application has faced several drawbacks, such as high price, fuel permeability (i.e., methanol crossover in DMFC application), and low proton conductivity at low relative humidity and elevated temperature (> 90°C). To address these issues, extensive efforts have been initiated on

modifying Nafion membrane and developing alternative membrane materials [31].

2.3 DMFC-Electrochemical Reactions

2.3.1 CH_3OH Oxidation Reaction

Methanol oxidation reaction (MOR) can proceed through a dual, parallel pathway mechanism (i.e., direct and indirect pathways) [32]. A simplified schematic of this mechanism is shown in Figure 2-3. As presented, the direct pathway proceeds through the formation of soluble intermediates such as formaldehyde and formic acid. In the indirect pathway, the adsorbed carbon monoxide (CO_{ads}) can be formed on the electrode surface, which subsequently reacts with oxygen-containing species to form carbon dioxide (CO_2).

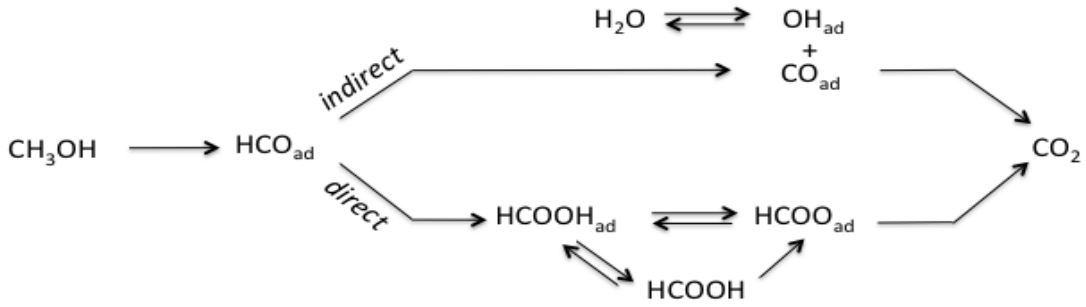

Figure 2-3: A simplified reaction pathway of methanol oxidation reaction. Adapted with permission from ref [33]. Copyright (2019) American Chemical Society.

Although the thermodynamic potential of methanol oxidation is at E = 0.02 V, relatively close to the hydrogen equilibrium potential, this reaction occurs at more positive potential range (E > 0.7 V) on the Pt-based catalysts. It is generally accepted that

the adsorption and dehydrogenation of CH_3OH on the electrode surface is the first elementary step for the methanol oxidation, which requires three adjacent Pt catalyst sites [34,35]. As methanol cannot displace the adsorbed hydrogen at lower potential range, hence, the methanol adsorption can only occur at more positive potential (E > 0.2 V), where the hydrogen is desorbed from the Pt surface and the electrode is relatively hydrogen free [36]. The adsorption-dehydrogenation of methanol results in the formation of adsorbed carbon monoxide (CO_{ads}) intermediates, which are very stable at the potential range of E = 0.2 - 0.5 V and can block the Pt active sites from the adsorption of water and methanol. To further oxidize the CO_{ads}, the oxygenated species should be formed on the Pt surface through water dissociative-adsorption. The oxidation of the CO_{ads} to CO_2 may take place at high positive potential (E = 0.7 V) due to insufficient activated water and/or adsorbed oxygenated species on the Pt surface at lower potential ranges [37]. However, this high anodic overpotential is not desirable for the DMFCs application. To address this issue, modification of Pt-based catalysts with foreign metals (e.g., Ru, Ni, etc.) has been investigated through bifunctional mechanism and/or ligand effect (electronic effect). Through the bifunctional mechanism, the secondary metal can facilitate the adsorption of oxygen-containing species at lower potential range, which promotes the oxidative removal rate of CO_{ads} [38]. Pt-Ru shows the best catalytic activity toward methanol oxidation, as the water dissociative-adsorption on ruthenium sites occurs at a potential as low as 0.2 V [39]. Through the ligand effect, the electronic properties of Pt can be modified by the electronic interaction with foreign metal. The CO adsorption occurs on Pt sites through electron

donation from 5σ-orbital of CO to the empty d-orbital of Pt with a subsequent electron back-donation from d-orbital of Pt to the 2π* anti-bonding orbital of CO [40]. The modification of Pt by foreign metal can result in a reduction in the electron back-donation of Pt d-orbital to the 2π* orbital of CO, resulting in a decrease in the stability of Pt-CO bonding and subsequently CO coverage (poisoning effect) on Pt active sites [41,42].

2.3.2 O_2 Reduction Reaction

Oxygen reduction reaction (ORR) is a multi-electron process with several steps and various reaction intermediates. The ORR can proceed through two primarily reaction pathways, a two-electron and a four-electron processes [43]. The simplified mechanism of ORR process is illustrated in Figure 2-4. As shown, oxygen can be electrochemically reduced to water through a 4-electron process with a rate constant k_1 and no intermediate formation (i.e., H_2O_2). Alternatively, oxygen can be electrochemically reduced to the adsorbed hydrogen peroxide ($H_2O_{2,ad}$) through a 2-electron process with a rate constant k_2. The adsorbed intermediate may be further reduced to H_2O with a rate constant k_3, chemically decomposed to $O_{2,ad}$ with a rate constant k_4, and/or desorbed to the bulk electrolyte with a rate constant k_5.

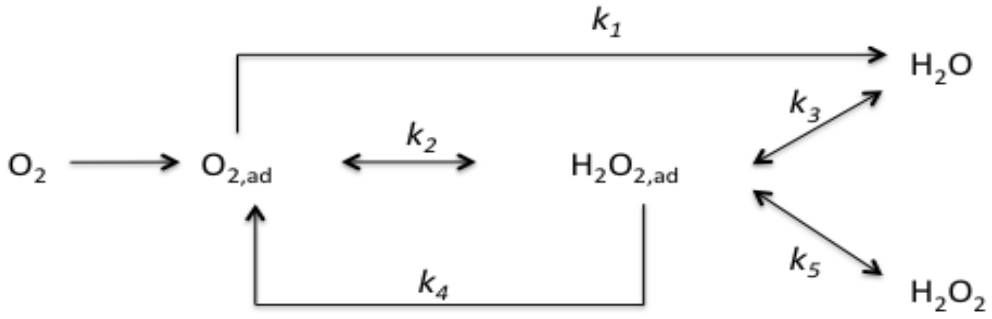

Figure 2-4: Oxygen reduction reaction on Pt electrocatalyst. Adapted with permission from ref [43]. Copyright (2019) Elsevier.

The ORR mechanism is also theoretically proposed as dissociative and associative pathways [44]. Through dissociative pathway (direct pathway), the O_2 initially adsorbs on the active sites of metal electrode through side-on mode. Immediately after the adsorption, the O-O bond is dissociated into the adsorbed atomic O, which can be further protonated by transported protons (from anode) and reduced by the transferred electrons to form adsorbed hydroxyl (OH_{ads}) species. The OH_{ads} can be consequently protonated and reduced to H_2O. This reaction pathway is considered as a direct form of 4-electron pathway, since no H_2O_2 is formed during this process. In the associative pathway, O_2 adsorbs on the active sites of metal electrode through end-on mode, which can further undergo a 2-electron transfer and form adsorbed intermediate $H_2O_{2,ads}$. This reaction intermediate may be either desorbed from the metal surface and form H_2O_2, or reduced through additional 2-electron transfer to form water. In fuel cell, the formation of water through the direct 4-electron pathway is highly preferred. However, the

dissociative mechanism (direct pathway) is energetically less favorable due to its higher activation barrier as compared to the associative mechanism. Platinum is the most commonly used cathode catalyst for the PEM fuel cells owing to its high catalytic activity toward ORR and good stability in the fuel cell acidic media. Although the thermodynamic potential of ORR is at 1.23 V, the open circuit potential of ORR is observed at 1.0 V. This is attributed to the strength of O=O bond (498 KJ/mol) that needs to be activated in the course of this reaction, resulting in sluggish kinetics of ORR [45]. This ~200 mV energy loss may result in a decrease in the overall fuel cell efficiency, which can be addressed by increasing the Pt content in the cathode catalyst layer. However, the high cost and low availability of Pt have led to the development of alternative catalysts with lower Pt content (e.g., Pt based-alloy). Alloying Pt with other transition metals (e.g., Pt-M, M = Cr, Ni, Co) can result in increased d-band vacancy, which may lead to a stronger metal-oxygen bond and subsequently enhanced O-O bond dissociation [46]. In addition, using transition metal with smaller size than Pt may result in lattice contraction, as these metals may enter into the Pt crystal structure and lower the Pt-Pt interatomic distance (the structure effect). This leads the Pt sites to be more favorable for the O_2 adsorption [47–49].

2.4 Challenges in the Development of DMFCs

2.4.1 Methanol Crossover

One of the most crucial issues that prevent the commercialization of DMFCs is the methanol crossover from anode to cathode through polymer electrolyte membrane (PEM) [50]. Diffusion as well as electro-osmotic drag are two main mechanisms

responsible for the methanol crossover [51,52]. When methanol is transported to the cathode side, two electrochemical reactions (i.e., MOR and ORR) can occur simultaneously, leading to a mixed potential and eventually a cell voltage drop. The permeated methanol can also be oxidized by O_2 through a purely chemical reaction, which may result in the CO_2 formation on the cathode [53]. Moreover, the adsorption of methanol on the cathode catalyst can result in the CO_{ads} formation, which can lower the catalyst active sites available for the oxygen reduction reaction (ORR). Methanol crossover depends on many factors, such as: methanol concentration, Nafion membrane permeability/thickness, and operating temperature of fuel cell. In order to minimize the negative impacts of methanol crossover on the fuel cell performance, a number of strategies have been investigated including the development of new membrane with low methanol permeability and the design of methanol-tolerant cathode catalysts for the DMFC system [54-56].

2.4.2 Impurities in Fuel Cells

Another critical issue facing the fuel cell commercialization is the degradation effect of contaminants (including air impurities and metal cations) on the fuel cell performance.

Air impurities (e.g., CO, NO_x, SO_2, and H_2S) can enter the fuel cell system along with the air stream. The effect of these impurities on the fuel cell has been the focus of many studies [57–62]. It has been shown that even very low concentrations of contaminants can result in a significant degradation in the fuel cell performance [4].

In addition to the air stream impurities, metal cation contaminants (e.g., Fe^{2+}, Cr^{3+},

Ni^{2+} and Cu^{2+}) can be introduced to the fuel cell system through the degradation of cell components (i.e., catalyst layer and bipolar plate) [5–11,63]. Metal cation contaminants can affect various functionalities of fuel cell (e.g., activities of catalyst layers, and ionic conductivity of Nafion membrane), resulting in a significant loss in the cell performance [11]. Although many studies have focused on the durability of Nafion membrane and fuel cell in the presence of cation contaminants, the effect of these contaminants on the electro-catalysts of fuel cell is not clearly understood and requires further investigation. The effect of metal cation contaminants on various components of fuel cell is further discussed in the following sections.

2.4.2.1 Effect of Cation Contaminants on the Overall PEM Fuel Cell Performance

Extensive studies have been conducted to identify the effect of cation contaminants on the overall fuel cell performance. In a study by Pozio et al., Fe cation contaminants originated from stainless steel (SS136L) endplate were shown to degrade the membrane, resulting in a significant decrease in the PEM fuel cell performance [64]. The effect of Fe^{3+} and Al^{3+} (using $Fe(ClO_4)_3$ and $Al_2(SO_4)_3$) in the cathode air stream on the PEM fuel cell performance was investigated by Li et al. [65]. The results showed an increase in charge and mass transfer resistances as well as a significant degradation in the cell performance in the presence of 5 ppm of Fe^{3+} and Al^{3+}. In another study by Li et al., the effect of various concentrations (i.e., 5 ppm and 300 ppm) of Co^{2+} cation contaminants (using $CoSO_4$) in the cathode air stream on the PEM fuel cell performance was investigated [66]. The results showed a decrease in the cell performance as the

concentration of Co^{2+} contaminants increased. Furthermore, a significant increase in the charge and mass transfer resistances as compared to the membrane resistance was observed in the presence of cation contaminants. It was suggested that Co^{2+} adsorption on the Pt active sites of cathode catalyst may result in a decrease in the ORR rate as well as a change in the ORR mechanism. Further in this study, the effect of operating temperature on the fuel cell performance was investigated in the presence of 5 ppm of Co^{2+} contaminants. Results showed a significant decrease in cell performance with decreasing the temperature. It was suggested that the stronger adsorption of Co^{2+} on Pt active sites at lower temperature is responsible for the decrease in the ORR activity and eventually the cell performance. The effect of various metal chloride salts (i.e., $AlCl_3$, $FeCl_3$, $CrCl_3$, $NiCl_2$ and $MgCl_2$) and HCl in the cathode air steam on the PEM fuel cell performance was studied by Uddin et al. [67]. The results showed a stronger degradation effect of HCl on the fuel cell performance as compared to metal chloride salts. It was suggested that the metal cations may play a positive role to lower the degradation effect of chloride on the cell performance.

The effect of Na^+, Mg^{2+} and Cr^{3+} (using metal sulfates) in the anode and cathode feed streams on the DMFC performance was investigated by Jie et al. [68]. The anode feed contaminants resulted in a decrease in DMFC performance as follow: $Na^+ > Mg^{2+} > Cr^{3+}$. It was suggested that the fast transfer and low affinity of lower valence cations toward the sulfonic acid groups of ionomer may result in increased proton losses. Unlike the anode feed contaminants, cation contaminants in the cathode feed suppressed the DMFC performance as follow: $Cr^{3+} > Mg^{2+} > Na^+$. It was suggested that the higher valence

cation, Cr^{3+}, may easily displace the protons of ionomer as compared to the lower valence cations (e.g., Na^{+} and Mg^{2+}), resulting in more proton losses and subsequently increased cathode overpotential. The effect of Cr^{3+} and Fe^{3+} in the anode feed stream on DMFC performance was investigated by Chen et al. [69]. It was suggested that the degradation effect of Cr^{3+} on the anode electro-catalytic activity and Fe^{3+} on the ionic conductivity of membrane are responsible for the decrease in DMFC performance. Yang et al. showed the presence of metal nitrates (e.g., $Ni(NO_3)_2$, $Fe(NO_3)_3$, $Cr(NO_3)_3$ and $Al(NO_3)_3$) in the DMFC anode feed stream resulted in a decrease in the DMFC performance [70]. Decrease in the proton conductivity of membrane was also observed in the presence of metal cation contaminants.

2.4.2.2 Effect of Cation Contaminants on Nafion Membrane

As shown in previous studies, the degradation of Nafion membrane properties increases in the presence of cation contaminants [12–16]. Metal cation contaminants can interact with the sulfonate sites of Nafion membrane and critically affect the conductivity and water management property of Nafion membrane. The multivalent cations can easily displace the proton (H^{+}) of Nafion membrane due to their higher affinity toward the sulfonic acid groups of Nafion as compared to the monovalent protons [12,71]. This high affinity is attributed to the strong electrostatic interaction between the high valence cations and sulfonate sites, resulting in a lower mobility of cations, thus decreasing the Nafion conductivity. In a study by Kelly et al., a significant decrease in the conductivity of Nafion membrane was observed in the presence of multivalent cations (e.g., Fe^{3+}> Cu^{2+} and Ni^{2+}) as compared to monovalent cation, Na^{+}

[72,73]. Furthermore, Okada et al. showed that the displaced multivalent cations in the Nafion membrane can suppress the number of water molecule per sulfonate site of Nafion, as well as the water movement [12]. It was suggested that the lower hydrophilic property of multivalent cations as compared to proton (H^+) is responsible for the decrease in the water content in the Nafion membrane, thus affecting its ionic conductivity. In a study by Sulek et al., the polymer electrolyte membrane (PEM) was immersed in various metal solutions (i.e., $FeSO_4$, $NiSO_4$, $Cr_2(SO_4)_3$ and $Al_2(SO_4)_3$) to identify their effects on the overall PEM fuel cell performance [74]. The results showed that the cation contaminated membrane suppressed the fuel cell performance as follow: Al^{3+}>> Fe^{2+} > Ni^{2+}, Cr^{3+}. It was suggested that the high affinity of multivalent cations toward the sulfonic sites of Nafion membrane and ionomer of catalyst layer results in a decrease in the proton conductivity and eventually fuel cell performance.

In addition, the presence of metal cation contaminants in Nafion membrane can result in a chemical membrane degradation in the presence of H_2O_2 at the electrode and Nafion interface. As discussed in section 2.3.2, H_2O_2 can be formed during ORR, which is the potential factor for the degradation of Nafion membrane. The decomposition of H_2O_2 can be catalyzed in the presence of contaminated Nafion, resulting in the formation of highly active oxygen containing radicals, thus accelerating the membrane decomposition [75,76]. In a study by Li et al, it was shown that the presence of Fe^{3+} cation contaminants can accelerate the decomposition of H_2O_2 (formed during ORR) into free radicals, resulting in the membrane pinhole formation and eventually the sudden cell death [65]. In a study by Kinumoto et al., the chemical stability of Fe^{2+} and Cu^{2+}

contaminated Nafion in the presence of H_2O_2 was investigated [77]. The results showed a significant increase in the membrane degradation due to the formation of strong radical species (e.g., OH• and OOH•) as the result of H_2O_2 decomposition in the presence of Fe^{2+} and Cu^{2+}. These radical species can attack various parts of membrane, which eventually results in the membrane pinhole formation. The formation mechanism of radical species is shown as follow [78]:

$$H_2O_2 + M^{2+}\text{ (in the membrane)} \rightarrow M^{3+} + HO\bullet + OH^- \qquad \text{Equation 2-4}$$

$$HO\bullet + H_2O_2 \rightarrow H_2O + HOO\bullet \qquad \text{Equation 2-5}$$

2.4.2.3 Effect of Cation Contaminants on ORR and MOR

Despite its importance, the effect of metal cation contaminants on the ORR and MOR activities of electro-catalysts has only been investigated in a few studies. Li et al. investigated the effect of various concentrations (i.e., 0.05 and 0.2 M) of Al^{3+} (using $Al_2(SO_4)_3$ salt) on the ORR activity of Pt/C catalysts using RDE technique [65]. The result showed changes in kinetic and mechanism (e.g., decrease in the overall electron transfer number from $4e^-$ to $2e^-$) of ORR with an increase in the concentration of Al^{3+}. In a separate study by Li et al., the effect of Co^{2+} (using $CoSO_4$ salt) on the ORR activities of bare Pt and Pt/C catalysts was investigated using RDE and rotating rink disk electrode (RRDE) techniques [79]. The RDE results showed a decrease in the overall electron transfer number of ORR, indicating a change in the ORR mechanism. Consistent with this result, the RRDE measurement conducted on Pt/C catalysts showed an increase in H_2O_2 formation in the presence of Co^{2+} contaminants. It was suggested that the adsorbed Co^{2+}

on Pt active sites may react with H_2O_2, resulting in Co^{2+}-H_2O_2 formation, which may eventually inhibit the H_2O_2 reduction to H_2O. In a study by Durst et al., a decrease in the ORR activity of Pt/C catalyst was observed in the presence of Co^{2+} contaminants (using $CoSO_4$) [80]. It was suggested that the enhanced OH formation on Pt surface in the presence of Co^{2+} resulted in a decrease in the ORR kinetic. In this study, the effect of Co^{2+} on the ORR activity of Nafion-coated Pt/C with different ionomer contents was further investigated. The results showed a lower Co^{2+} effect on Nafion-coated Pt/C catalyst as the ionomer content increased. It was suggested that the interaction between Co^{2+} and sulfonate sites of Nafion-ionomer may suppress the Co^{2+} effect on the Pt active sites as compared to the Nafion-free bare Pt/C catalyst. The effect of alkali metal sulfates (i.e., Li_2SO_4, Na_2SO_4, K_2SO_4, Rb_2SO_4 and Cs_2SO_4) on the ORR activity of Pt(111) in acidic media was investigated by Tymoczko et al. [81]. A decrease in ORR activity of electrode in the presence of alkaline cations (with no clear trend from Li^+ to Cs^+) and (bi)sulfate anions was reported. It was suggested that the presence of (bi)sulfate anions can result in a complicated interaction at Pt interface.

In a study by Zhou et al., a decrease in the MOR activity of Pt catalyst was observed in the presence of metal sulfates (i.e., Li_2SO_4, $MnSO_4$, $NiSO_4$, $CuSO_4$ and $Ce(SO_4)_2$) [82]. It was suggested that the adsorption of metal cations on Pt surface as well as a change in the potential distribution of electrochemical double layer were responsible for the decrease in MOR activity. It was also suggested that the adsorption of Mn^{2+} and Cu^{2+} on Pt active sites is stronger as compared to other cation contaminants. Durst et al. also investigated the effect of metal cation contaminants (using metal sulfate

such as Al^{3+}, Co^{2+}, K^{+}, Li^{+}) on the CO electro-oxidation using CO stripping voltammetry [80]. The results showed that the presence of metal cations resulted in a decrease in the onset potential of CO electro-oxidation. The effect of Co^{2+} was further investigated on the Pt/C electrodes with different Nafion contents. The results showed a decrease in metal cation effect on the CO electro-oxidation of Nafion-coated Pt/C electrode with higher Nafion content.

2.4.2.4 Effect of Metal Solutions on the Voltammetric Properties of Pt Catalysts

Understanding the effect of metal cation contaminants on the voltammetric properties of electro-catalysts is essential in order to characterize the metal cations influence on the electrode catalytic activities. However, few studies have investigated the influence of cation contaminants on the voltammetric properties of various Pt based electrodes (e.g., Nafion-coated Pt, bare Pt, and Pt/C). The effect of Co^{2+} (using $CoSO_4$) containing 0.5 M H_2SO_4 on the voltammetric properties of polycrystalline Pt was investigated by Li et al.[79]. The results showed a slight decrease in the electrochemical surface area (ECSA) of Pt electrode due to Co^{2+} adsorption on the Pt active sites. In a study by Chen et al., the presence of Cr^{3+} and Fe^{3+} resulted in 19.6 % and 7.8% decrease, respectively, in the ECSA of anode electro-catalyst (i.e., PtRu/C) of DMFC [69].

In addition to this, the presence of metal cations (e.g., Co^{2+}, Ni^{2+} and Zn^{2+}) can result in underpotential deposition (UPD) of metal on Pt active sites in an acidic media [80,83-85]. The UPD of metal refers to a less than a monolayer of adsorbed metal at a potential more positive than that for the bulk deposition of metal [84]. Durst et al.

investigated the effect of Co^{2+} (using $CoSO_4$) containing 0.1 M H_2SO_4 on the voltammetric property of Pt/C catalysts [80]. The results showed a change in hydrogen adsorption-desorption peak current in the presence of cobalt solution, which was attributed to the UPD of Co^{2+} on Pt active sites at lower potential range.

2.5 Experimental Techniques

2.5.1 Three-electrode Method

During this study, a three-electrode electrochemical cell was used to separately examine the anode and cathode half reactions occurring in a DMFC. In this method, methanol oxidation and oxygen reduction reactions are isolated to understand the effect of metal contaminants on the catalyst-solution interface. As shown in Figure 2-5, the three-electrode cell contains a working electrode (WE), a counter electrode (CE) and a reference electrode (RE). The working electrode provides a dominant reaction site across its interface, where the electrochemical reaction of interest can occur. The selected working electrode (i.e., polycrystalline Pt, Nafion-coated Pt and Pt/C) materials used during the study are discussed in the following chapters. The counter electrode is utilized to allow the current flow to or from the working electrode. It also has a large surface area with a negligible resistance to prevent any limitation (interfacial resistance) in the current flow. It is usually made of electrochemically inert materials (e.g., platinum, gold) to prevent its dissolution at the potential of interest during the experiments. The reference electrode has a known and constant potential with no current flow through it, which provides a standard to measure the potential of working electrode. In order to minimize the ohmic potential drop (iR drop), which is due to the solution resistance

between working electrode and reference electrode, the reference electrode is placed in a Luggin capillary with the tip positioned very close to the working electrode.

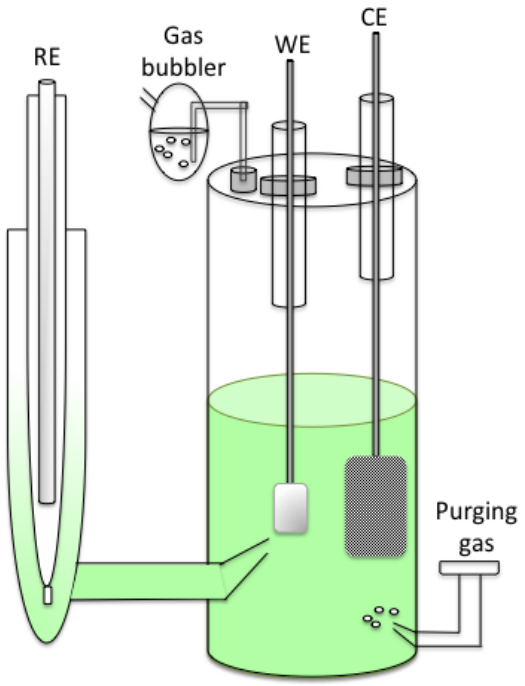

Figure 2-5: Schematic of three-electrode electrochemical cell setup used for this study.

2.5.2 Cyclic Voltammetry

Cyclic voltammetry is an electrochemical technique used to characterize the electrochemical processes (e.g., adsorption, desorption) occurring on the electro-catalyst surface. In this technique, a linear ramp potential is applied to the working electrode with respect to the reference electrode. As shown in Figure 2-6, the potential is scanned between two set values ($E_{initial}$ and E_{final}) at a fixed scan rate. When the potential E_{final} is reached, the direction of potential is reversed until the $E_{initial}$ is reached.

During the potential scanning, the generated current is recorded and normalized with respect to the geometric surface area of electro-catalyst, and is referred to as current density. The recorded current density is plotted versus the applied potential, and the resulting plot is termed as cyclic voltammogram (CV).

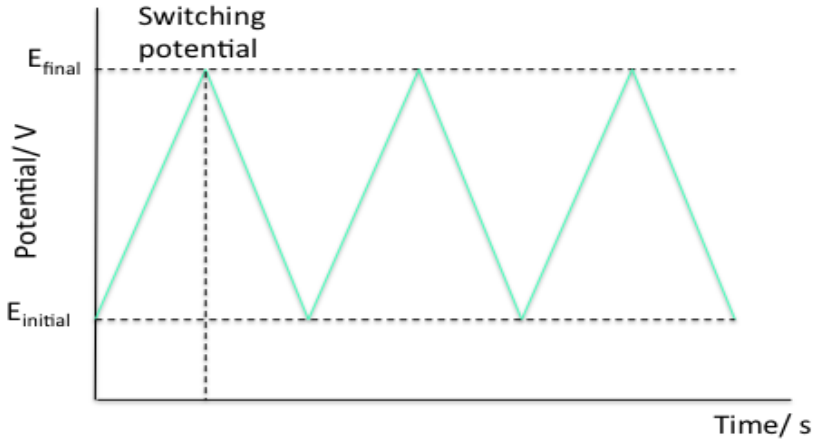

Figure 2-6: The waveform potential applied to the working electrode.

2.5.3 Rotating Disk Electrode

Rotating disk electrode (RDE) is a hydrodynamic electrochemical method commonly used in ORR studies. The RDE consists of a metal disk of the selected electrode (e.g., platinum, gold) embedded in a cylinderal non-conductive material (e.g., Teflon). In this technique, the RDE is placed with face down toward the electrolyte solution and can be rotated under a well-controlled condition. The rotation of electrode

can develop a controlled mass-transport of the fresh electrolyte and reactant to the electrode surface through a laminar flow formed across the disk surface, as illustrated in Figure 2-7a.

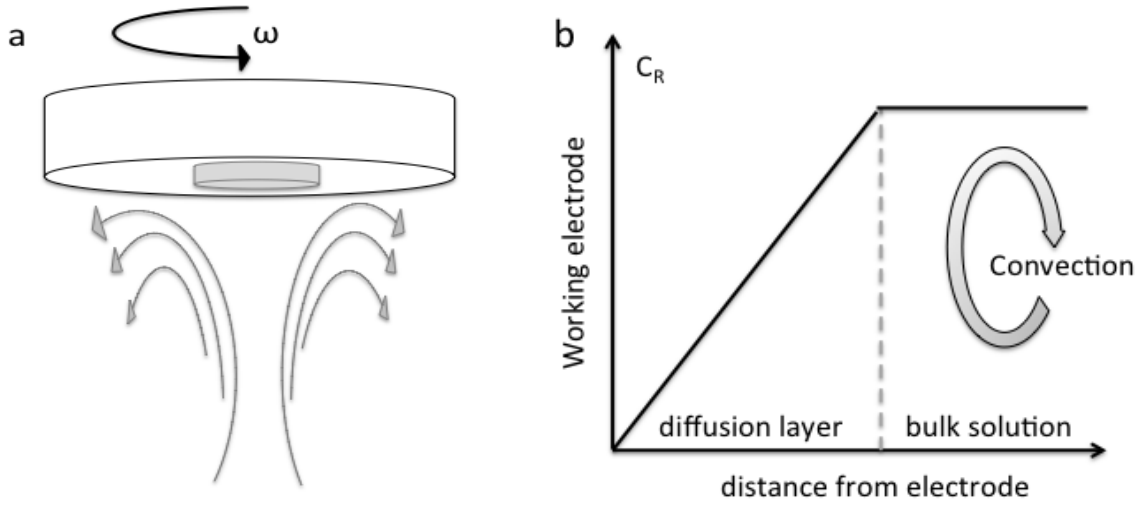

Figure 2-7: (a) Schematic of rotating disk electrode (RDE) with laminar flow. (b). Concentration profile of reactant transport to the rotating disk electrode (RDE).Adapted with permission from ref [86]. Copyright (2019) Elsevier.

As the RDE rotates, a stagnant layer of electrolyte forms adjacent to the electrode surface, known as diffusion layer, in which the reactant reaches to the electrode surface through diffusion. The thickness of this layer depends on the rotation rate of electrode and can be calculated as follows:

$$\delta = 1.61\, D^{1/3}\, \nu^{1/6}\, \omega^{-1/2} \qquad \text{Equation 2-6}$$

where δ is the thickness of diffusion layer, D is the diffusion coefficient of reactant in the electrolyte ($cm^2\ s^{-1}$), ν is the kinematic viscosity of the electrolyte ($cm^2\ s^{-1}$) and ω is

the angular rotation rate of RDE (rad s^{-1}).

The concentration of reactants varies inside of diffusion layer (shown in Figure 2-7 b), which is equal to bulk concentration at the starting point of diffusion layer and decreases toward the electrode surface. When the reaction rate at the electrode surface is faster than the diffusion rate of reactant to the electrode, the concentration of reactant at the surface becomes close to zero and the reaction rate is in under mass-transport control. Levich equation (below) is used to calculate the mass-transport limited current:

$$i_L = 0.62\, nFAC D^{2/3} \nu^{-1/6} \omega^{1/2} \qquad \text{Equation 2-7}$$

where n is the number of electron involved in the reaction, F is the Faraday's constant (C mol^{-1}), A is the geometric surface area of the electrode (cm^2), C is the bulk concentration of reactant (mol cm^{-3}), D is the diffusion coefficient of reactant in the electrolyte (cm^2 s^{-1}), ν is the kinematic viscosity of the electrolyte (cm^2 s^{-1}) and ω is the angular rotation rate of RDE (rad s^{-1}).

2.5.4 Electrochemical Impedance Spectroscopy (EIS)

Electrochemical impedance spectroscopy (EIS) is a powerful technique to evaluate the electrochemical reactions on the electrode surface, as it can separate various electrochemical processes occurring at different time scales as a function of frequency [87]. During the EIS measurement, the working electrode is first held at a constant voltage and then a small amplitude sinusoidal voltage perturbation is applied over a wide frequency range and subsequently the amplitude and phase shift of sinusoidal

current response is recorded. The sinusoidal applied voltage and current response can be calculated using the following equations:

$$E_t = E_0 \sin \omega t \qquad \text{Equation 2-8}$$

$$i_t = i_0 \sin (\omega t + \theta) \qquad \text{Equation 2-9}$$

where E_0 and i_0 are the amplitude of the voltage and current, respectively, $\omega = 2\pi f$ is the angular frequency, θ is the phase shift between the current perturbation and the voltage perturbation, and t is time.

The impedance can be calculated from Ohm's law using voltage and current perturbation, shown below:

$$Z(\omega) = \frac{E_t}{i_t} \qquad \text{Equation 2-10}$$

The impedance can further be expressed as a complex number, shown below:

$$Z(\omega) = Z' + jZ'' \qquad \text{Equation 2-11}$$

where the Z' and Z" are the real and the imaginary components of the impedance, respectively.

The measured impedance spectra is commonly represented by Nyquist plot or complex plane with the real component in the x-axis and imaginary component in the y-axis, shown in Figure 2-8. As shown, the frequency decreased from high to low clockwise along the loop.

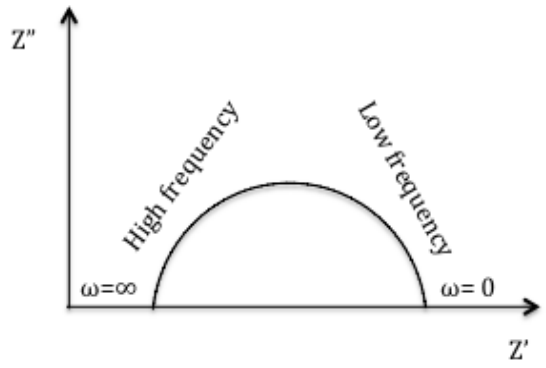

Figure 2-8: Nyquist plot with real and imaginary components.

In order to analyze the impedance spectra, an equivalent circuit can be used to better understand the electrochemical processes occurring at the specific applied potential. The equivalent circuit is comprised of various elements, (i.e., resistor, capacitor and inductor), as described in this section.

Resistor:

When a sinusoidal voltage is applied to a pure resistor, the resultant current is in phase with the voltage with no time lag, and a phase angle of zero. The impedance of a resistor can be calculated as follow:

$$E_t = E_0 \sin \omega t \qquad \text{Equation 2-12}$$

$$i_t = E_t / R = E_0 \sin (\omega t) / R \qquad \text{Equation 2-13}$$

$$Z(\omega) = E_t / i_t = R \qquad \text{Equation 2-14}$$

where R is the resistance.

Capacitor:

When a sinusoidal voltage is applied to a capacitor with charge (q) and capacity (C), the resultant current has the same frequency as sinusoidal voltage but leads the voltage by a phase difference of $\pi/2$. The impedance of this capacitor can be calculated as follow:

$$q = CE \qquad \text{Equation 2-15}$$

$$i = dq/dt = CdE/dt \qquad \text{Equation 2-16}$$

$$i = \omega C E_0 \cos(\omega t) = \omega C E_0 \sin(\omega t + \pi/2) \qquad \text{Equation 2-17}$$

$$Z_C(\omega) = \frac{1}{j\omega C} \qquad \text{Equation 2-18}$$

Inductor:

When the current passes through an inductor, a magnetic flux (φ) is created, which can be calculated using the following equation:

$$\varphi = Li(t) \qquad \text{Equation 2-19}$$

where L is the inductance of a inductor.

Unlike the capacitor, when a sinusoidal voltage is applied to an inductor, the resultant current lags behind the voltage with a phase difference of $\pi/2$. The impedance of an inductor can be calculated as follow:

$$E = d\varphi/dt = d\, Li(t)/dt \qquad \text{Equation 2-20}$$

$$E = L\, d\, i_0 \sin(\omega t) / dt \qquad \text{Equation 2-21}$$

$$E = L\, \omega\, i_0 \sin(\omega t + \pi/2) \qquad \text{Equation 2-22}$$

$$Z_L(\omega) = j\omega L \qquad \text{Equation 2-23}$$

Constant Phase Element (CPE):

CPE is another circuit element used during this study. The CPE is considered as a non-ideal capacitor to represent an inhomogeneity of the electrode surface and, or rough/porous electrode structure [88,89]. Various factors are proposed to contribute to the CPE properties including surface roughness, varying thickness or composition of electrode and non-uniform distribution of current [88]. The impedance of CPE can be calculated using the equation below:

$$Z_C(\omega) = \frac{1}{q(j\omega)^{\alpha}} \qquad \text{Equation 2-24}$$

where q is a constant (with unit of F cm^{-2} $s^{\alpha-1}$) and α is the CPE exponent [90]. The CPE represent as an ideal capacitor when α = 1, as a resistor when α = 0, and as an inductor when α = -1.

2.6 Summary

According to the preceding discussion in this chapter, the majority of the available literature on the effect of metal contaminants on fuel cells has focused on identifying the change in the overall fuel cell performance and Nafion membrane properties. Despite its importance, the degradation effect of metal cation contaminants on the anode and cathode electro-catalyst activities of DMFCs has not been systematically investigated. The overall goal of this dissertation is to better understand the effect of metal solution contaminants on different parts of electro-catalyst layers of DMFC during MOR and ORR by utilizing various Pt based electrodes, including polycrystalline Pt, Nafion-coated Pt and Pt/C electrodes with different Nafion contents.

2.7 References

[1] L. Carrette, K.A. Friedrich, U. Stimming, Fuel cells: Principles, types, fuels, and applications, ChemPhysChem. 1 (2000) 163–193.

[2] K. Kordesch, Fuel Cells and Their Applications, 1996.

[3] S.K. Kamarudin, F. Achmad, W.R.W. Daud, Overview on the application of direct methanol fuel cell (DMFC) for portable electronic devices, Int. J. Hydrogen Energy. 34 (2009) 6902–6916. doi:10.1016/j.ijhydene.2009.06.013.

[4] B.D. Gould, O.A. Baturina, K.E. Swider-Lyons, Deactivation of Pt/VC proton exchange membrane fuel cell cathodes by SO2, H2S and COS, J. Power Sources. 188 (2009) 89–95. doi:10.1016/j.jpowsour.2008.11.072.

[5] L. Dubau, L. Castanheira, F. Maillard, O. Lottin, G. Maranzana, J. Dillet, J. Perrin, E. Moukheiber, G. De Moor, C. Bas, L. Flandin, N. Caqué, A review of PEM fuel cell durability: Materials degradation, local heterogeneities of aging and possible mitigation strategies, Wiley Interdiscip. Rev. Energy Environ. 3 (2014) 540–560. doi:10.1002/wene.113.

[6] T. Cochell, W. Li, A. Manthiram, Effects of Pt coverage in Pt@PdCu5/C core-shell electrocatalysts on the oxygen reduction reaction and methanol tolerance, J. Phys. Chem. C. 117 (2013) 3865–3873. doi:10.1021/jp3126522.

[7] N. Zamel, X. Li, Effect of contaminants on polymer electrolyte membrane fuel cells, Prog. Energy Combust. Sci. 37 (2011) 292–329. doi:10.1016/j.pecs.2010.06.003.

[8] L. Ma, S. Warthesen, D.A. Shores, Evaluation of materials for bipolar plates in PEMFCs, J. New Mater. Electrochem. Syst. 3 (2000) 221–228. http://www.groupes.polymtl.ca/jnmes/modules/journal/index.php/content0647.html.

[9] J. Wind, R. Späh, W. Kaiser, G. Böhm, Metallic bipolar plates for PEM fuel cells, J. Power Sources. 105 (2002) 256–260. doi:10.1016/S0378-7753(01)00950-8.

[10] J.W. Guo, X.F. Xie, J.H. Wang, Y.M. Shang, Effect of current collector corrosion

made from printed circuit board (PCB) on the degradation of self-breathing direct methanol fuel cell stack, Electrochim. Acta. 53 (2008) 3056–3064. doi:10.1016/j.electacta.2007.11.044.

[11] X. Cheng, Z. Shi, N. Glass, L. Zhang, J. Zhang, D. Song, Z.S. Liu, H. Wang, J. Shen, A review of PEM hydrogen fuel cell contamination: Impacts, mechanisms, and mitigation, J. Power Sources. 165 (2007) 739–756. doi:10.1016/j.jpowsour.2006.12.012.

[12] T. Okada, H. Satou, M. Okuno, M. Yuasa, Ion and water transport characteristics of perfluorosulfonated ionomer membranes with H+ and alkali metal cations, J. Phys. Chem. B. 106 (2002) 1267–1273. doi:10.1021/jp013195l.

[13] J.G. Goodwin Jr., K. Hongsirikarn, S. Greenway, S. Creager, Effect of cations (Na+, Ca2+, Fe3+) on the conductivity of a Nafion membrane, J. Power Sources. 195 (2010) 7213–7220. doi:10.1016/j.jpowsour.2010.05.005.

[14] Y. Legras, M.a, Hirata, Q.T. Nguyen, D. Langevin, M. Métayer, Sorption and diffusion behaviors of water in Nafion 117 membranes with different counter ions, Desalination. 147 (2002) 351–357. doi:10.1016/S0011-9164(02)00608-2.

[15] H.L. Yeager, A. Steck, Cation and water diffusion in nafion ion exchange membranes: Influence of polymer structure, J. Electrochem. Soc. 128 (1981) 1880–1884. doi:10.1149/1.2127757.

[16] S. Shi, A.Z. Weber, A. Kusoglu, STRUCTURE-TRANSPORT RELATIONSHIP OF PERFLUOROSULFONIC-ACID MEMBRANES IN DIFFERENT CATIONIC FORMS, Electrochim. Acta. 220 (2016) 517–528.

[17] B.C.H. Steele, A. Heinzel, Materials for fuel-cell technologies, Nature. 414 (2001) 345–352. doi:10.1038/35104620.

[18] H. Wang, M.A. Sweikart, J.A. Turner, Stainless steel as bipolar plate material for polymer electrolyte membrane fuel cells, J. Power Sources. 115 (2003) 243–251. doi:10.1016/S0378-7753(03)00023-5.

[19] H. Tawfik, Y. Hung, D. Mahajan, Metal bipolar plates for PEM fuel cell-A review, J. Power Sources. 163 (2007) 755–767. doi:10.1016/j.jpowsour.2006.09.088.

[20] H.-C. Kuan, C.-C.M. Ma, K.H. Chen, S.-M. Chen, Preparation, electrical, mechanical and thermal properties of composite bipolar plate for a fuel cell, J. Power Sources. 134 (2004) 7–17. doi:10.1016/j.jpowsour.2004.02.024.

[21] A. Hermann, T. Chaudhuri, P. Spagnol, Bipolar plates for PEM fuel cells: A review, Int. J. Hydrogen Energy. 30 (2005) 1297–1302. doi:10.1016/j.ijhydene.2005.04.016.

[22] V. Mehta, J.S. Cooper, Review and analysis of PEM fuel cell design and manufacturing, J. Power Sources. 114 (2003) 32–53. doi:10.1016/S0378-7753(02)00542-6.

[23] M.V. Williams, E. Begg, L.. Bonville, H.R. Kunz, J.M. Fenton, Characterization of gas diffusion layers for PEMFC, J. Electrochem. Soc. 151 (2004) A1173–A1180. doi:10.1149/1.1764779.

[24] U. Pasaogullari, C.Y. Wang, Liquid Water Transport in Gas Diffusion Layer of Polymer Electrolyte Fuel Cells, J. Electrochem. Soc. 151 (2004) A399–A406. doi:10.1149/1.1646148.

[25] S. Banerjee, D.E. Curtin, Nafion® perfluorinated membranes in fuel cells, J. Fluor. Chem. 125 (2004) 1211–1216.

[26] R.E. White, T.V. Nguyen, A Water and Heat Management Model for Proton-Exchanae-Membrane Fuel Cells, J. Electrochem. Soc. 140 (1993) 2178–2186. doi:10.1149/1.2220792.

[27] S. Motupally, A.J. Becker, J.W. Weidner, Diffusion of water in Nafion 115 membranes, J. Electrochem. Soc. 147 (2000) 3171–3177. doi:10.1149/1.1393879.

[28] K.A. Mauritz, R.B. Moore, State of understanding of Nafion, Chem. Rev. 104 (2004) 4535–4585. doi:10.1021/cr0207123.

[29] N. Agmon, The Grotthuss mechanism, Chem. Phys. Lett. 244 (1995) 456–462. doi:10.1016/0009-2614(95)00905-J.

[30] T.A. Zawodzinski, J. Davey, J. Valerio, S. Gottesfeld, The water content dependence of electro-osmotic drag in proton-conducting polymer electrolytes, Electrochim. Acta. 40 (1995) 297–302. doi:10.1016/0013-4686(94)00277-8.

[31] M. Gil, X. Ji, X. Li, H. Na, J.E. Hampsey, Y. Lu, Direct synthesis of sulfonated aromatic poly(ether ether ketone) proton exchange membranes for fuel cell applications, J. Memb. Sci. 234 (2004) 75–81. doi:10.1016/j.memsci.2003.12.021.

[32] R. Parsons, T. VanderNoot, The oxidation of small organic molecules. A survey of recent fuel cell related research, J. Electroanal. Chem. 257 (1988) 9–45. doi:10.1016/0022-0728(88)87028-1.

[33] R. Nagao, D.A. Cantane, F.H.B. Lima, H. Varela, Influence of anion adsorption on the parallel reaction pathways in the oscillatory electro-oxidation of methanol, J. Phys. Chem. C. 117 (2013) 15098–15105. doi:10.1021/jp4028047.

[34] H.A. Gasteiger, N. Marković, P.N. Ross Jr., E.J. Cairns, Electro-oxidation of small organic molecules on well-characterized PtRu alloys, Electrochim. Acta. 39 (1994) 1825–1832. doi:10.1016/0013-4686(94)85171-9.

[35] T. Iwasita, Electrocatalysis of methanol oxidation, Electrochim. Acta. 47 (2002) 3663–3674. doi:10.1016/S0013-4686(02)00336-5.

[36] T. Iwasita, Methanol and CO electrooxidation. In: Handbookof fuel cells – fundamentals, technology and applications,vol. 2. John Wiley & Sons, Ltd, 2003.

[37] B.E. Angerstein-Kozlowska, H., Conway, W.B.A. Sharp, The real condition of electrochemically oxidized platinum surfaces. Part I. Resolution of component processes, J. Electroanal. Chem. 43 (1973) 9–36. doi:10.1016/S0022-0728(73)80307-9.

[38] M. Watanabe, M. Uchida, S. Motoo, Preparation of highly dispersed Pt + Ru alloy clusters and the activity for the electrooxidation of methanol, J. Electroanal. Chem. 229 (1987) 395–406. doi:10.1016/0022-0728(87)85156-2.

[39] M. Watanabe, S. Motoo, Electrocatalysis by ad-atoms part II. Enhancement of the oxidation of methanol on platinum by ruthenium ad-atoms, J. Electroanal. Chem. 60 (1975) 267–273.

[40] G. Blyholder, Molecular orbital view of chemisorbed carbon monoxide, J. Phys. Chem. 68 (1964) 2772–2778.

[41] M. Igarashi, H., Fujino, T., Zhu, Y., Uchida, H., Watanabe, CO tolerance of Pt alloy

electrocatalysts for polymer electrolyte fuel cells and the detoxification mechanism, Phys. Chem. Chem. Phys. 3 (2001) 306–314. doi:10.1039/b007768m.

[42] S. Giorgi, L., Pozio, A., Bracchini, C., Giorgi, R., Turtù, H2 and H2/CO oxidation mechanism on Pt/C, Ru/C and Pt-Ru/C electrocatalysts, J. Appl. Electrochem. 31 (2001) 325–334. doi:10.1023/A:1017595920726.

[43] H. Wroblowa, Y. C. Pan, J. Razumney., Electroreduction of Oxygen: A new mechanism criterion, J. Electroanal. Che., (1976) 195–229.

[44] J.K. Nørskov, J. Rossmeisl, A. Logadottir, L. Lindqvist, J.R. Kitchin, T. Bligaard, H. Jónsson, Origin of the overpotential for oxygen reduction at a fuel-cell cathode, J. Phys. Chem. B. 108 (2004) 17886–17892. doi:10.1021/jp047349j.

[45] A.A. Gewirth, M.S. Thorum, Electroreduction of dioxygen for fuel-cell applications: Materials and challenges, Inorg. Chem. 49 (2010) 3557–3566. doi:10.1021/ic9022486.

[46] T. Toda, H. Igarashi, H. Uchida, M. Watanabe, Enhancement of the electroreduction of oxygen on Pt alloys with Fe, Ni, and Co, J. Electrochem. Soc. 146 (1999) 3750–3756. doi:10.1149/1.1392544.

[47] M. Min, J. Cho, K. Cho, H. Kim, Particle size and alloying effects of Pt-based alloy catalysts for fuel cell applications, Electrochim. Acta. 45 (2000) 4211–4217. doi:10.1016/S0013-4686(00)00553-3.

[48] L. Xiong, A. Manthiram, Influence, of atomic ordering on the electrocatalytic activity of Pt-Co alloys in alkaline electrolyte and proton exchange membrane fuel cells, J. Mater. Chem. 14 (2004) 1454–1460. doi:10.1039/b400968c.

[49] S. Mukerjee, Role of Structural and Electronic Properties of Pt and Pt Alloys on Electrocatalysis of Oxygen Reduction An In Situ XANES and EXAFS Investigation, J. Electrochem. Soc. 142 (1995) 1409–1422. doi:10.1149/1.2048590.

[50] A. Heinzel, V.M. Barragán, A review of the state-of-the-art of the methanol crossover in direct methanol fuel cells, J. Power Sources. 84 (1999) 70–74. doi:10.1016/S0378-7753(99)00302-X.

[51] Z. Qi, A. Kaufman, Open circuit voltage and methanol crossover in DMFCs, J.

Power Sources. 110 (2002) 177–185. doi:10.1016/S0378-7753(02)00268-9.

[52] R. Dillon, S. Srinivasan, A.S. Aricò, V. Antonucci, International activities in DMFC R&D: Status of technologies and potential applications, J. Power Sources. 127 (2004) 112–126. doi:10.1016/j.jpowsour.2003.09.032.

[53] W. Paganin, V.A., Sitta, E., Iwasita, T., Vielstich, Methanol crossover effect on the cathode potential of a direct PEM fuel cell, J. Appl. Electrochem. 35 (2005) 1239–1243. doi:10.1007/s10800-005-9035-5.

[54] H. Yang, N. Alonso-Vante, J.-M. Léger, C. Lamy, Tailoring, Structure, and Activity of Carbon-Supported Nanosized Pt-Cr Alloy Electrocatalysts for Oxygen Reduction in Pure and Methanol-Containing Electrolytes, J. Phys. Chem. B. 108 (2004) 1938–1947.

[55] N. Jia, M.C. Lefebvre, J. Halfyard, Z. Qi, P.G. Pickup, Modification of Nafion proton exchange membranes to reduce methanol crossover in PEM fuel cells, Electrochem. Solid-State Lett. 3 (2000) 529–531. doi:10.1149/1.1391199.

[56] S.P. Jiang, Z. Liu, Z.Q. Tian, Layer-by-layer self-assembly of composite polyelectrolyte-nafion membranes for direct methanol fuel cells, Adv. Mater. 8 (2006) 1068–1072. doi:10.1002/adma.200502462.

[57] Y. Zhai, G. Bender, S. Dorn, R. Rocheleau, The Multiprocess Degradation of PEMFC Performance Due to Sulfur Dioxide Contamination and Its Recovery, J. Electrochem. Soc. 157 (2010) B20–B26. doi:10.1149/1.3247546.

[58] R. Mohtadi, W. -k. Lee, J.W. Van Zee, Assessing durability of cathodes exposed to common air impurities, J. Power Sources. 138 (2004) 216–225. doi:10.1016/j.jpowsour.2004.06.036.

[59] R. Mohtadi, W. -k. Lee, S. Cowan, J.W. Van Zee, M. Murthy, Effects of Hydrogen Sulfide on the Performance of a PEMFC, Electrochem. Solid-State Lett. 6 (2003) A272. doi:10.1149/1.1621831.

[60] J.M. Moore, P.L. Adcock, J.B. Lakeman, G.O. Mepsted, The effects of battlefield contaminants on PEMFC performance, J. Power Sources. 85 (2000) 254–260. doi:10.1016/S0378-7753(99)00341-9.

[61] Y. Nagahara, S. Sugawara, K. Shinohara, The impact of air contaminants on PEMFC performance and durability, J. Power Sources. 182 (2008) 422–428. doi:10.1016/j.jpowsour.2007.12.091.

[62] R. Borup, J. Meyers, B. Pivovar, Y.S. Kim, R. Mukundan, N. Garland, D. Myers, M. Wilson, F. Garzon, D. Wood, P. Zelenay, K. More, K. Stroh, T. Zawodzinski, X.J. Boncella, J.E. Mcgrath, O.M. Inaba, K. Miyatake, M. Hori, K. Ota, Z. Ogumi, S. Miyata, A. Nishikata, Z. Siroma, Y. Uchimoto, K. Yasuda, K. Kimijima, N. Iwashita, Scientific aspects of polymer electrolyte fuel cell durability and degradation, Chem. Rev. 107 (2007) 3904–3951. doi:10.1021/cr050182l.

[63] J. Xie, D.L. Wood, D.M. Wayne, T. a. Zawodzinski, P. Atanassov, R.L. Borup, Durability of PEFCs at High Humidity Conditions, J. Electrochem. Soc. 152 (2005) A104–A113. doi:10.1149/1.1830355.

[64] A. Pozio, R.F. Silva, M. De Francesco, L. Giorgi, Nafion degradation in PEFCs from end plate iron contamination, Electrochim. Acta. 48 (2003) 1543–1549. doi:10.1016/S0013-4686(03)00026-4.

[65] H. Li, K. Tsay, H. Wang, J. Shen, S. Wu, J. Zhang, N. Jia, S. Wessel, R. Abouatallah, N. Joos, J. Schrooten, Durability of PEM fuel cell cathode in the presence of Fe3+ and Al3+, J. Power Sources. 195 (2010) 8089–8093. doi:10.1016/j.jpowsour.2010.07.003.

[66] H. Li, J. Gazzarri, K. Tsay, S. Wu, H. Wang, J. Zhang, S. Wessel, R. Abouatallah, N. Joos, J. Schrooten, PEM fuel cell cathode contamination in the presence of cobalt ion (Co2+), Electrochim. Acta. 55 (2010) 5823–5830. doi:10.1016/j.electacta.2010.05.031.

[67] M. a. Uddin, X. Wang, J. Qi, M.O. Ozdemir, U. Pasaogullari, L. Bonville, T. Molter, Effect of Chloride on PEFCs in Presence of Various Cations, J. Electrochem. Soc. 162 (2015) F373–F379. doi:10.1149/2.0291504jes.

[68] X. Jie, Z.G. Shao, B. Yi, The effect of different valency cations on DMFC performance, Electrochem. Commun. 12 (2010) 700–702. doi:10.1016/j.elecom.2010.03.010.

[69] W. Chen, Q. Xin, G. Sun, S. Yang, Z. Zhou, Q. Mao, P. Sun, Effects of dissolved iron and chromium on the performance of direct methanol fuel cell, Electrochim. Acta. 52 (2007) 7115–7120. doi:10.1016/j.electacta.2007.05.047.

[70] M.-J. Yang, K.-Y. Park, K.-B. Kim, H. Cho, H. Choi, J.-Y. Park, Degradation mechanisms and mitigation strategies of metal cations in recycled fuel for direct methanol fuel cell membrane electrode assembly, J. Power Sources. 242 (2013) 646–655. doi:10.1016/j.jpowsour.2013.05.141.

[71] T.. Okada, N. Nakamura, M. Yuasa, I. Sekine, Ion and water transport characteristics in membranes for polymer electrolyte fuel cells containing H+ and Ca2+ cations, J. Electrochem. Soc. 144 (1997) 2744–2750.

[72] M.J. Kelly, G. Fafilek, J.O. Besenhard, H. Kronberger, G.E. Nauer, Contaminant absorption and conductivity in polymer electrolyte membranes, J. Power Sources. 145 (2005) 249–252. doi:10.1016/j.jpowsour.2005.01.064.

[73] M.J. Kelly, B. Egger, G. Fafilek, J.O. Besenhard, H. Kronberger, G.E. Nauer, Conductivity of polymer electrolyte membranes by impedance spectroscopy with microelectrodes, Solid State Ionics. 176 (2005) 2111–2114. doi:10.1016/j.ssi.2004.07.071.

[74] M. Sulek, J. Adams, S. Kaberline, M. Ricketts, J.R. Waldecker, In situ metal ion contamination and the effects on proton exchange membrane fuel cell performance, J. Power Sources. 196 (2011) 8967–8972. doi:10.1016/j.jpowsour.2011.01.086.

[75] A.P. Young, J. Stumper, S. Knights, E. Gyenge, Ionomer degradation in polymer electrolyte membrane fuel cells, J. Electrochem. Soc. 157 (2010) B425–B436. doi:10.1149/1.3281899.

[76] A. Collier, H. Wang, X. Zi Yuan, J. Zhang, D.P. Wilkinson, Degradation of polymer electrolyte membranes, Int. J. Hydrogen Energy. 31 (2006) 1838–1854. doi:10.1016/j.ijhydene.2006.05.006.

[77] T. Kinumoto, M. Inaba, Y. Nakayama, K. Ogata, R. Umebayashi, A. Tasaka, Y. Iriyama, T. Abe, Z. Ogumi, Durability of perfluorinated ionomer membrane against

hydrogen peroxide, J. Power Sources. 158 (2006) 1222–1228. doi:10.1016/j.jpowsour.2005.10.043.

[78] C. Walling, Perfluorinated Ionomer Membranes, Acc. Chem. Res. 8 (1975) 125–131. doi:10.1021/ar50088a003.

[79] H. Li, K. Tsay, H. Wang, S. Wu, J. Zhang, N. Jia, S. Wessel, R. Abouatallah, N. Joos, J. Schrooten, Effect of Co2+ on oxygen reduction reaction catalyzed by Pt catalyst, and its implications for fuel cell contamination, Electrochim. Acta. 55 (2010) 2622–2628. doi:10.1016/j.electacta.2009.12.037.

[80] J. Durst, M. Chatenet, F. ́de ́ric Maillard, Impact of metal cations on the electrocatalytic properties of Pt/C nanoparticles at multiple phase interfaces, Phys. Chem. Chem. Phys. 14 (2012) 13000–13009. doi:10.1039/c2cp42191g.

[81] J. Tymoczko, V. Colic, A. Ganassin, W. Schuhmann, A.S. Bandarenka, Influence of the alkali metal cations on the activity of Pt(1 1 1) towards model electrocatalytic reactions in acidic sulfuric media, Catal. Today. 244 (2015) 96–102. doi:10.1016/j.cattod.2014.07.007.

[82] X. Zhou, T. Lu, W. Xing, C. Liu, Effect of cations in solution on the oxidation of methanol on the surface of platinum electrode, Electrochim. Acta. 52 (2006) 1688–1691. doi:10.1016/j.electacta.2006.03.100.

[83] M. Chatenet, Y. Soldo-olivier, E. Chainet, Electrochemical quartz crystal microbalance determination of nickel formal partial charge number during nickel-underpotential deposition on platinum in sulphate media, 9 (2007) 1463–1468. doi:10.1016/j.elecom.2007.02.001.

[84] E. Guerra, G.H. Kelsall, M. Bestetti, D. Dreisinger, K. Wong, K.A.R. Mitchell, D. Bizzotto, Use of Underpotential Deposition for Evaluation of Overpotential Deposition Kinetics of Reactive Metals, J. Electrochem. Soc. 151 (2004) E1–E6. doi:10.1149/1.1631282.

[85] S. Kim, J.P. Meyers, Electrochimica Acta The influence of hydrogen- and cation-underpotential deposition on oxide-mediated Pt dissolution in proton-exchange membrane fuel cells, Electrochim. Acta. 56 (2011) 8387–8393.

doi:10.1016/j.electacta.2011.07.031.

[86] C. Du, Q. Tan, G. Yin, J. Zhang, Rotating Disk Electrode Methode, Rotating Electrode Methods and Oxygen Reduction Electrocatalysts, (2014) pp. 171-198. doi: 10.1016/B978-0-444-63278-4.00005-7

[87] M.E. Orazem, B. Tribollet, Electrochemical Impedance Spectroscopy, John Wiley & Sons, 2011.

[88] G.J. Brug, A.L.G. van den Eeden, M. Sluyters-Rehbach, J.H. Sluyters, The analysis of electrode impedances complicated by the presence of a constant phase element, J. Electroanal. Chem. 176 (1984) 275–295. doi:10.1016/S0022-0728(84)80324-1.

[89] R. De Levie, The influence of surface roughness of solid electrodes on electrochemical measurements, Electrochim. Acta. 10 (1965) 113–130. doi:10.1016/0013-4686(65)87012-8.

[90] A. Lasia, Electrochemical Impedance Spectroscopy and its Applications, in: Electrochem. Impedance Spectrosc. Its Appl., 2014: p. 38. doi:10.1007/978-1-4614-8933-7.

3 The Effect of Metal Solution Contaminants on the Platinum Electro-catalyst during Methanol Oxidation and Oxygen Reduction Reactions

Abstract

Understanding the effect of metal solution contaminants on the methanol oxidation reaction (MOR) and oxygen reduction reaction (ORR) activities of direct methanol fuel cells (DMFCs) is critical in the enhancement of this technology. In this study, the effect of various concentrations of metal salt solutions (i.e., Co, Ni and Zn with sulfate and nitrate as counter-anions) on polycrystalline Pt and Pt_xRu_y electro-catalytic activities during MOR and ORR are systematically investigated. The results show a decrease in MOR and ORR activities as the concentration of metal salt solutions increased. The influence of counter-anions (i.e., NO_3^- and SO_4^{2-}) adsorption on the Pt electro-catalyst activity was further investigated. The results showed that a combined effect of adsorbed counter-anions as well as hydrated metal cations may be responsible for the decrease in the electro-catalytic activity of Pt during the MOR and ORR.

3.1 Introduction

DMFC is a promising power source for portable application due to its high energy density, low pollution and simple system design. Despite considerable progress in DMFC research, there are many issues need to be addressed before widespread commercial adoption will be realized [1]. These include membrane and electro-catalyst degradation, cell contamination and fuel crossover [2–6]. Impurities may be introduced to the fuel cell through the fuel and/or air (oxidant) streams, or from the degradation of fuel cell components. The effect of air impurities (e.g., CO, NO_x, SO_2, and NH_3) on the proton exchange membrane fuel cells (PEMFCs) has been extensively studied in the literature, showing a significant degradation in the fuel cell performance [7–11]. In addition, metal cation contaminants (e.g., Co^{2+}, Ni^{2+}, and Fe^{2+}) introduced to the fuel cell system through the degradation of its components (via corrosion of the catalyst, current collector and/or bipolar plates [12-14]) can result in a significant decrease in the fuel cell performance.

The detrimental effect of metal cations on Nafion membrane of PEMFCs is well established [15]. Nafion membrane is composed of sulfonate sites, which have a higher affinity for the multivalent cations (e.g., Fe^{3+} and Cu^{2+}) than for protons. The higher valence cations displace the protons in the Nafion membrane, resulting in decreased membrane water content and proton mobility, which detrimentally affect the fuel cell performance [16,17]. Li et al. studied the effect of Fe^{3+} on the PEMFC performance. It was shown that the presence of Fe^{3+} can result in the pinhole formation in the membrane, leading to a sudden cell death [18]. In a study by Chen et al., the proton

conductivity of the Nafion membrane decreased in the presence of Cr^{3+}, leading to a drop in DMFC performance [19].

The effect of metal cation contaminants on the fuel cell performance has been focused by ongoing research studies in recent years. Yang et al. investigated the effect of various metal cation impurities (including Ni^{2+}, Fe^{3+}, Al^{3+}, and Cr^{3+}) on the membrane electrode assembly (MEA) of DMFC [20]. The results showed that Ni^{2+} has the highest adverse effect on the anode electro-catalytic activity, showing a significant anode polarization loss as compared to other cation impurities (i.e., Fe^{3+}, Al^{3+}, and Cr^{3+}). The effect of Fe^{3+} on DMFC performance was investigated by Chen et al. [19]. It was shown that the presence of Fe^{3+} resulted in a decrease in the anode electrochemical surface area, leading to a degradation in the anode electro-catalytic activity and DMFC performance. Li et al. studied the effect of Co^{2+}, Fe^{3+} or Al^{3+} on the cathode side of a PEMFC using the electrochemical impedance spectroscopy (EIS) [18,21]. The results showed an increase in ORR charge-transfer and mass-transfer resistances, resulting in a significant decrease in the PEMFC performance.

While previous research has primarily focused on the effect of metal cation contaminants on the membrane properties and fuel cell performance, little is known regarding their influence on the electro-catalysts of fuel cell. The effect of alkali metal cations on the Pt electro-catalytic activity in the alkaline media was investigated by Strmcnik et al. [22]. It was suggested that the non-covalent interaction between the non-adsorbed hydrated alkali metal cations in outer Helmholtz plane (OHP) and the adsorbed

oxygenated (OH_{ad}) species in the inner Helmholtz plane (IHP) can affect the electro-catalytic activity of Pt during the MOR and ORR. In a thermodynamic analysis conducted by Garcia et al., the effect of K_2SO_4 on the electrochemical properties of Pt(111) in the acidic media was investigated [23]. It was suggested that the adsorption of K^+ metal cations can occur through ion-pair formation (K^+-SO_4^{2-}) with adsorbed SO_4^{2-} anions. It was also reported in the previous studies that the alkali metal cations as well as adsorbed anions can affect the Pt (111) electrochemical properties in the acidic media [24–26].

Despite its importance, the effect of metal solution contaminants on the electro-catalyst activities of fuel cell is not systematically investigated. The primary objective of this study is to understand the effect of metal solution contaminants including Co, Ni, and Zn salts on the Pt electro-catalytic activities during the MOR and ORR. Cobalt and nickel cation contaminants were selected as they may be introduced into a DMFC system through the dissolution of Pt alloy catalysts [13,27,28]. To consider metal cations with a wide range of reduction potentials, Zn-containing salts with low standard potential (-0.76 V) relative to other transition metals were selected. The individual influence of counter-anions (i.e., NO_3^- and SO_4^{2-}) on the Pt catalytic activity was also quantified. Through this work, the effects of cations and counter-anions of six metal salts were separately examined on the voltammetric properties of Pt and its activity during MOR and ORR using cyclic voltammetry and RDE measurements. It also should be noted that during this study, exposures to metal salt solutions were performed in a relatively small

time frame compared to expected life span of fuel cells, explaining the higher concentrations of metal solutions selected in this study.

3.2 Experimental Methods

3.2.1 Solution Preparation

The electrolyte solution used during background and MOR voltammetries was 0.5 M H_2SO_4, which was prepared by diluting measured amount of H_2SO_4 (Fisher Scientific, ACS grade, 98%) with deionized (DI) water (Millipore Milli-Q, 18.2 MΩ cm). As sulfate anions are known to suppress the ORR activity [29,30], 0.1 M $HClO_4$ (Fisher Scientific, ACS grade, 70 %) solution was used as the electrolyte solution during the ORR studies. Various concentrations (i.e., $2x10^{-x}$ M (x=1-7)) of metal solution contaminants were prepared using $CoSO_4 \cdot 7H_2O$ (Alfa Aesar, 98 %), $Co(NO_3)_2 \cdot 6H_2O$ (Sigma Aldrich, > 98 %), $NiSO_4 \cdot 6H_2O$ (Alfa Aesar, 98 %), $Ni(NO_3)_2 \cdot 6H_2O$ (Alfa Aesar, 98 %), $ZnSO_4 \cdot 7H_2O$ (Sigma-Aldrich, > 99 %), $Zn(NO_3)_2 \cdot 6H_2O$ (Anachemia, > 99 %) and HNO_3 (Fisher Scientific, ACS grade). In order to evaluate the effect of the metal solution contaminants on the electro-catalyst activity within a reasonable experimental time frame, high concentrations of metal solutions were also selected through this study. This approach has been commonly used in the literature for similar investigations [31-33].

3.2.2 Electrode Preparation

A polycrystalline Pt foil (1 cm × 0.8 cm, Alfa Aesar, 99.99% metal basis) was used during the background and MOR voltammetry measurements. To perform the ORR study, a polycrystalline Pt disk electrode (0.5 cm diameter, embedded in Teflon, Pine

Instruments, 99.99 %) was used as a rotating disc electrode (RDE). In this study, the polycrystalline Pt electrodes are used to achieve well-controlled measurements and to avoid the complications that arise when using bimetallic or carbon-supported catalysts. As the planar Pt is not a true representation of real DMFC electrodes, the MOR measurements were also performed using Pt_xRu_y electro-catalysts to prove that our findings also apply to the type of anode materials typically used in DMFCs.

The unsupported Pt_xRu_y electrodes were prepared through two different methods. In the first method, a polycrystalline Pt foil was immersed in a solution containing 0.2 M $RuCl_3$ (Alfa Aesar, 99.9 %) and 0.1 M $HClO_4$ for 60 s, which induces spontaneous Ru deposition onto the electrode surface [34]. The electrode was then rinsed with excessive amounts of DI water. In the second method, Pt_xRu_y electrodes were prepared from powder sample prepared during a previous study [35]. The Pt_xRu_y powder was transformed into ink and transferred by pipette onto Au foil (1 cm × 0.58 cm, 99.9%, Goodfellow) electrodes.

3.2.3 Electrochemical Cell

Electrochemical measurements were performed in a standard two-compartment glass cell. The working (main) compartment was shared with the working electrode and a large surface area of Pt mesh as the counter electrode. The reference electrode was placed in the reference compartment, which was separated from the working compartment by a Luggin capillary. A saturated calomel electrode (SCE) was used as the reference electrode during background and MOR voltammetry measurements. Selected

experiments were repeated using the reversible hydrogen electrode (RHE) to confirm that the short-term use of the SCE did not result in the chloride contamination in the working compartment. During the ORR studies, the RHE was used as the reference electrode. For measurements using RHE, a small surface area Pt gauze electrode was immersed in the electrolyte solution purged with electrolytically generated H_2 gas (Parker Hannifin H2PEM-165L, 99.9999 %). All potentials reported in this work are referenced to the RHE. Current densities were calculated by the measured current divided by the geometric area of the electrode.

3.2.4 Electrochemical Measurements

Prior to each electrochemical measurement, the polycrystalline Pt electrode was cleaned by cycling the potential (at least fifty times) between 0.08 and 1.48 V at a scan rate of 100 mV s^{-1} in 0.5 M H_2SO_4, until the voltammogram remained stable. To clean the Pt_xRu_y electrodes, the cycling potential was performed for approximately 10 times at potential range of 0.08 - 0.88 V with a scan rate of 20 mV s^{-1} in 0.5 M H_2SO_4. In this case, the potential range and the number of potential cycling were limited in order to avoid the degradation of Pt_xRu_y during the cleaning process.

In order to determine the effect of metal solution contaminants (i.e., Co, Ni and Zn with sulfate and nitrate as counter-anions) on the Pt voltammetric properties, cyclic voltammetry measurements were performed in metal-free and metal containing 0.5 M H_2SO_4 solutions at the potential range of 0.08 - 1.28 V with a 20 mV s^{-1} scan rate. Prior to background and MOR voltammetries, the electrolyte solutions were purged with argon

(purity grade 5.0) for a minimum of 30 minutes to remove dissolved oxygen.

To characterize the effect of metal solution contaminants on the Pt electro-catalytic activity during MOR, cyclic voltammetry measurements were performed in metal-free and metal containing Ar-saturated 0.5 M H_2SO_4 + 0.5 M CH_3OH (Fisher Scientific, 99.9 %) solutions at the potential range of 0.08 - 1 V with a 20 mV s^{-1} scan rate. To further investigate the effect of counter-anions on the Pt catalytic activity, the background and MOR voltammetries were performed in the presence of HNO_3. The MOR voltammetry of Pt_xRu_y electrodes was also conducted in the absence and presence of metal solution contaminants in Ar-saturated 0.5 M H_2SO_4 + 0.5 M CH_3OH solutions at the potential range of 0.08 – 0.88 V with a 20 mV s^{-1} scan rate.

To examine the effect of metal solution contaminants on the Pt electro-catalytic activity during the ORR, linear sweep voltammograms were obtained at Pt RDE in the metal-free and metal containing O_2 (The Linde Group, grade 4.5) saturated 0.1 M $HClO_4$ solutions. The electrode potential was scanned at the potential range of 0.002 - 1.1 V at a 10 mV s^{-1} scan rate with the electrode rotation rate of 400 rpm. To further investigate the effect of counter-anions of metal solution contaminants on Pt electro-catalytic activity during the ORR, the linear sweep voltammetry was separately conducted in the presence of H_2SO_4 and HNO_3 solutions. All voltammetric measurements were performed using a Solartron Analytical 1285 potentiostat controlled with Corrware software (v. 3.1c, Scribner Associates Inc.). A modulated speed rotator (AFMSRX, Pine Instruments) was also used to control the rotation speed of the RDE.

3.3 Results and Discussion

3.3.1 General Considerations of Pt Voltammetry

The background voltammetry of polycrystalline Pt electrode in the acidic media was examined in the absence of metal solution contaminants, in order to better understand the electro-catalytic properties of this electrode. Figure 3-1a shows a cyclic voltammogram (CV) of polycrystalline Pt in 0.5 M H_2SO_4. The CV is divided into three potential regions: (i) 0 – 0.3 V, (ii) 0.3 – 0.7 V, and (iii) 0.7 – 1.28 V. In the first potential region, (i), the reduction and oxidation peak currents correspond to the adsorption and desorption of hydrogen ($H_{ads/des}$) on the Pt surface, respectively. The peak currents observed at ~ 0.1 V and ~ 0.25 V are associated with $H_{ads/des}$ on Pt (110) and Pt (100)/(111) sites, respectively [36]. In the second potential region, (ii), the current is primarily attributed to the double layer charging at the electrode-solution interface. Finally, in the third potential region, (iii), the oxidation and reduction peak currents are associated with the formation of Pt-OH/Pt-O surface species and the subsequent electrochemical reduction of these species back to Pt metal, respectively.

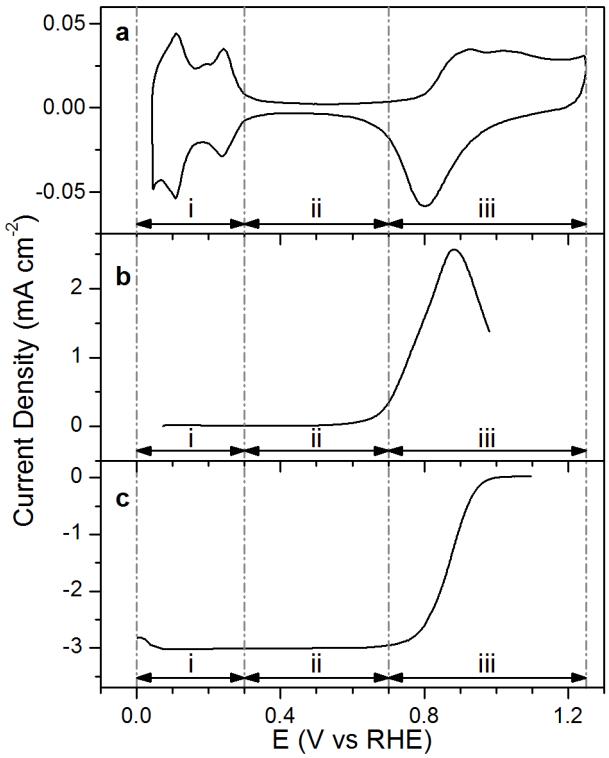

Figure 3-1: Cyclic voltammograms of polycrystalline Pt electrode in: a) Ar-saturated 0.5 M H_2SO_4 solution at a scan rate of 20 mV s^{-1}., b) Ar-saturated 0.5M CH_3OH + 0.5M H_2SO_4 solution (forward direction) at a scan rate of 20 mV s^{-1}., c) O_2-saturated 0.1 M $HClO_4$ solution (reverse direction) at a scan rate of 10 mV s^{-1} and ω = 400 rpm.

Figure 3-1b shows the anodic linear sweep voltammogram of Pt in 0.5 M H_2SO_4 containing 0.5 M CH_3OH solution. The MOR onset potential appears at ~ 0.6 V, followed by a fully developed oxidation peak current at 0.87 V. The MOR onset potential occurs well above the standard potential, E^0 = 0.06 V, as Pt-OH must form in order to oxidize CH_3OH to CO_2. It should be noted that the MOR onset potential on bi-metallic catalysts (e.g., Pt_xRu_y) that are typically used in DMFCs is as low as 0.3 V. Therefore, the potential region (ii) is the focus of practical interest for the MOR in DMFCs.

Figure 3-1c shows the linear potential sweep (reverse-direction) of Pt obtained in

an O_2-saturated 0.1 M $HClO_4$ solution. The onset potential of the ORR appears at ~ 1 V, well below the standard potential, E^0 = 1.2 V. This occurs due to the Pt-OH surface coverage at E> 1 V, which must be reduced to the Pt metallic state. The diffusion-limited current is reached at potential below 0.7 V, i.e., potential regions (i) and (ii). Therefore, the activation-controlled region at potential region (iii) is considered the greatest interest for the ORR in fuel cell systems.

Having established the potential regions of interest for the MOR and ORR, the question to be asked is what effects transition metal cations such as Co^{2+}, Ni^{2+} and Zn^{2+} could have on either of these processes. From their E^0 values (-0.28 V for Co^{2+}/Co and -0.25 V for Ni^{2+}/Ni), neither Co^{2+} nor Ni^{2+} ions is expected to reduce on the Pt surface in the potential regions (ii) or (iii). The E^0 value for the Zn^{2+}/Zn pair is even more negative (-0.76 V). Nevertheless, the results presented in this work demonstrate that metal solution contaminants can detrimentally affect the MOR and ORR activities.

3.3.2 Effect of Metal Solution Contaminants on the Pt Voltammetric Properties

The first elementary step in this study is to charactrize the effect of metal solution contaminants on the voltammetric properties of polycrystalline Pt, which is responsible for the MOR and ORR activities. The cyclic voltammetries were conducted on the Pt in 0.5 M H_2SO_4 solutions in the absence and presence of various concentrations (i.e., $2x10^{-x}$ M (x=1-7)) of metal salt solutions (i.e., Co, Ni and Zn with sulfate and nitrate as counter-anions). The results obtained in the presence of low concentrations (< $2x10^{-3}$)

of metal solutions showed no significant changes in $H_{ads/des}$ (E < 0.3 V) and Pt-OH/Pt-O formation/reduction (E > 0.7 V) peak currents. Therefore, only the results obtained in the presence of high concentration (i.e., 0.2 M) of metal solutions are discussed in the following sections.

3.3.2.1 Pt Voltammetry in the Presence of Metal Sulfates

Figure 3-2a shows the CVs of polycrystalline Pt obtained in the metal-free (dash-dotted black curve) and 0.2 M metal sulfate containing (i.e., (i) $CoSO_4$, (ii) $NiSO_4$ and (iii) $ZnSO_4$ (solid gray curves)) 0.5 M H_2SO_4 solutions at a 20 mV s^{-1} scan rate.

Figure 3-2a-i and Figure 3-2a-ii (solid gray curve) respectively show the CVs of Pt in the presence of 0.2 M $CoSO_4$ and 0.2 M $NiSO_4$. The results show an increase in the cathodic and anodic current densities in the hydrogen adsorption-desorption region (E < 0.3 V). However, by scanning the potential to more positive range (E > 0.3 V), no significant changes in the electrochemical double-layer and Pt-OH/Pt-O formation/reduction peak currents are observed, as compared to the CV obtained in the metal-free 0.5 M H_2SO_4 solution (shown in Figure 3-2a, dash-dotted black curve). The increase in peak current densities in the hydrogen adsorption-desorption region may be associated with the underpotential deposition (UPD) of M^{2+} (i.e., Co^{2+} and Ni^{2+} [37]) on the Pt surface and the subsequent removal of the deposited metal during the anodic potential sweep. As the UPD of M^{2+} is a 2-electron involved process, the resulting current density is higher as compared to the 1-electron hydrogen adsorption-desorption process. The UPD process may kinetically compete with concurrent hydrogen

adsorption, which may result in a partial UPD coverage on the Pt surface.

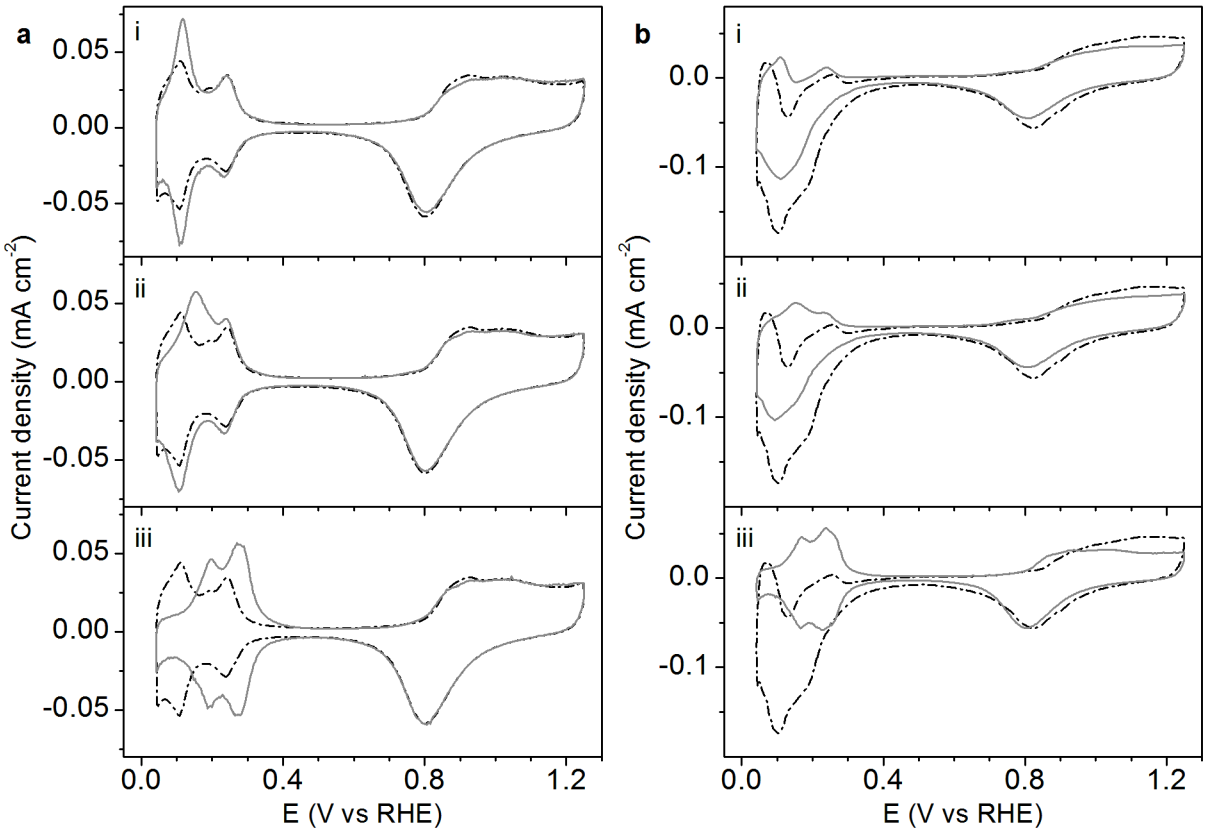

Figure 3-2: a) Cyclic voltammograms of polycrystalline Pt in the metal-free (dash-dotted black curve) and 0.2 M metal sulfates containing (solid gray curve) (i.e., (i) $CoSO_4$, (ii) $NiSO_4$ and (iii) $ZnSO_4$) 0.5 M H_2SO_4 solutions., b) Cyclic voltammograms of polycrystalline Pt in 0.4 M HNO_3 containing (dash-dotted black curve) and 0.2 M metal nitrates containing (solid gray curve) (i.e., (i) $Co(NO_3)_2$, (ii) $Ni(NO_3)_2$, (iii) $Zn(NO_3)_2$) 0.5 M H_2SO_4 solutions. All CVs were obtained at a scan rate of 20 mV s^{-1}.

Figure 3-2a-iii (solid gray curve) shows the CV of Pt in the presence of 0.2 M $ZnSO_4$. The result shows an increase in the cathodic and anodic current densities in the hydrogen adsorption-desorption region, which are only stable up to E= 0.38 V, disappearing at more positive potential range (E > 0.38 V). This increase in current

densities at hydrogen adsorption-desorption region may be associated with the UPD of Zn^{2+} on Pt [38,39]. Although the standard reduction potential of Zn^{2+}/Zn is at −0.76 V, the UPD of Zn^{2+} appeared at ~ 0.38 V in this study (Figure 3-2a-iii). According to the literature, the positive potential shift in the Zn UPD on Pt relative to its standard reduction potential is associated with the work function difference between Pt and Zn [38].

3.3.2.2 Pt Voltammetry in the Presence of Metal Nitrates

In order to further understand the possible influence of counter-anions of metal solution contaminants on the Pt voltammetric properties, additional experiments were performed using metal nitrates solutions. Figure 3-2b (solid gray curves) shows the CVs of Pt obtained in the presence of 0.2 M metal nitrate containing (i.e., (i) $Co(NO_3)_2$, (ii) $Ni(NO_3)_2$ and (iii) $Zn(NO_3)_2$) 0.5 M H_2SO_4 solutions. To better distinguish the effect of nitrate counter-anions on the Pt voltammetric properties, the cyclic voltammetry was performed in the metal-free 0.4 M HNO_3 containing 0.5 M H_2SO_4 solution (shown in Figure 3-2b, dash-dotted black curves). The result shows an increase in the current density during cathodic potential scanning at lower potential range (~ 0.08 - 0.3 V) as well as a slight decrease in Pt-OH/Pt-O formation/reduction current densities at higher potentials (E > 0.8 V), as compared to the cyclic voltammetry obtained in 0.5 M H_2SO_4 solution (shown in Figure 3-2a, dash-dotted black curve). The increase in the cathodic current density at lower potential range (E < 0.3 V) may be associated with the nitrate anion reduction initiated at the potentials of double layer region [40,41]. Further, the

adsorbed species formed during the nitrate anion reduction may partially block the Pt surface, which may result in a slight decrease in Pt-OH/Pt-O formation/reduction current densities.

Figure 3-2b-i (solid gray curve) shows the CV of Pt in the presence of 0.2 M $Co(NO_3)_2$. The results show a decrease in the cathodic current density as well as an increase in the anodic current density at lower potential range (E < 0.3 V) in the presence of cobalt solution as compared to the CV obtained in metal-free 0.4 M HNO_3 solution (shown in Figure 3-2b-i, dash-dotted black curve). The anodic peak current occurs at a potential similar to that observed in the presence of $CoSO_4$, assigned to the removal of Co UPD from the Pt surface. These observations may indicate that the UPD of Co^{2+} may partially occur on the Pt surface at lower potential range, blocking the Pt active sites, which may lower the nitrate anion reduction on Pt surface. A similar voltammogram result is observed in the presence of 0.2 M $Ni(NO_3)_2$ (shown in Figure 3-2b-ii, solid gray curve). In this case, the partial UPD of Ni^{2+} and the subsequent removal of Ni from the Pt surface may be responsible for the decrease in cathodic peak current density and increase in anodic peak current density at lower potential range, respectively. These observations may indicate that the partial UPD of Ni^{2+} on Pt surface may lower the nitrate anion reduction on the Pt surface at lower potential range.

Figure 3-2b-iii (solid gray curve) shows the CV of Pt in the presence of 0.2 M $Zn(NO_3)_2$. The results show two voltammetric peaks at ~ 0.18 and ~ 0.23 V with no cathodic peak current associated with the nitrate anion reduction in the presence of zinc

solution, as compared to the CV obtained in the metal-free 0.4 M HNO_3 solution (shown in Figure 3-2b-iii, dash-dotted black curve). The Pt voltammogram in the presence of $Zn(NO_3)_2$ shows a similar behavior to that of observed in the presence of $ZnSO_4$ (shown in Figure 3-2a-iii, solid gray curve). Based on these observations, it appears that the UPD of Zn^{2+} on Pt surface may occur at lower potential range, blocking the Pt active sites and diminishing the nitrate anion reduction on Pt surface [42].

3.3.3 Effect of Metal Solution Contaminants on the CH_3OH Oxidation Reaction

In order to determine the effect of metal solution contaminants on the Pt electro-catalytic activity during MOR, cyclic voltammetry was performed in Ar-saturated 0.5 M CH_3OH + 0.5 M H_2SO_4 in the absence and presence of various concentrations (i.e., $2x10^{-x}$ M (x=1-7)) of metal salt solutions (i.e., Co, Ni and Zn with sulfate and nitrate as counter-anions). The results showed a minimal change in the MOR activity of Pt in the presence of low concentrations (< $2x10^{-3}$ M) of metal salt solutions. Figure 3-3a shows the anodic linear sweep voltammograms of MOR obtained in the absence and presence of 0.002 M and 0.2 M $NiSO_4$. The results show no significant changes in the MOR onset potential in the presence of nickel solutions. However, the maximum MOR peak current decreases with increasing $NiSO_4$ concentration.

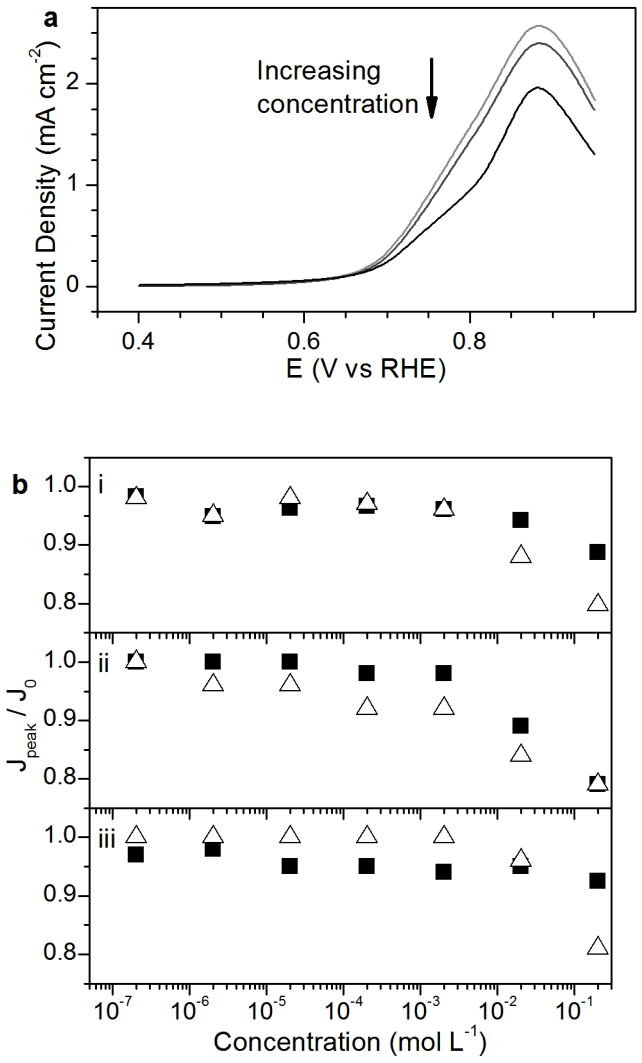

Figure 3-3: a) Anodic linear sweep voltammograms of polycrystalline Pt in the metal-free (light gray curve) and $NiSO_4$ containing (0.002 M (dark gray curve), and 0.2 M (black curve)) 0.5 M H_2SO_4 + 0.5 M CH_3OH solutions at a scan rate of 20 mV s^{-1}., b) Normalized MOR peak current in the presence of various concentrations (i.e., $2x10^{-7}$ M - $2x10^{-1}$ M) of metal containing (i) Co^{2+}, (ii) Ni^{2+}, and (iii) Zn^{2+} (■ = SO_4^{2-}, Δ = NO_3^-) 0.5 M H_2SO_4 + 0.5 M CH_3OH solutions obtained relative to the MOR peak current measured in the metal-free solution.

Figure 3-3b summarizes the normalized MOR peak currents in the presence of various concentrations (i.e., $2x10^{-7}$ -$2x10^{-1}$) of the six metal salt solutions, which were obtained dividing by the MOR peak current obtained in the metal-free solution. As shown, the changes in MOR peak current in the presence of low concentrations (< 10^{-3} M) of metal sulfates and metal nitrates are insignificant (≤ 5 %). However, by increasing the concentration of metal solutions, decrease in MOR peak current is more evident, with a maximum of 22% decrease in MOR peak current in the presence of 0.2 M metal sulfates and metal nitrates.

As presented in Figure 3-3b (black squares), the MOR activity of Pt electro-catalyst decreases in the presence of high concentration of metal sulfates. These results are inconsistent with the changes observed in the Pt voltammetric properties in the presence of metal sulfates (presented in section 3.3.2.1), where the UPD species appeared to be fully removed at E > 0.4 V and no significant changes were observed in Pt-OH/Pt-O formation/reduction peak currents at higher potential range. The decrease in MOR activity in the presence of metal sulfates may be attributed to the (bi)sulfate counter-anion adsorption on the Pt surface [43,44], which may partially inhibit methanol dissociative adsorption. In addition, it can be expected that the hydrated metal cations may not approach the positively charged Pt electrode surface, which may localize at the OHP and play an additional inhibiting role on the MOR activity of Pt.

As presented in Figure 3-3b (open triangles), the MOR activity of Pt electro-catalyst decreases in the presence of high concentration of metal nitrates. These results

are consistent with the changes observed in the Pt voltammetric properties in the presence of metal nitrate solutions (presented in section 3.3.2.2). To better characterize the effect of nitrate counter-anions of metal nitrate solutions on the MOR activity of Pt, the cyclic voltammetry was performed in 0.4 M HNO_3 containing methanol solution (shown in Figure 3-4, light gray curve). The linear sweep voltammograms in the absence and presence of 0.2 M $Ni(NO_3)_2$ solutions are also presented in Figure 3-4. The results show a decrease in MOR peak current in the presence of metal-free HNO_3 solution as compared to the MOR peak current obtained in metal-free H_2SO_4 solution (shown in Figure 3-4, black curve). This result may be attributed to the partial blockage of the Pt surface by adsorbed species formed during the nitrate anion reduction at lower potential range [41]. The linear sweep voltammogram in the presence of $Ni(NO_3)_2$ shows a further decrease in the MOR activity of Pt, as compared to metal-free HNO_3. Based on the results, it appears that the nitrate counter-anion adsorption on the positively charged Pt surface as well as the hydrated metal cations localized at OHP may be responsible for the decrease in MOR activity in the presence of metal nitrate solutions.

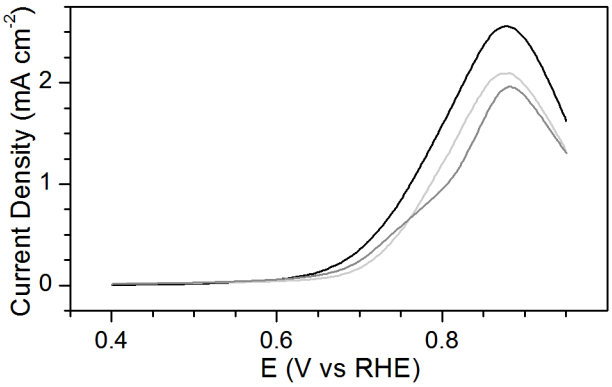

Figure 3-4: Anodic linear sweep voltammograms of polycrystalline Pt in 0.5 M CH_3OH + 0.5 M H_2SO_4 (black curve), 0.4 M HNO_3 containing (light gray curve) and 0.2 M $Ni(NO_3)_2$ containing (gray curve) 0.5 M CH_3OH + 0.5 M H_2SO_4 solution. All CVs were obtained at a scan rate of 20 mV s^{-1}.

3.3.4 Effect of Metal Solution Contaminants on the Pt_xRu_y Electrodes

Based on the results presented thus far, it appears that a combined effect of adsorbed counter-anions and hydrated metal cations (localized at OHP) of metal solution contaminants can impede CH_3OH oxidation on planar Pt electrodes. The relevance of these results is extended to the anode electro-catalyst of DMFCs by introducing high surface area Pt_xRu_y electro-catalysts that are commonly used in DMFC systems. As the fuel cell electro-catalysts may undergo changes (e.g., corrosion of the carbon support) during electrochemical tests [6,45–47], two representative unsupported Pt_xRu_y electro-catalysts were used during this study.

Prior to performing the MOR voltammetry, the cyclic voltammetry of Pt_xRu_y was obtained in Ar-saturated 0.5 M H_2SO_4 solution at a scan rate of 20 mV s^{-1}, shown in

Figure 3-5a (gray curve) and Figure 3-5b. Results show a decrease in the $H_{ads/des}$ peak currents for both Pt_xRu_y voltammograms as compared to the voltammogram of polycrystalline Pt (shown in Figure 3-5a, black curve). This decrease in $H_{ads/des}$ peak currents may be associated with the lower activity of Ru species toward hydrogen adsorption [48]. Furthermore, the Pt_xRu_y voltammograms show an increase in double-layer current due to the formation of ruthenium oxide at this potential range as compared to the voltammogram of polycrystalline Pt.

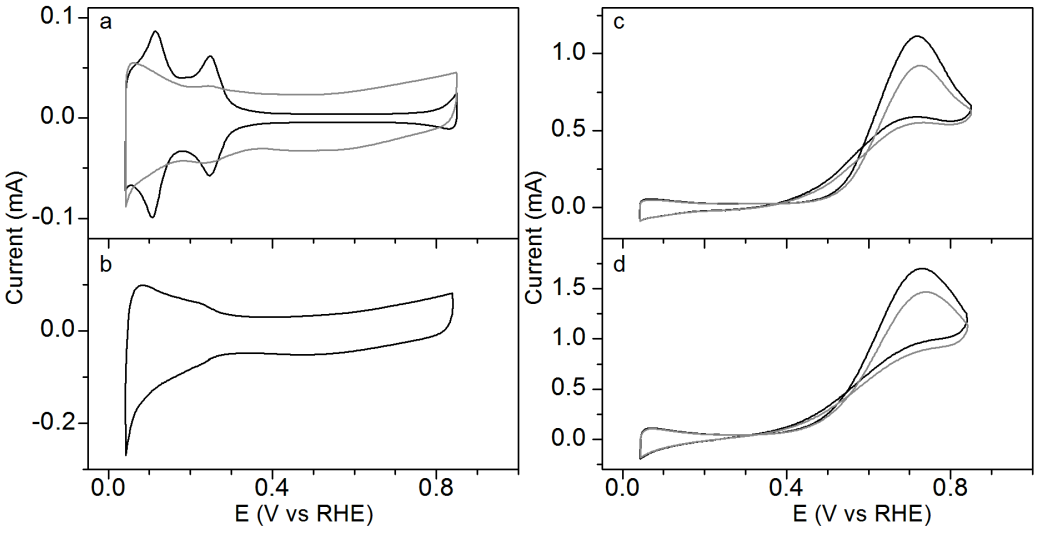

Figure 3-5: Cyclic voltammograms obtained in a) 0.5 M H_2SO_4 on polycrystalline Pt (black curve), spontaneously deposited Pt_xRu_y (gray curve)., b) 0.5 M H_2SO_4 on $Pt_{75}Ru_{25}$ electrode., c) in metal-free (black curve) and 0.2 M $CoSO_4$ containing (gray curve) 0.5 M H_2SO_4 + 0.5 M CH_3OH solutions on spontaneously deposited Pt_xRu_y and (d) in metal-free (black curve) and 0.2 M $CoSO_4$ containing (gray curve) 0.5 M H_2SO_4 + 0.5 M CH_3OH solutions on $Pt_{75}Ru_{25}$ electrode. All CVs were obtained at a scan rate of 20 mV s^{-1}.

To further investigate the effect of metal solution contaminants on Pt_xRu_y catalytic activity during the MOR, cyclic voltammetry was performed in Ar-saturated 0.5 M CH_3OH + 0.5 M H_2SO_4 in the absence and presence of 0.2 M metal (i.e., Co, Ni and Zn) sulfates. Figure 3-5c and Figure 3-5d (black curves) show the MOR voltammograms of Pt_xRu_y electro-catalysts in the metal-free 0.5 M CH_3OH + 0.5 M H_2SO_4 solution. The results shows that the MOR onset potential appears at lower potentials (~ 0.4 V) as compared to the polycrystalline Pt electrodes (~ 0.6 V), shown in Figure 3-1b. These results are in agreement with the results previously reported in the literature and associated with the oxygenated species formation on Ru at lower potential range [49]. Figure 3-5c and Figure 3-5d (gray curves) show the MOR voltammograms of Pt_xRu_y electro-catalysts in the presence of 0.2 M $CoSO_4$ solution. The results show that MOR peak currents decreased in the presence of Co solution. Similar results were obtained in the presence of $NiSO_4$ and $ZnSO_4$ (results not presented to avoid repetition). From these results, it appears that metal solution contaminants (under condition described in this study) can negatively affect high surface area Pt_xRu_y electro-catalysts during the MOR. These results are consistent with the results obtained for the polycrystalline Pt presented in section 3.3.3.

3.3.5 Effect of Metal Solution Contaminants on the O_2 Reduction Reaction

In order to evaluate the effect of metal solution contaminants on the electro-catalytic activity of Pt during the ORR, cyclic voltammetry was performed in O_2-saturated 0.1 M $HClO_4$ solution in the absence and presence of various concentrations (i.e., $2x10^{-x}$

M (x=1-3)) of metal solutions (i.e., Co, Ni and Zn with sulfate and nitrate as counter-anions). In this section, the ORR voltammograms of Pt in the absence and presence of various concentrations of $CoSO_4$ (shown in Figure 3-6a) are selected to present the overall behavior of polycrystalline Pt in the presence of metal solution contaminants during the ORR. Figure 3-6a (black curve) shows a linear potential sweep measured in O_2-saturated metal-free 0.1 M $HClO_4$ solution. As previously reported in the literature [50], the ORR is under activation control at E > 0.9 V, under mixed activation/diffusion control at 0.8 < E < 0.9 V, and is diffusion-limited at E < 0.8 V. The results show that by increasing $CoSO_4$ concentrations, the diffusion-limited current density (J_L) decreases along with a negative potential shift in the half-wave potential ($E_{1/2}$). In this work, $E_{1/2}$ is used as an indicator of the ORR kinetics. Figure 3-6b summarizes the effects of various concentrations (i.e., $2x10^{-x}$ M (x=1-3)) of the six metal salts on the $E_{1/2}$ of the ORR. The overall results show that the measured $E_{1/2}$ decreases by increasing metal salt concentration, indicating a decrease in the ORR rate. In a similar study by Li et al., the effect of $CoSO_4$ on the ORR activity of Pt was investigated [31]. The results showed that the presence of 0.05 M $CoSO_4$ resulted in an increase in H_2O_2 formation on a Pt surface during the ORR by ~ 9 % and decrease in the electron transfer number by a corresponding amount. It was suggested that the decrease in kinetic parameters as well as diffusion-limited current may rationalize the increase in H_2O_2 formation in the presence of high metal solution concentrations. The same general conclusions may be drawn for $CoSO_4$ contaminants used in this study, although their experimental methods (e.g., Koutecky-Levich analyses, RRDE experiments) were somewhat different from those

employed in this study. However, further work is still necessary to examine the effects of Ni^{2+} and Zn^{2+} solution contaminants.

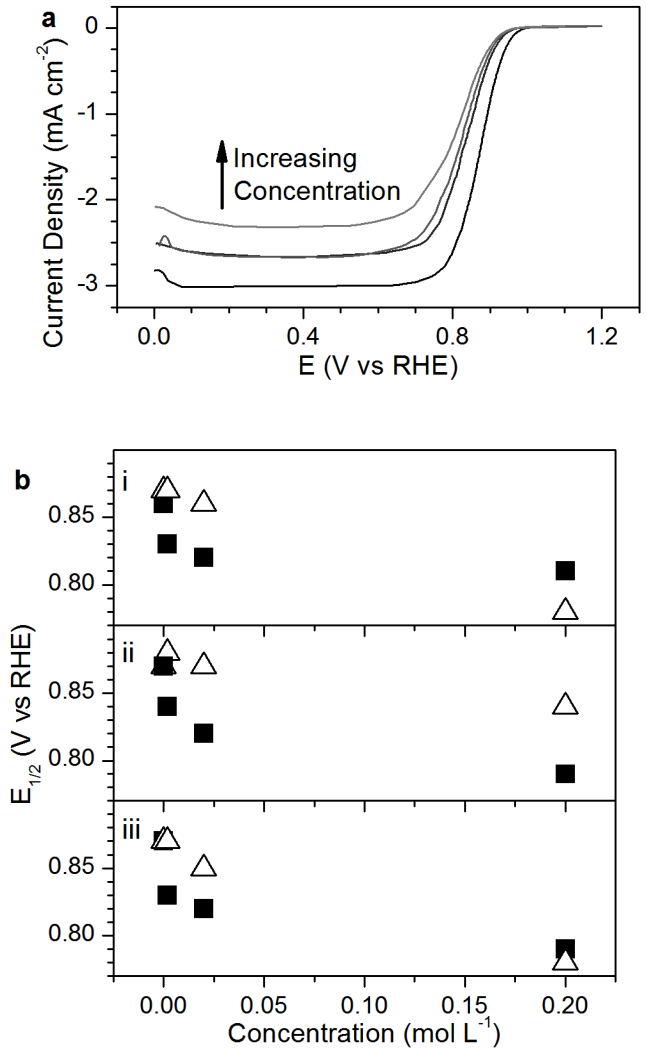

Figure 3-6: a) Linear potential sweeps of polycrystalline Pt RDE in O_2-saturated: metal-free (black curve) and $CoSO_4$ containing: 0.002 M (dark gray curve), 0.02 M (gray), and 0.2 M (light gray curve) 0.1 M $HClO_4$ solutions., b) The half-wave potentials ($E_{1/2}$) from linear potential sweeps measured in 0.1 M $HClO_4$ with various concentrations (i.e., $2x10^{-3}$ M-$2x10^{-1}$ M) of added metal salts: (i) Co^{2+}, (ii) Ni^{2+}, and (iii) Zn^{2+} (■ = SO_4^{2-}, Δ = NO_3^-). All CVs were obtained at the scan rate of 10 mV s^{-1} and ω = 400 rpm.

Although the overall results presented in Figure 3-6 show that the ORR activities decrease in the presence of metal solution contaminants, the specific role played by the metal cations and counter-anions is still unclear. The effect of anion adsorption on the Pt activity during the ORR has been significantly investigated [51,52]. The chloride anion adsorption on the Pt shows an increase in H_2O_2 formation during ORR [51,53]. Moreover, adsorbed (bi)sulfate on Pt electro-catalysts is also shown to negatively affect the ORR kinetics by blocking the initial adsorption of molecular O_2 [30,53]. In order to better distinguish the individual effect of metal cations and counter-anions of metal salts on the Pt activity during the ORR, additional experiments were further conducted using H_2SO_4 and HNO_3 in this study. Results are discussed in details in the following sections.

3.3.5.1 O_2 Reduction Reaction in the Presence of Metal Sulfates

In order to understand the effect of (bi)sulfate counter-anions of metal sulfate solutions on the electro-catalytic activity of Pt during the ORR, the cyclic voltammetry was obtained in O_2-saturated 0.1 M $HClO_4$ solution containing various concentrations of H_2SO_4 (shown in Figure 3-7). Results were further compared with the ORR voltammetry in the presence of $CoSO_4$. Figure 3-7a shows comparative ORR voltammograms obtained in the presence of low concentrations (0.002 M) of $CoSO_4$ and H_2SO_4 solutions. The results show a similar negative effect of both H_2SO_4 and $CoSO_4$ on the ORR current density. This result may indicate that (bi)sulfate counter-anions may be responsible for the decrease in ORR current density (with no significant effect of Co^{2+}) in the presence of low concentration of metal sulfate solution. This change in the ORR activity may be

associated with the (bi)sulfate counter-anions adsorption on the Pt surface [29,30,53], which may block the initial adsorption of O_2, resulting in decreased ORR rate. Figure 3-7b shows the ORR voltammograms of Pt in the presence of 0.2 M $CoSO_4$ and 0.2 M H_2SO_4. The result shows a significant decrease (by about twice) in the ORR current density in the presence of $CoSO_4$ as compared to H_2SO_4. This result shows that (bi)sulfate counter-anions adsorption on the Pt surface may not be the only inhibiting factor for the change in ORR current density, indicating additional negative effect of the hydrated metal cations on the ORR activity. From these results, it appears that a combined effect of adsorbed (bi)sulfate counter-anions and hydrated metal cations may be responsible for the decrease in ORR current density in the presence higher concentration of metal sulfate solutions. This decrease in ORR activity in the presence of metal sulfate solutions may be accompanied by the increased production of H_2O_2 on the Pt surface and the corresponding decrease of the electron transfer number during ORR.

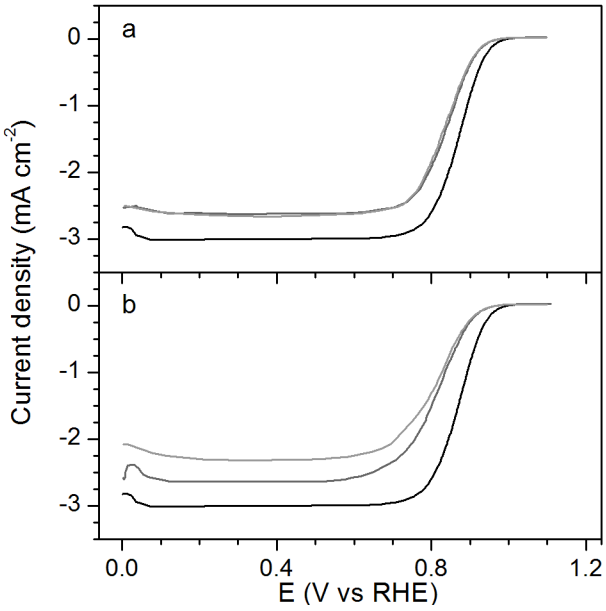

Figure 3-7: Linear potential sweeps of polycrystalline Pt RDE in O_2-saturated: a) metal-free 0.1 M $HClO_4$ (black curve), 0.1 M $HClO_4$ + 0.002 M H_2SO_4 (gray curve), and 0.1 M $HClO_4$ + 0.002 M $CoSO_4$ (light gray curve)., b) metal-free 0.1 M $HClO_4$ (black curve), 0.1 M $HClO_4$ + 0.2 M H_2SO_4 (gray curve), and 0.1 M $HClO_4$ + 0.2 M $CoSO_4$ (light gray curve). All CVs were obtained at the scan rate of 10 mV s^{-1} and ω = 400 rpm.

3.3.5.2 O_2 Reduction Reaction in the Presence of Metal Nitrates

In order to characterize the effect of nitrate counter-anions of metal nitrate solutions on the electro-catalytic activity of Pt during ORR, the cyclic voltammetry was performed in O_2-saturated 0.1 M $HClO_4$ in the presence of various concentrations of HNO_3 (shown in Figure 3-8). Results were further compared with the ORR voltammetry obtained in the presence of $Co(NO_3)_2$. Figure 3-8a shows comparative ORR voltammograms in the presence of 0.004 M HNO_3 and 0.002 M $Co(NO_3)_2$ solutions. The results show that the diffusion-limited current density decreases in the presence of $Co(NO_3)_2$ and HNO_3 solutions. It also appears that the effect of metal-free HNO_3 solution

is slightly smaller than the effect of metal salt solutions. The poisoning effect of nitrate counter-anions on the Pt active sites [54] may be responsible for the decrease in ORR activity in the presence of low concentration of metal nitrate solutions. Figure 3-8b shows the ORR voltammograms obtained in the presence of 0.4 M HNO_3 and 0.2 M $Co(NO_3)_2$ solutions. The results show that the ORR current density decreases more significantly in the presence of metal nitrate as compared to HNO_3 solution. These results indicate that a combined effect of adsorbed nitrate counter-anions and hydrated metal cations may be responsible for the decrease in the ORR current density in the presence of high concentration of metal nitrate solutions.

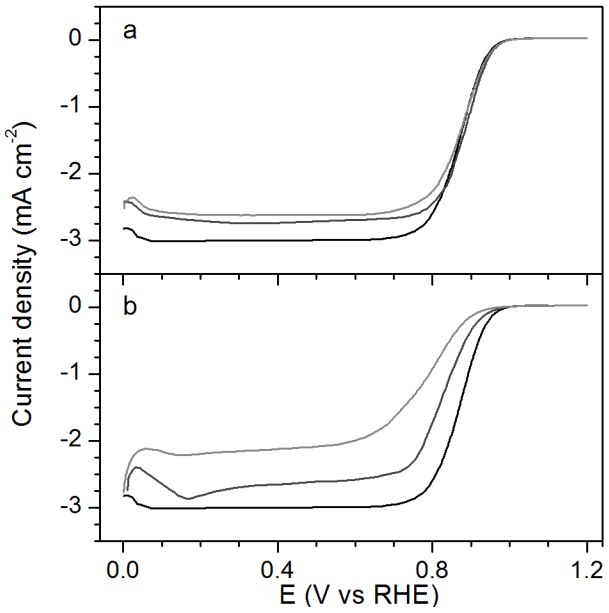

Figure 3-8: Linear potential sweeps of polycrystalline Pt RDE in O_2-saturated: a) metal-free 0.1 M $HClO_4$ (black curve), 0.1 M $HClO_4$ + 0.004 M HNO_3 (gray curve), and 0.1 M $HClO_4$ + 0.002 M $Co(NO_3)_2$ (light gray curve)., b) metal-free 0.1 M $HClO_4$ (black curve), 0.1 M $HClO_4$ + 0.4 M HNO_3 (gray curve), and 0.1 M $HClO_4$ + 0.2 M $Co(NO_3)_2$ (light gray curve). All CVs were obtained at the scan rate of 10 mV s^{-1} and ω = 400 rpm.

3.4 Conclusions

While previous studies have primarily focused on the influence of metal cation contaminants on Nafion membranes and overall performance of fuel cells, the influence of these contaminants on the electro-catalysts activities of fuel cell is not well understood. In this study, the effect of various concentrations (i.e., $2x10^{-x}$ M (x=1-7)) of metal salt solutions (i.e., Co, Ni and Zn with sulfate and nitrate as counter-anions) and their corresponding counter-anions on the voltammetric properties and electro-catalytic activities of polycrystalline Pt during MOR and ORR were systematically investigated. The cyclic voltammetry of polycrystalline Pt obtained in the acidic media showed that the presence of high concentration of metal sulfates and zinc nitrate resulted in the UPD of Co^{2+}, Ni^{2+} and Zn^{2+} on Pt at lower potentials, E < 0.3 V. These deposition processes may compete with concurrent hydrogen adsorption, which can result in a partial UPD layer on the Pt surface. On the other hand, the UPD of Co^{2+} and Ni^{2+} was partially inhibited in the presence of high concentration of metal nitrate (i.e., Co and Ni) solutions due to nitrate counter-anions reduction on the Pt active sites at lower potential ranges.

The effect of various concentrations of metal solutions on the MOR activities of Pt and Pt_xRu_y as well as ORR activity of Pt was further investigated. The results show a decrease in MOR and ORR activities in the presence of higher concentration of metal solutions. In addition, the influence of counter-anion adsorption on the electro-catalytic activity of Pt during MOR and ORR was investigated. Based on the results obtained, it appears that a combined effect of adsorbed counter-anions and the hydrated metal

cations (localized in OHP) may be responsible for the partial blockage of the Pt active sites, resulting in a decrease in the electro-catalytic activity of Pt during the MOR and ORR.

3.5 References

[1] X. Zhao, M. Yin, L. Ma, L. Liang, C. Liu, J. Liao, T. Lu, W. Xing, Recent advances in catalysts for direct methanol fuel cells, Energy Environ. Sci. 4 (2011) 2736. doi:10.1039/c1ee01307f.

[2] E. Antolini, J.R.C. Salgado, E.R. Gonzalez, The stability of Pt-M (M = first row transition metal) alloy catalysts and its effect on the activity in low temperature fuel cells. A literature review and tests on a Pt-Co catalyst, J. Power Sources. 160 (2006) 957–968. doi:10.1016/j.jpowsour.2006.03.006.

[3] S. Chen, H.A. Gasteiger, K. Hayakawa, T. Tada, Y. Shao-Horn, Platinum-Alloy Cathode Catalyst Degradation in Proton Exchange Membrane Fuel Cells: Nanometer-Scale Compositional and Morphological Changes, J. Electrochem. Soc. 157 (2010) A82. doi:10.1149/1.3258275.

[4] B.N. Popov, Stability of platinum based alloy cathode catalysts in PEM fuel cells, 155 (2006) 253–263. doi:10.1016/j.jpowsour.2005.05.011.

[5] A. Heinzel, V.M. Barragán, A review of the state-of-the-art of the methanol crossover in direct methanol fuel cells, J. Power Sources. 84 (1999) 70–74. doi:10.1016/S0378-7753(99)00302-X.

[6] J. Wu, X.Z. Yuan, J.J. Martin, H. Wang, J. Zhang, J. Shen, S. Wu, W. Merida, A review of PEM fuel cell durability: Degradation mechanisms and mitigation strategies, J. Power Sources. 184 (2008) 104–119. doi:10.1016/j.jpowsour.2008.06.006.

[7] J.J. Baschuk, X. Li, Carbon monoxide poisoning of proton exchange membrane fuel cells, Int. J. Energy Res. 25 (2001) 695–713. doi:10.1002/er.713.

[8] R. Mohtadi, W. -k. Lee, S. Cowan, J.W. Van Zee, M. Murthy, Effects of Hydrogen Sulfide on the Performance of a PEMFC, Electrochem. Solid-State Lett. 6 (2003) A272–A274. doi:10.1149/1.1621831.

[9] F. a. Uribe, S. Gottesfeld, T. a. Zawodzinski, Effect of Ammonia as Potential Fuel Impurity on Proton Exchange Membrane Fuel Cell Performance, J. Electrochem. Soc. 149 (2002) A293. doi:10.1149/1.1447221.

[10] D. Yang, J. Ma, L. Xu, M. Wu, H. Wang, The effect of nitrogen oxides in air on the performance of proton exchange membrane fuel cell, Electrochim. Acta. 51 (2006) 4039–4044. doi:10.1016/j.electacta.2005.11.018.

[11] Y. Zhai, G. Bender, S. Dorn, R. Rocheleau, The Multiprocess Degradation of PEMFC Performance Due to Sulfur Dioxide Contamination and Its Recovery, J. Electrochem. Soc. 157 (2010) B20–B26. doi:10.1149/1.3247546.

[12] L. Ma, S. Warthesen, D.A. Shores, Evaluation of materials for bipolar plates in PEMFCs, J. New Mater. Electrochem. Syst. 3 (2000) 221–228. http://www.groupes.polymtl.ca/jnmes/modules/journal/index.php/content0647.html.

[13] J.W. Guo, X.F. Xie, J.H. Wang, Y.M. Shang, Effect of current collector corrosion made from printed circuit board (PCB) on the degradation of self-breathing direct methanol fuel cell stack, Electrochim. Acta. 53 (2008) 3056–3064. doi:10.1016/j.electacta.2007.11.044.

[14] A. Pozio, R.F. Silva, M. De Francesco, L. Giorgi, Nafion degradation in PEFCs from end plate iron contamination, Electrochim. Acta. 48 (2003) 1543–1549. doi:10.1016/S0013-4686(03)00026-4.

[15] H.L. Yeager, A. Steck, Cation and Water Diffusion in Nation Ion Exchange Membranes : Influence of Polymer Structure, J. Electrochem. Soc. 128 (1981) 1880–1884. doi:10.1149/1.2127757.

[16] M. Sulek, J. Adams, S. Kaberline, M. Ricketts, J.R. Waldecker, In situ metal ion contamination and the effects on proton exchange membrane fuel cell performance, J. Power Sources. 196 (2011) 8967–8972. doi:10.1016/j.jpowsour.2011.01.086.

[17] T. Okada, Y. Ayato, M. Yuasa, I. Sekine, The Effect of Impurity Cations on the Transport Characteristics of Perfluorosulfonated Ionomer Membranes, J. Phys. Chem. B. 103 (1999) 3315–3322. doi:10.1021/jp983762d.

[18] H. Li, K. Tsay, H. Wang, J. Shen, S. Wu, J. Zhang, N. Jia, S. Wessel, R. Abouatallah, N. Joos, J. Schrooten, Durability of PEM fuel cell cathode in the presence of Fe3+

and Al3+, J. Power Sources. 195 (2010) 8089–8093. doi:10.1016/j.jpowsour.2010.07.003.

[19] W. Chen, Q. Xin, G. Sun, S. Yang, Z. Zhou, Q. Mao, P. Sun, Effects of dissolved iron and chromium on the performance of direct methanol fuel cell, Electrochim. Acta. 52 (2007) 7115–7120. doi:10.1016/j.electacta.2007.05.047.

[20] M.-J. Yang, K.-Y. Park, K.-B. Kim, H. Cho, H. Choi, J.-Y. Park, Degradation mechanisms and mitigation strategies of metal cations in recycled fuel for direct methanol fuel cell membrane electrode assembly, J. Power Sources. 242 (2013) 646–655. doi:10.1016/j.jpowsour.2013.05.141.

[21] H. Li, J. Gazzarri, K. Tsay, S. Wu, H. Wang, J. Zhang, S. Wessel, R. Abouatallah, N. Joos, J. Schrooten, PEM fuel cell cathode contamination in the presence of cobalt ion (Co 2+), Electrochim. Acta. 55 (2010) 5823–5830. doi:10.1016/j.electacta.2010.05.031.

[22] D. Strmcnik, K. Kodama, D. van der Vliet, J. Greeley, V.R. Stamenkovic, N.M. Marković, The role of non-covalent interactions in electrocatalytic fuel-cell reactions on platinum, Nat. Chem. 1 (2009) 466–472. doi:10.1038/nchem.330.

[23] N. Garcia-araez, V. Climent, P. Rodriguez, J.M. Feliu, Thermodynamic evidence for K+-SO4 2- ion pair formation on Pt(111). New insight into cation specific adsorption, Phys. Chem. Chem. Phys. 12 (2010) 12146–12152. doi:10.1039/c0cp00247j.

[24] V. Climent, N. García-Araez, J.M. Feliu, Influence of alkali cations on the infrared spectra of adsorbed (bi)sulphate on Pt(111) electrodes, Electrochem. Commun. 8 (2006) 1577–1582. doi:10.1016/j.elecom.2006.07.027.

[25] J. Tymoczko, V. Colic, A. Ganassin, W. Schuhmann, A.S. Bandarenka, Influence of the alkali metal cations on the activity of Pt(111) towards model electrocatalytic reactions in acidic sulfuric media, Catal. Today. 244 (2015) 96–102. doi:10.1016/j.cattod.2014.07.007.

[26] N. García, V. Climent, J.M. Orts, J.M. Feliu, A. Aldaz, Effect of pH and alkaline metal cations on the voltammetry of Pt(111) single crystal electrodes in sulfuric acid

solution, ChemPhysChem. 5 (2004) 1221–1227. doi:10.1002/cphc.200400047.

[27] L. Dubau, F. Maillard, M. Chatenet, L. Guetaz, J. André, E. Rossinot, Durability of Pt[sub 3]Co/C Cathodes in a 16 Cell PEMFC Stack: Macro/Microstructural Changes and Degradation Mechanisms, J. Electrochem. Soc. 157 (2010) B1887. doi:10.1149/1.3485104.

[28] L. Dubau, J. Durst, F. Maillard, L. Guétaz, M. Chatenet, J. André, E. Rossinot, Further insights into the durability of Pt3Co/C electrocatalysts: Formation of "hollow" Pt nanoparticles induced by the Kirkendall effect, Electrochim. Acta. 56 (2011) 10658–10667. doi:10.1016/j.electacta.2011.03.073.

[29] F.C. Nart, T. Iwasita, An FTIR study of adsorbed sulfate species on polycrystalline platinum with application of group theory to the problem of band assignment for adsorbed species, J. Electroanal. Chem. 322 (1992) 289–300. doi:10.1016/0022-0728(92)80083-G.

[30] N.M. Markovic, H.A. Gasteiger, P.N. Ross Jr., Oxygen Reduction on Platinum Low-Index Single-Crystal Surfaces in Sulfuric Acid Solution: Rotating Ring-Pt(hkl) Disk Studies, J. Phys. Chem. 99 (1995) 3411–3415. doi:10.1021/j100011a001.

[31] H. Li, K. Tsay, H. Wang, S. Wu, J. Zhang, N. Jia, S. Wessel, R. Abouatallah, N. Joos, J. Schrooten, Effect of Co2+ on oxygen reduction reaction catalyzed by Pt catalyst, and its implications for fuel cell contamination, Electrochim. Acta. 55 (2010) 2622–2628. doi:10.1016/j.electacta.2009.12.037.

[32] X. Jie, Z.G. Shao, B. Yi, The effect of different valency cations on DMFC performance, Electrochem. Commun. 12 (2010) 700–702. doi:10.1016/j.elecom.2010.03.010.

[33] X. Jie, Z.-G. Shao, J. Hou, G. Sun, B. Yi, The influence of sodium ion as a potential fuel impurity on the direct methanol fuel cells, Electrochim. Acta. 55 (2010) 4783–4788. doi:10.1016/j.electacta.2010.03.035.

[34] P.A. Christensen, J.M. Jin, W.F. Lin, A. Hamnett, Identification of CO Adsorbed at Ru and Pt Sites on a Polycrystalline Pt/Ru Electrode and the Observation of Their Oxidation and Free Interchange under Open Circuit Conditions, J. Phys. Chem. B.

108 (2004) 3391–3394. doi:10.1021/jp037520b.

[35] C. Bock, B. MacDougall, Y. LePage, Dependence of CH3OH Oxidation Activity for a Wide Range of PtRu Alloys, J. Electrochem. Soc. 151 (2004) A1269. doi:10.1149/1.1768545.

[36] J. Solla-Gullón, P. Rodríguez, E. Herrero, A. Aldaz, J.M. Feliu, Surface characterization of platinum electrodes., Phys. Chem. Chem. Phys. 10 (2008) 1359–1373. doi:10.1039/b709809j.

[37] M. Chatenet, R. Faure, Y. Soldo-Olivier, Nickel-underpotential deposition on Pt (1 1 0) in sulphate-containing media, J. Electroanal. Chem. 580 (2005) 275–283. doi:10.1016/j.jelechem.2005.03.037.

[38] A. Aramata, M.A. Quaiyyum, W.A. Balais, T. Atoguchi, M. Enyo, UPD of zinc on polycrystalline platinum in various pH solutions, J. Electroanal. Chem. 338 (1992) 367–372. doi:10.1016/0022-0728(92)80436-8.

[39] E. Guerra, G.H. Kelsall, M. Bestetti, D. Dreisinger, K. Wong, K.A.R. Mitchell, D. Bizzotto, Use of Underpotential Deposition for Evaluation of Overpotential Deposition Kinetics of Reactive Metals, J. Electrochem. Soc. 151 (2004) E1–E6. doi:10.1149/1.1631282.

[40] G.E. Dima, G.L. Beltramo, M.T.M. Koper, Nitrate reduction on single-crystal platinum electrodes, Electrochim. Acta. 50 (2005) 4318–4326. doi:10.1016/j.electacta.2005.02.093.

[41] O.A. Petrii, T.Y. Safonova, Electroreduction of nitrate and nitrite anions on platinum metals: A model process for elucidating the nature of the passivation by hydrogen adsorption, J. Electroanal. Chem. 331 (1992) 897–912. doi:10.1016/0022-0728(92)85013-S.

[42] J. Yang, F. Calle-Vallejo, M. Duca, M.T.M. Koper, Electrocatalytic reduction of nitrate on a Pt electrode modified by p-block metal adatoms in acid solution, ChemCatChem. 5 (2013) 1773–1783. doi:10.1002/cctc.201300075.

[43] E.A. Batista, G.R.P. Malpass, A.J. Motheo, T. Iwasita, New mechanistic aspects of methanol oxidation, J. Electroanal. Chem. 571 (2004) 273–282.

doi:10.1016/j.jelechem.2004.05.016.

[44] E.A. Batista, G.R.P. Malpass, A.J. Motheo, T. Iwasita, New insight into the pathways of methanol oxidation, Electrochem. Commun. 5 (2003) 843–846. doi:10.1016/j.elecom.2003.08.010.

[45] J. Wang, G. Yin, Y. Shao, S. Zhang, Z. Wang, Y. Gao, Effect of carbon black support corrosion on the durability of Pt/C catalyst, J. Power Sources. 171 (2007) 331–339. doi:10.1016/j.jpowsour.2007.06.084.

[46] J.P. Meyers, J.E. Mcgrath, R. Borup, J. Meyers, B. Pivovar, Y.S. Kim, R. Mukundan, N. Garland, D. Myers, M. Wilson, F. Garzon, D. Wood, P. Zelenay, K. More, K. Stroh, T. Zawodzinski, X.J. Boncella, J.E. Mcgrath, O.M. Inaba, K. Miyatake, M. Hori, K. Ota, Z. Ogumi, S. Miyata, A. Nishikata, Z. Siroma, Y. Uchimoto, Scientific Aspects of Polymer Electrolyte Fuel Cell Durability and Degradation . Chemical Scientific Aspects of Polymer Electrolyte Fuel Cell Durability and Degradation, Chem. Rev. 107 (2007) 3904–3951. doi:10.1021/cr050182l.

[47] L.M. Roen, C.H. Paik, T.D. Jarvi, Electrocatalytic Corrosion of Carbon Support in PEMFC Cathodes, Electrochem. Solid-State Lett. 7 (2004) A19–A22. doi:10.1149/1.1630412.

[48] H.A. Gasteiger, N.M. Markovic, P.N. Ross Jr., H2 and CO electrooxidation on well-characterized Pt, Ru, and Pt-Ru. 1. Rotating disk electrode studies of the pure gases including temperature effects, J. Phys. Chem. 99 (1995) 8290–8301. doi:10.1021/j100020a063.

[49] M. Watanabe, S. Motoo, Electrocatalysis by ad-atoms part II. Enhancement of the oxidation of methanol on platinum by ruthenium ad-atoms, J. Electroanal. Chem. 60 (1975) 267–273.

[50] U.A. Paulus, A. Wokaun, G.G. Scherer, T.J. Schmidt, V. Stamenkovic, N.M. Markovic, P.N. Ross, Oxygen reduction on high surface area Pt-based alloy catalysts in comparison to well defined smooth bulk alloy electrodes, Electrochim. Acta. 47 (2002) 3787–3798. doi:10.1016/S0013-4686(02)00349-3.

[51] V. Stamenkovic, N.M. Markovic, P.N. Ross, Structure-relationships in

electrocatalysis: Oxygen reduction and hydrogen oxidation reactions on Pt(111) and Pt(100) in solutions containing chloride ions, J. Electroanal. Chem. 500 (2001) 44–51. doi:10.1016/S0022-0728(00)00352-1.

[52] T.J. Schmidt, U. a. Paulus, H. a. Gasteiger, R.J. Behm, The oxygen reduction reaction on a Pt/carbon fuel cell catalyst in the presence of chloride anions, J. Electroanal. Chem. 508 (2001) 41–47. doi:10.1016/S0022-0728(01)00499-5.

[53] N.M. Markovic, T.J. Schmidt, V. Stamenkovic, P.N. Ross, Oxygen Reduction Reaction on Pt and Pt Bimetallic Surfaces: A Selective Review, Fuel Cells. 1 (2001) 105–116. doi:10.1002/1615-6854(200107)1:2<105::AID-FUCE105>3.0.CO;2-9.

[54] K.. Nakata, Y.. Kayama, K.. Shimazu, A.. Yamakata, S.. Ye, M.. Osawa, Surface-enhanced infrared absorption spectroscopic studies of adsorbed nitrate, nitric oxide, and related compounds 2: Nitrate ion adsorption at a platinum electrode, Langmuir. 24 (2008) 4358–4363. doi:10.1021/la703476m.

4. Analysis of Ni Solution Contaminants on Nafion-coated and Bare Pt Electrodes during Methanol Oxidation Reaction

Abstract

Understanding the influence of metal contaminants on the electro-catalyst activities of direct methanol fuel cell (DMFC) is critical in the enhancement of this technology. In this study, the effect of Ni solution contaminant on the methanol oxidation reaction (MOR) activity of Nafion-coated and bare Pt electrodes was examined using cyclic voltammetry and electrochemical impedance spectroscopy (EIS). The background voltammetry results showed a significant decrease in the voltammetric properties of bare Pt electrode compared to Nafion-coated Pt electrode after Ni solution exposure. The MOR voltammetry was further obtained. The results showed a similar behavior after Ni solution exposure of both electrodes, where only a slightly higher decrease in MOR activity is observed for the Ni exposed bare Pt electrode as compared to Ni exposed Nafion-coated Pt electrode. Furthermore, the EIS measurement was conducted at various potential ranges (0.38 – 0.78 V). The results showed that the charge transfer resistance (R_{ct}) of the CO_{ads} oxidation reaction significantly increases in the presence of Ni exposed bare Pt electrode, which may be attributed to the slow H_2O dissociative-adsorption. Based on these results, it appears that the presence of Nafion-ionomer film may play as a barrier and slow down the access of Ni solution contaminants to the Pt catalyst active sites. The recovery tests further revealed some degree of recovery for both Ni exposed electrodes. However, a higher degree of recovery is observed for the Ni

exposed Nafion-coated Pt electrode.

4.1 Introduction

The direct methanol fuel cell (DMFC) is a promising energy conversion device due to its high energy density, efficiency, easy handling and distribution of liquid fuel [1]. However, the commercial deployment of DMFCs has been limited due to the slow kinetics of the methanol oxidation reaction (MOR), methanol crossover [2-4], fuel cell component degradation and cell contamination [5-8]. Contaminants such as Na^{+}, Cr^{3+}, Co^{2+}, Ni^{2+}, Cu^{2+} can be introduced to the fuel cell system through the degradation of bipolar plates/electro-catalyst layers, resulting in a degradation in the fuel cell performance [9–15].

The degradation effects of metal contaminants on the Nafion membrane properties and overall fuel cell performance have been significantly focused on previous studies [16-20]. Yang et al. studied the effect of various metal contaminants (i.e., Ni^{2+}, Fe^{3+}, Al^{3+}, and Cr^{3+}) on the membrane electrode assembly (MEA) of DMFCs [21]. The results showed that the degradation of DMFC performance increased as the concentration of metal solution contaminants increased. In a study by Chen et al., the effect of Fe^{3+} and Cr^{3+} in the anode feed stream on the DMFC performance was investigated [22]. It was suggested that decreases in the electrochemical surface area (ECSA) of the anode catalyst and proton conductivity of the Nafion membrane in the presence of Fe^{3+} and Cr^{3+}, respectively, are responsible for the decrease in the DMFC performance.

Despite its importance, the effect of metal contaminants on the cathode and anode electro-catalyst activities of fuel cell is not well understood. The effect of Co^{2+} and

Al^{3+} on the oxygen reduction reaction (ORR) activity of Pt was studies by Li et al. [23,24]. The results showed a change in ORR mechanism in the presence of metal solution contaminants. Durst et al. also studied the effect of various concentrations of Co^{2+} solution on the ORR activity of Pt/C catalyst [25]. The result showed a decrease in ORR activity as the concentration of Co^{2+} solution increased. As discussed in chapter 3, the effect of various concentrations of Co^{2+}, Ni^{2+} and Zn^{2+} solutions on the MOR and ORR activities on the polycrystalline Pt was investigated. The results showed a decrease in MOR and ORR activities in the presence of high concentrations of metal solutions. It was suggested that a combined effect of metal cations and counter-anions may be responsible for the decrease in electro-catalytic activities of Pt.

The anode electro-catalyst layer typically used in a DMFC system consists of carbon supported Pt-Ru catalyst and a Nafion ionomer, each of which may be affected in the presence of metal solution contaminants. The primary objective of this work is to understand the effect of Ni solution contaminants on the activity and mechanism of MOR on the Nafion-coated polycrystalline Pt and bare polycrystalline Pt electrodes. Nickel is chosen due to a higher negative effect on the MOR activity relative to other metal cation contaminants (i.e., Co^{2+}, Zn^{2+}, Al^{3+}, Fe^{2+}, Cr^{3+}) [21]. The presence of Ni in DMFC system due to the anode electro-catalyst dissolution was also previously suggested as a source of contaminant by Alia et al. [26].

4.2 Experimental Methods

4.2.1 Electrode Preparation

a) Bare Polycrystalline Pt Electrode

During this study, a polycrystalline Pt disk electrode (99.99 %, 0.5 cm diameter, embedded in Teflon, Pine Instruments) was employed as the working electrode. This electrode was used due to its simple structure, and in order to avoid the complications that arise when using bimetallic or carbon-supported catalysts.

b) Nafion-coated Polycrystalline Pt Electrode

Nafion-coated Pt electrodes were prepared by applying 10 µL of Nafion (Sigma-Aldrich- 5 wt.% Nafion in lower alcohols) onto an electrochemically cleaned (described in section 4.2.3) polycrystalline Pt disk surface. Then, a glass vial was placed over the prepared electrode to avoid rapid evaporation of the alcohol in the Nafion solution, thus allowing for the preparation of a smooth and uniform Nafion film. The Nafion coated electrode was left to dry at room temperature for approximately 24 hours. The average thickness of the Nafion film was estimated to be approximately 12 µm, according to the volume and density of the Nafion solution. This Nafion film thickness exceeds the typical ionomer content used in fuel cell electro-catalysts, however, this thickness was found to be essential to guarantee the adhesion of the Nafion film to the Pt surface during the experiments carried out in this work. Nafion film with similar thickness was also prepared in previous studies [27,28].

c) Preparation of Ni Exposed Electrodes

Nickel solutions were prepared using $NiSO_4$ (Alfa Aesar, 99%) dissolved in 0.5 M H_2SO_4 (Fisher Scientific, ACS grade, 98%) to reach a 0.2 M Ni solution concentration. This concentration was selected to allow the evaluation of the contaminant effect on the MOR activity within a reasonable experimental time frame. This approach was commonly used as a practical procedure for such investigations [10,29,30].

To prepare Ni exposed Nafion-coated and bare Pt electrodes, the electrochemically cleaned electrode was immersed in 0.2 M $NiSO_4$ + 0.5 M H_2SO_4 for approximately 24 hours at open circuit potential. This duration was chosen to allow the Ni solution contaminants to diffuse through the Nafion film and interact with the sulfonate sites of Nafion-ionomer.

4.2.2 Electrochemical Cell

Electrochemical measurements were carried out in a two-compartment glass cell. The working electrode and a high surface area Pt mesh counter electrode were placed in the working electrode compartment. A saturated calomel electrode (SCE) was used as the reference electrode and placed in the reference electrode compartment, which was connected to the working compartment via a Luggin capillary with the tip positioned close to the working electrode. All potentials reported in this study are referred to a reversible hydrogen electrode (RHE). Current densities are normalized by dividing the measured current by the geometric surface area of working electrode.

4.2.3 Electrochemical Measurements

The electrolyte solution used in this study was 0.5 M H_2SO_4, which was prepared by diluting measured amount of H_2SO_4 with high purity water (Millipore Milli-Q, 18.2 MΩ cm). All electrolyte solutions were purged with argon (purity grade 5.0) for a minimum of 30 minutes to remove dissolved oxygen before each electrochemical measurement.

Prior to each experiment, the bare Pt electrodes were cleaned electrochemically by cycling the potential between 0.08 and 1.48 V at 100 mV s^{-1} in 0.5 M H_2SO_4 for at least 30 cycles in order to remove the potential impurities from Pt active sites. To clean Nafion-coated Pt electrodes, the potential was cycled between 0.08 and 1.28 V at 100 mV s^{-1} in 0.5 M H_2SO_4 till stable appearances of cyclic voltammogram (CV) were obtained. The upper potential and the number of cycles were limited in order to avoid the detachment of the Nafion film.

The effect of the Ni solution contaminant on the voltammetric properties of Nafion-coated and bare Pt electrodes was investigated by conducting cyclic voltammetry on the unexposed and Ni exposed electrodes in metal-free Ar-saturated 0.5M H_2SO_4. In this case CVs were collected between 0.08 and 1.28 V at 20 mV s^{-1}.

The effect of Ni solution contaminants on the MOR activities of Nafion-coated and bare Pt electrodes was further investigated. The MOR voltammograms were collected on unexposed electrodes in 0.5 M CH_3OH (Fisher Scientific, 99.9%) + 0.5 M H_2SO_4. Furthermore, the MOR voltammograms of Ni exposed Nafion-coated and bare Pt electrodes were obtained in 0.2 M nickel sulfate containing 0.5 M CH_3OH + 0.5 M H_2SO_4 solutions. The MOR voltammetries were conducted between 0.08 and 1 V at 20 mV s^{-1}.

All voltammetric measurements were performed using a Solartron Analytical 1285 potentiostat controlled with Corrware software (v. 3.1c, Scribner Associates Inc.).

Electrochemical impedance spectroscopy (EIS) measurements were also performed on the unexposed and Ni exposed electrodes in metal-free and 0.2 M nickel sulfate containing 0.5 M CH_3OH + 0.5 M H_2SO_4 solutions, respectively. Prior to each EIS measurement, the electrode was held at a specific potential, (E= 0.38 - 0.78 V), for 30 minutes to obtain a quasi-steady state current. Then, the EIS was performed by sweeping the frequency from 100 kHz to 0.1 Hz at the specific constant electrode potential with a root mean square (rms) amplitude of 10 mV. EIS measurements were conducted with a Solartron 1260 frequency response analyzer and Solartron 1285 potentiostat controlled by ZPlot (v. 3.3c, Scribner Associates Inc.). The impedance data were fitted to equivalent circuits using ZView software (Scribner Associates Inc). Throughout all experiments, the electrochemical cell was placed in a Faraday cage, in order to reduce any potential electrical noise and/or vibration.

4.3 Results and Discussion

4.3.1 Cyclic Voltammetries of Unexposed and Ni Exposed Bare Pt Electrodes

In order to better understand the effect of Ni solution contaminants on the voltammetric properties of bare Pt electrode, cyclic voltammetry was conducted on the unexposed and Ni exposed bare Pt electrodes. Figure 4-1a (black curve) shows the CV of the unexposed bare Pt electrode. The result exhibits an expected characteristic behavior of polycrystalline Pt in 0.5 M H_2SO_4, where the hydrogen adsorption/desorption ($H_{ads/des}$)

reaction takes place between ~ 0.08 and 0.28 V followed by the Pt-oxide (Pt-OH/O) formation/reduction at more positive potentials (~ 0.78 - 1.28 V). The CV of Ni exposed bare Pt electrode is presented in Figure 4-1a (gray curve). The result shows a significant decrease in the $H_{ads/des}$ peak current density, as well as a positive shift in the onset potential of Pt-oxide formation for the Ni exposed bare Pt electrode as compared to the unexposed condition. The corresponding electrochemical surface area (ECSA) of both electrodes was also calculated, assuming a correlation value of 210 μC cm_{Pt}^{-2} (the charge associated with a monolayer formation of adsorbed-hydrogen on a polycrystalline Pt surface). The results showed a 88% decrease in the ECSA of bare Pt electrode after Ni solution exposure. In a separate experiment, cyclic voltammetry of bare Pt was conducted immediately after exposure to H_2SO_4 solution. Results did not show any major change in $H_{ads/des}$ and Pt-OH/O formation/reduction peak currents, indicating insignificant effect of counter-anion adsorption on the bare Pt electrode.

To further investigate the nature of adsorbed species on the Pt active sites after exposure to the Ni solution, exposed electrodes were analyzed using x-ray photoelectron spectroscopy (XPS). The XPS analysis, however, only revealed the presence of $NiSO_4$ on the Pt surface and failed to detect any further details regarding to the adsorbed species. The XPS result is presented in Appendix. The detection of $NiSO_4$ by XPS is likely the result of carried over contaminant from the Ni stock solution, which may not allow distinguishing whether an adsorbed Ni-species is present on the Pt surface.

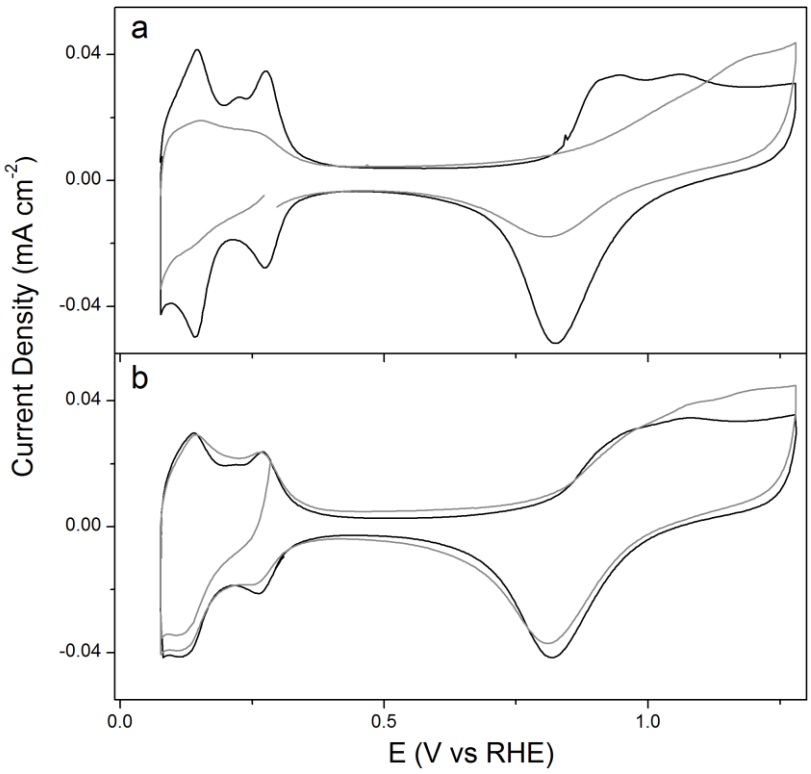

Figure 4-1: Cyclic voltammograms of: a) unexposed bare Pt electrode (black curve) and Ni exposed bare Pt electrode (gray curve)., b) unexposed Nafion-coated Pt electrode (black curve) and Ni exposed Nafion-coated Pt electrode (gray curve). All CVs were obtained at a scan rate of 20 mV s^{-1}.

4.3.2 Cyclic Voltammetries of Unexposed and Ni Exposed Nafion-coated Pt Electrodes

In order to evaluate the influence of Ni solution contaminants on the voltammetric properties of Nafion-coated Pt, cyclic voltammetry was conducted on the unexposed and Ni exposed Nafion-coated Pt electrodes. Figure 4-1b (black curve) shows the CV of unexposed Nafion-coated Pt electrode. As shown, the $H_{ads/des}$ and Pt-OH/O formation/reduction peak currents are suppressed in the presence of Nafion-ionomer as compared to the CV characteristics of bare Pt electrode, shown in Figure 4-1a (black curve). The ECSA of unexposed Nafion-coated Pt electrode was further calculated. The result showed a 15% decrease in the ECSA in the presence of Nafion-ionomer film as compared to the ECSA of unexposed bare Pt electrode. This result may be associated with the hydrophobic backbone of Nafion-ionomer, which may block Pt active sites, resulting in a decrease in the active surface area [28,31,32].

Figure 4-1b (gray curve) shows the CV of the Ni exposed Nafion-coated Pt electrode. The result shows a decrease in the H_{ads} peak current during the cathodic potential scan between 0.08 and 0.28 V and no significant change in the H_{des} peak current during the anodic potential scan. Further, no significant change in the onset potential of the Pt-oxide formation is observed for the Ni exposed electrode as compared to the unexposed condition (both occurring at ~ 0.6 - 0.7 V). However, a higher oxidative current is observed in the Pt-oxide formation region between 1 and 1.28 V for the Ni exposed Nafion-coated Pt electrode. Okada et al. reported no significant change in the voltammetric properties of the Na^+ exposed Nafion coated Pt electrode as

compared to unexposed condition [27]. Subbaraman et al. also reported no significant changes in $H_{ads/des}$ peak current for the cation-exchanged (e.g., K^+ and Mg^{2+}) Nafion-coated Pt(111) electrode as compared to the unexposed conditions [33].

Based on the CVs presented in section 4.3.1 and section 4.3.2, it appears that the presence of Nafion-ionomer film on the Pt electrode may partially block the Pt active sites through its hydrophobic domains. This may hinder the hydrogen adsorption on the Pt in the Nafion-coated electrode, as compared to the bare Pt electrode. The results also reveal a significant poisoning effect of Ni solution contaminants on the bare Pt electrode, contrary to the observations for the Nafion-coated Pt electrode, where only minor changes in the voltammetric properties were observed. This indicates that the Nafion-ionomer may act as a barrier for Ni solution contaminants, reducing their impact on the Pt active sites.

4.3.3 MOR Voltammetries of Unexposed and Ni Exposed Bare Pt Electrodes

In order to understand the effect of Ni solution contaminants on the Pt electro-catalytic activity during the MOR, cyclic voltammetry was conducted on the unexposed and Ni exposed bare Pt electrodes. Figure 4-2a (black curve) shows a typical MOR voltammogram of unexposed bare Pt electrode, where the MOR onset potential appears at ~ 0.5 - 0.6 V, followed by a fully developed oxidation peak at 0.86 V. At more positive potentials (E > 0.86 V), a decrease in MOR current is observed due to the increase in Pt-oxide formation, leading to a passivation and loss in Pt activity [34,35]. Figure 4-2a (gray curve) shows the MOR voltammogram of Ni exposed bare Pt electrode. The result shows

a positive shift in the MOR onset potential, followed by a significant drop in the MOR anodic peak current density (89%), as compared to the unexposed condition. This result is consistent with the changes observed in the voltammetric property of bare Pt electrode after Ni solution exposure, presented in section 4.3.1. The changes observed in the background and MOR voltammetries indicate that Ni solution contaminants may partially block the Pt active sites, resulting in a significant decrease in Pt electro-catalytic activity.

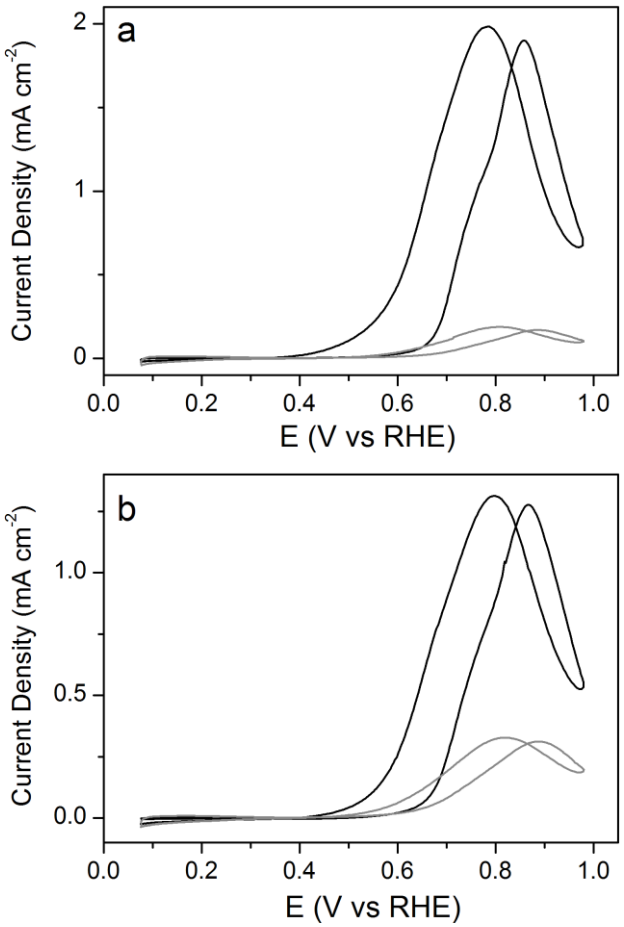

Figure 4-2: MOR voltammograms of: a) unexposed bare Pt electrode (black curve) and Ni exposed bare Pt electrode (gray curve)., b) unexposed Nafion-coated Pt electrode (black curve) and Ni exposed Nafion-coated Pt electrode (gray curve). All CVs were obtained at a scan rate of 20 mV s^{-1}.

4.3.4 MOR Voltammetries of Unexposed and Ni Exposed Nafion-coated Pt Electrodes

To further understand the effect of Ni solution contaminants on the Nafion-coated Pt electrode activity during the MOR, cyclic voltammetry was conducted on the unexposed and Ni exposed Nafion-coated Pt electrodes. Figure 4-2b (black curve) shows

the MOR voltammogram of the unexposed Nafion-coated Pt electrode. The result shows a slight positive shift in the MOR onset potential, as well as a decrease in the MOR anodic peak current as compared to the MOR voltammogram of the unexposed bare Pt electrode, shown in Figure 4-2a (black curve). This behavior may be attributed to the hydrophobic property of Nafion-ionomer, which may partially block the Pt active sites, resulting in a decrease in the Pt electro-catalytic activity during the MOR. Similar results were previously reported in the literature, showing a decrease in the MOR activity of electro-catalysts with higher Nafion-ionomer contents [36,37]. It is also suggested that the presence of Nafion-ionomer may result in CO_2 (a MOR product) entrapment within the hydrophilic part of Nafion-ionomer, blocking the microchannels pathways within its structure, leading to a decrease in CH_3OH access to the Pt active sites [38].

Figure 4-2b (gray curve) shows the MOR voltammogram of the Ni exposed Nafion-coated Pt electrode. The result shows that the MOR peak current density diminishes after exposure of the electrode to the Ni solution. This decrease in the MOR activity is inconsistent with the background voltammetry results (presented in section 4.3.2), where no significant change in the voltammetric property of Ni exposed Nafion-coated Pt electrode was observed. In a similar work, Okada et al. studied the effect of Na^+ solution contaminants on Nafion-coated Pt electrodes during the ORR [27]. The results showed a significant drop in the ORR rate for the Na^+ contaminated Nafion-coated Pt electrode, while, no significant changes in the background cyclic voltammogram was reported. It was suggested that the changes in the polymer flexibility and electric double layer at the platinum-ionomer interface may lead to the drop in the ORR activity after

Na^+ solution exposure of Nafion-coated Pt electrodes.

Based on the MOR voltammetries presented in the sections 4.3.3 and 4.3.4, it appears that Ni solution contaminants have a significant poisoning effect on both Nafion-coated and bare Pt electrodes. However, this decrease in MOR activity is slightly higher on the Ni exposed bare Pt electrode as compared to Ni exposed Nafion-coated Pt electrode.

4.3.5 Electrochemical Impedance Spectroscopy (EIS) of CH_3OH Oxidation Reaction

As it is well established, MOR is a multistep electrochemical reaction with different rate constants [39-43]. In this study, electrochemical impedance spectroscopy (EIS) is used to separate the multistep reactions over a wide frequency range. The MOR impedance spectra (referred to as Nyquist plot) show different patterns at different potential ranges, where a mechanistic change in the MOR may occur [44-46]. In order to better understand the mechanistic aspect of MOR by the EIS measurements, a simple reaction pathway is modeled as summarized bellow:

$$Pt + CH_3OH \rightarrow Pt - CO_{ads} + 4H^+ + 4e^- \qquad \text{Equation 4-1}$$

$$H_2O + Pt \rightarrow Pt - OH_{ads} + H^+ + e^- \qquad \text{Equation 4-2}$$

$$Pt - CO_{ads} + Pt - OH_{ads} \rightarrow CO_2 + 2Pt + H^+ + e^- \qquad \text{Equation 4-3}$$

CH_3OH initially adsorbs on the Pt surface and subsequently undergoes several dehydrogenation steps, resulting in the formation of adsorbed carbon monoxide (CO_{ads})

(Equation 4-1). Water dissociative adsorption further occurs on the Pt surface to form oxygenated species (e.g., adsorbed hydroxyl (OH_{ads})) (Equation 4-2). Furthermore, the formed OH_{ads} oxidizes the CO_{ads} to CO_2, resulting in a decrease in CO_{ads} coverage (Equation 4-3) [47–49].

In this study, the EIS measurements were conducted within a potential range of 0.38 and 0.78 V. The equivalent circuit models used to analyze the Nyquist plots at each potential as well as a detailed schematic of MOR on the unexposed bare Pt electrode are summarized in Figure 4-3. The following sections present the EIS observations for unexposed and Ni exposed Nafion-coated and bare Pt electrodes at different potential ranges.

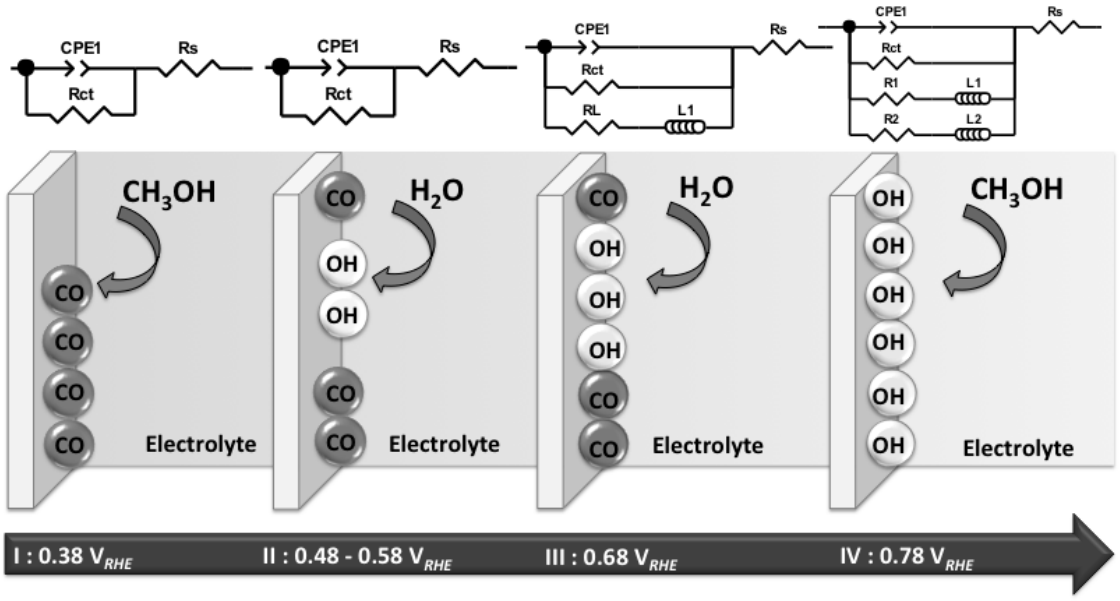

Figure 4-3: Schematic representation of the CH_3OH oxidation reaction on the unexposed bare Pt electrode at different potentials (E= 0.38 - 0.78 V) with the corresponding equivalent circuit models.

EIS at 0.38 V_{RHE}:

Dissociative adsorption and dehydrogenation of CH_3OH on the Pt surface (as shown in Equation 4-1) is the main reaction taking place at 0.38 V. The slow methanol dehydrogenation reaction results in the formation of CO_{ads}, which blocks the Pt surface from further methanol adsorption [47,50]. Figure 4-4 shows the Nyquist plots of unexposed and Ni exposed Nafion-coated and bare Pt electrodes at 0.38 V. A large arc with a deviation from straight line in the first quadrant of the Nyquist plot is observed in all cases, which may be associated with the slow methanol adsorption-dehydrogenation reaction at this potential [46,51]. The Nyquist plots of Ni exposed electrodes show a similar arc behavior with a slight increase in the arc diameter as compared to unexposed electrodes.

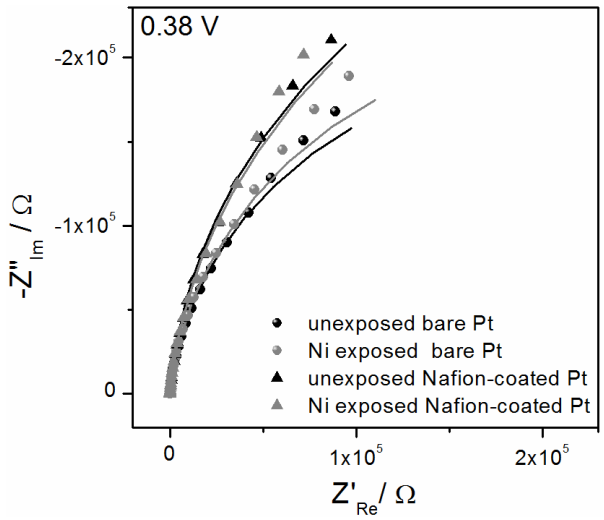

Figure 4-4: Nyquist plots of unexposed and Ni exposed electrodes obtained at 0.38 V.

In order to characterize the Nyquist plots at this potential, the equivalent circuit shown in Figure 4-3, region I is used to fit the data [52]. In this circuit, R_s represents the solution resistance between the working electrode and the reference electrode. The constant phase element (CPE) is used to represent the double layer capacitance. R_{ct} is the charge transfer resistance associated with the slow methanol adsorption-dehydrogenation reaction to CO_{ads}. As expected from the Nyquist plots and confirmed by fitted data shown in Table 4-1, the R_{ct} values of both electrodes slightly increase after Ni solution exposure relative to the unexposed electrodes. Based on this observation, it appears that Ni solution contaminants may have an insignificant inhibiting role on the slow methanol adsorption-dehydrogenation on the Pt active sites at this potential.

Table 4-1. Fitting parameters obtained from the Nyquist plot at E = 0.38 V shown in Figure 4-4.

Sample	R_s (Ω)	CPE1-T (F)	CPE1-P (F)	R_{ct} (Ω)
unexposed bare Pt	4.7	7.13E-06	0.94	4.18E05
Ni exposed bare Pt	5.1	6.36E-06	0.94	4.55E05
unexposed Nafion-coated Pt	5.0	6.63E-06	0.95	6.35E05
Ni exposed Nafion-coated Pt	5.3	6.61E-06	0.94	6.66E05

EIS at 0.48-0.58 V_{RHE}:

By increasing the potential to 0.48 - 0.58 V, the H_2O dissociative-adsorption rate starts to increase, resulting in the formation of oxygenated species, i.e., OH_{ads}, on the Pt surface (as shown in Equation 4-2). This can subsequently enhance the oxidative removal of CO_{ads}, as the presence of oxygenated species is essential in the oxidation of CO_{ads} to CO_2 [45]. The increase in the CO_{ads} oxidation rate results in a decrease in the arc diameter (semi circle appearance) of Nyquist plots for the unexposed bare Pt electrodes, shown in Figure 4-5 (black circle).

As shown in Figure 4-5 (black triangle), the arc diameter of Nyquist plots (at E= 0.48 and 0.58 V) is larger for the unexposed Nafion-coated Pt electrodes compared to the unexposed bare Pt electrodes. Moreover, the Nyquist plots of both Ni exposed electrodes show an increase in the arc diameters as compared to the corresponding unexposed electrodes. However, this increase is more significant for the Ni exposed bare Pt electrode compared to the Ni exposed Nafion-coated Pt electrode.

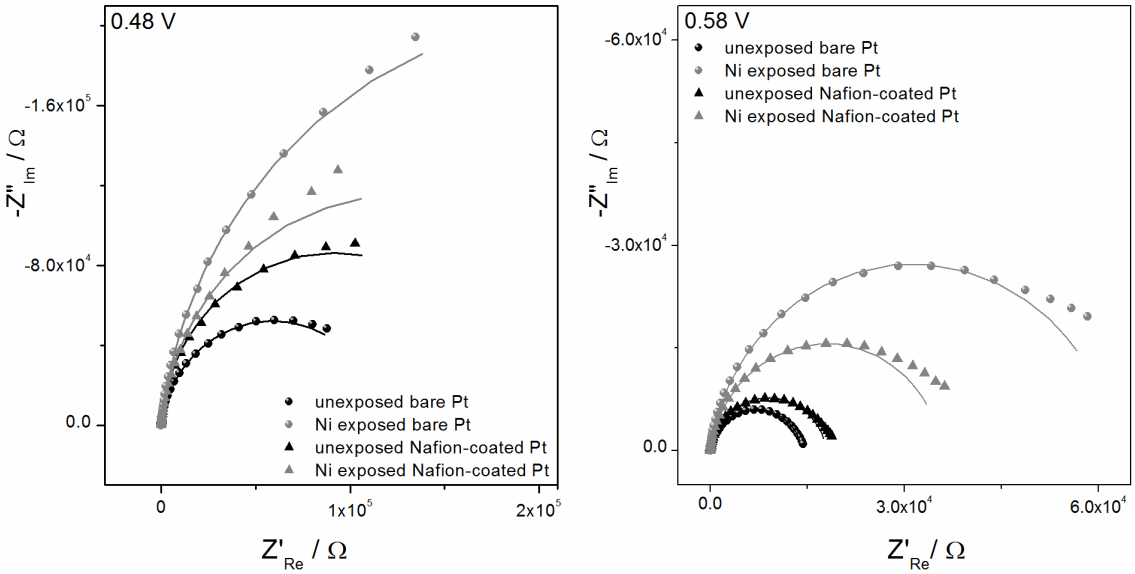

Figure 4-5: Nyquist plots of unexposed and Ni exposed electrodes obtained at 0.48 - 0.58 V.

To further analyze the Nyquits plots at this potential range, the equivalent circuit shown in Figure 4-3, region II is used to fit the data. Results are presented in Table 4-2 and Table 4-3, showing a higher R_{ct} values for the unexposed Nafion-coated Pt electrodes compared to the unexposed bare Pt electrodes. This behavior may be attributed to the presence of Nafion-ionomer film, which may decelerate the H_2O access to the Pt active sites (due to Nafion hydrophobic properties), resulting in a decrease in the formation of oxygenated species and subsequently leading to a decrease in the oxidative removal rate of the CO_{ads}. Moreover, the increase in R_{ct} values for the Ni exposed bare Pt is more significant as compared to Ni exposed Nafion-coated Pt electrode. These results indicate that the CO_{ads} oxidation rate significantly decreases on the bare Pt in the presence of Ni solution at the potential range of 0.48 - 0.58 V.

Table 4-2. Fitting parameters obtained from the Nyquist plot at E = 0.48 V shown in Figure 4-5.

Sample	R_s (Ω)	CPE1-T (F)	CPE1-P (F)	R_{ct} (Ω)
unexposed bare Pt	4.5	7.24E-06	0.93	1.02E05
Ni exposed bare Pt	4.9	5.45E-06	0.94	3.32E05
unexposed Nafion-coated Pt	4.6	6.70E-06	0.94	1.86E05
Ni exposed Nafion-coated Pt	4.8	6.35E-06	0.93	2.37E05

Table 4-3. Fitting parameters obtained from the Nyquist plot at E = 0.58 V shown in Figure 4-5.

Sample	R_s (Ω)	CPE1-T (F)	CPE1-P (F)	R_{ct} (Ω)
unexposed bare Pt	3.5	1.03E-05	0.89	1.31E04
Ni exposed bare Pt	3.7	8.21E-06	0.91	6.40E04
unexposed Nafion-coated Pt	3.6	8.11E-06	0.93	1.67E04
Ni exposed Nafion-coated Pt	3.9	7.80E-06	0.92	3.56E04

EIS at 0.68 V_{RHE}:

Figure 4-6 shows the Nyquist plots of unexposed and Ni exposed Nafion-coated and bare Pt electrodes at E = 0.68 V. A capacitive arc at high frequency, followed by an inductive loop in the fourth quadrant at low frequency are observed in the Nyquist plots of all cases. At this potential, the oxidative removal reaction of CO_{ads} with OH_{ads} (as shown in Equation 4-3) occurs more rapidly, resulting in the availability of more Pt sites for further CH_3OH adsorption-dehydrogenation and CO_{ads} coverage [46]. A similar inductive behavior was previously reported in the literature [45,51,53]. It was suggested that the appearance of inductive behavior at low frequency range is associated with the strong adsorption of CO_{ads}, which can result in the sluggish response to the change in the potential and subsequently a delay in the resulting alternative current [54].

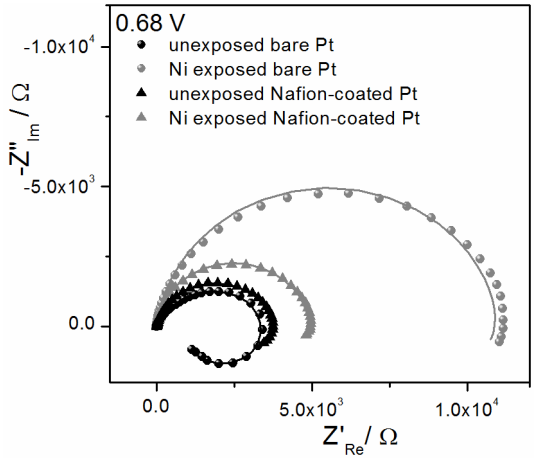

Figure 4-6: Nyquist plots of unexposed and Ni exposed electrodes obtained at 0.68 V.

After Ni solution exposure, the Nyquist plots of both electrodes show an increase in the arc diameter as compared to the unexposed condition. However, this increase in the arc diameter is more significant for the Ni exposed bare Pt electrode as compared to the Ni exposed Nafion-coated Pt electrode.

For the quantitative analysis of the Nyquist plots of unexposed and Ni exposed electrodes, the equivalent circuit shown in Figure 4-3, region III is used to fit the data [53]. According to this circuit, the R_{ct} is the charge-transfer resistance, L_1 is the inductance, and R_1 is the inductance resistance [53,55]. As presented in Table 4-4, the R_{ct} values significantly increased for the Ni exposed bare Pt electrode as compared to the Ni exposed Nafion-coated Pt electrode. This behavior may indicate that the formation of OH_{ads} through H_2O dissociative-adsorption becomes slower after Ni exposure of bare Pt electrode, leading to a decrease in the oxidative removal rate of CO_{ads}. The smaller change observed in R_{ct} value after Ni exposure of Nafion-coated Pt electrode compared to the Ni exposed bare Pt electrode is consistent with the results obtained at lower potentials (i.e., 0.48-0.58 V), which may be attributed to the prohibiting role of Nafion-ionomer film for the Ni solution contaminants to negatively affect the Pt active sites of Nafion-coated Pt electrode.

Table 4-4. Fitting parameters obtained from the Nyquist plot at E = 0.68 V shown in Figure 4-6.

Sample	R_s (Ω)	CPE1-T (F)	CPE1-P (F)	R_{ct} (Ω)	R_1(Ω)	L_1(H)
unexposed bare Pt	3.8	2.3E-05	0.89	3.8E03	1050	2.4E03
Ni exposed bare Pt	4.2	7.0E-06	0.90	1.9E04	1.5E4	9.0E4
unexposed Nafion-coated Pt	3.9	1.5E-05	0.90	3.9E03	5.7E03	2.5E03
Ni exposed Nafion-coated Pt	4.2	6.6E-06	0.94	4.8E03	7.5E03	3.1E04

EIS at 0.78 V_{RHE}:

Figure 4-7 shows the Nyquist plots of unexposed and Ni exposed Nafion-coated and bare Pt electrodes at E = 0.78 V. As shown in Figure 4-7 (black circle), the Nyquist plot of unexposed bare Pt electrode flips over to the second and third quadrants. By increasing the potential, the rates of CH_3OH adsorption-dehydrogenation (Equation 4-1) and oxidative removal of CO_{ads} by OH_{ads} (Equation 4-3) become faster and approaches each other. At more positive potentials, the oxygenated species form at a faster rate on the Pt surface through H_2O dissociative-adsorption. This can further enhance the CO_{ads} oxidation rate, and also inhibit the adsorption of CH_3OH on Pt. According to the literature, the rapid OH_{ads} formation may block the Pt active sites, resulting in the negative impedance at high frequency in the Nyquist plot at this potential [56]. Based on the previous studies, the negative impedance appeared in the Nyquist plot is described as hidden negative impedance, as no negative slope is observed in the polarization curve during voltammetry at this specific potential [57,58].

As shown in Figure 4-7 (black triangle), the Nyquist plot of unexposed Nafion-coated Pt shows a different behavior as compared to the unexposed bare Pt electrode, where the Nyquist arc appears in the first and fourth quadrants. The change in the arc behavior in the presence of Nafion-ionomer film is consistent with the changes observed in the Nyquist plots obtained at lower potential ranges (i.e., 0.48-0.68 V). This behavior indicates that hydrophobic property of Nafion-ionomer may affect H_2O permeation, leading to a decrease in the oxygenated species formation.

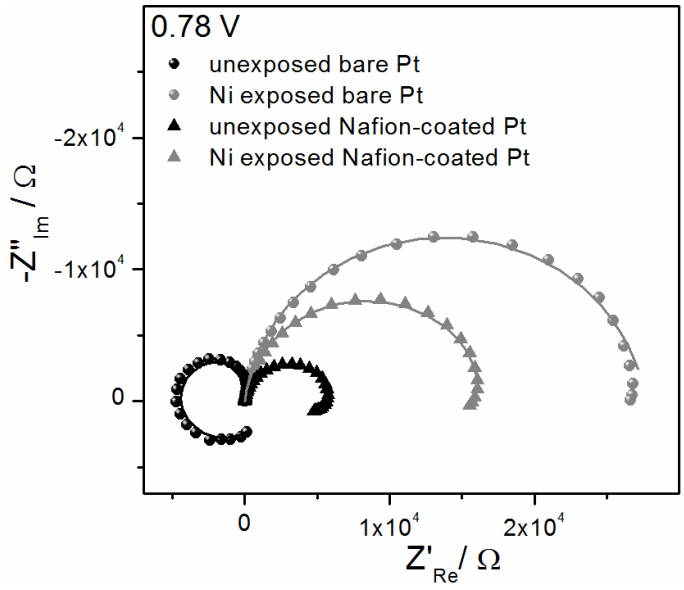

Figure 4-7: Nyquist plots of unexposed and Ni exposed electrodes obtained at 0.78 V.

After the Ni solution exposure, the Nyquist plots of both electrodes appear at first and fourth quadrants, shown in Figure 4-7 (gray triangle and gray circle). Consistent with the Nyquist plots obtained at lower potential ranges (i.e., 0.48-0.68 V), a higher increase in the arc diameter is observed for the Nyquist plot of Ni exposed bare Pt electrode as compared to Ni exposed Nafion-coated Pt electrode. This may indicate that the H_2O dissociative-adsorption rate decreased significantly after Ni solution exposure of bare Pt, resulting in the fewer active oxygenated species formation on the Pt surface.

To further analyze the Nyquist plot of unexposed bare Pt electrode at this potential, the equivalent circuit shown in Figure 4-3, region IV is used to fit the data [59]. As the Nyquist plots showed different behavior for the unexposed Nafion-coated Pt and Ni exposed electrodes, the equivalent circuit shown in Figure 4-3, region III is used for data analysis. As expected from the Nyquist plot and confirmed by the fitted

data shown in Table 4-5, a negative R_{ct} value was obtained for the unexposed bare Pt electrode. However, the R_{ct} value became positive in the presence of unexposed Nafion-coated Pt and increased for the Ni exposed electrodes. The changes in R_{ct} values from negative to positive may indicate a decrease in OH_{ads} formation on the unexposed Nafion-coated Pt and Ni exposed electrodes as compared to the unexposed bare Pt.

Table 4-5. Fitting parameters obtained from the Nyquist plot at E = 0.78 V shown in Figure 4-7.

Sample	R_s (Ω)	CPE1-T (F)	CPE1-P (F)	R_{ct} (Ω)	R_1(Ω)	L_1(H)	R_2(Ω)	L_2(H)
unexposed bare Pt	4.1	2.6E-05	0.89	-2653	6423	13.73	902	2882
Ni exposed bare Pt	4.9	5.64E-06	0.94	2.73E04	3.60E04	3.76E05	-	-
unexposed Nafion-coated Pt	4.8	6.37E-05	0.94	5.88E03	1.57E04	1.55E04	-	-
Ni exposed Nafion-coated Pt	5	7.95E-06	0.95	1.65E04	6.68E04	1.34E05	-	-

Changes in R_{ct} values as a function of potential obtained from the Nyquist plots of unexposed and Ni exposed electrodes are presented in Figure 4-8. Results show that the R_{ct} values are generally higher in presence of unexposed Nafion-coated Pt electrode, as compared to the unexposed bare Pt electrode. This behavior may be associated with the hydrophobic properties of Nafion-ionomer film, resulting in a decrease in CH_3OH adsorption-dehydrogenation as well as CO_{ads} oxidative removal rate (due to the decrease in oxygenated species formation). The results also reveal that the R_{ct} values of Ni exposed Nafion-coated Pt electrode are smaller than the R_{ct} values of Ni exposed bare Pt electrode. These results may indicate that the presence of Nafion-ionomer film may play as a barrier for the Pt surface, partially preventing Ni solution contaminants to negatively affect the Pt active sites. This behavior may be attributed to the negatively charged sulfonate groups of Nafion-ionomer, which may interact with the Ni cations and localize some of these cations away from the Pt active sites.

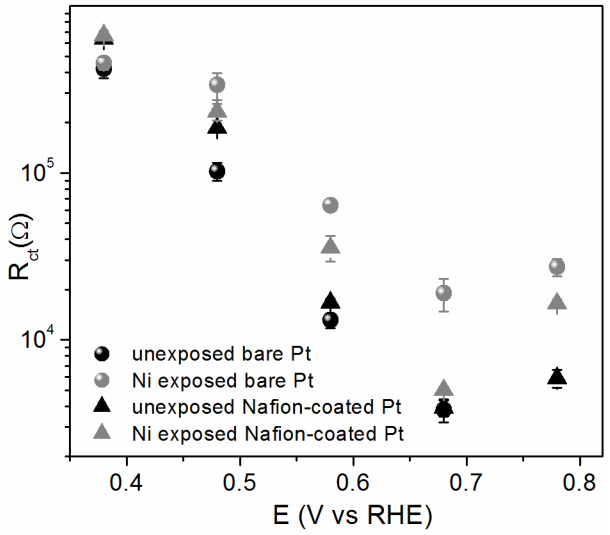

Figure 4-8: The R_{ct} values as a function of electrode potential on the unexposed and Ni exposed electrodes. The negative value of charge transfer resistance is not plotted.

4.3.6 Recovery of Catalytic Activity of Ni Exposed Electrodes

In order to estimate the recovery potential of the Ni exposed electrodes, cyclic voltammetry (referred to as CV-recovery) was conducted on the Ni exposed electrodes at potential range of 0.08 - 1.28 V in Ni-free 0.5 M H_2SO_4 for 7 cycles. This potential range was selected, in order to inhibit the degradation of Nafion film during the process. Figure 4-9a (gray curve) shows the CV-recovery scan of a Ni exposed bare Pt electrode. As shown, the $H_{ads/des}$ and Pt-oxide formation/reduction peak currents partially recovered compared to the unexposed condition. Figure 4-9b (gray curve) shows the CV-recovery scan of a Ni exposed Nafion-coated Pt electrode. The results show that cycling the potential may lead to a nearly complete recovery of the Ni exposed Nafion-coated Pt.

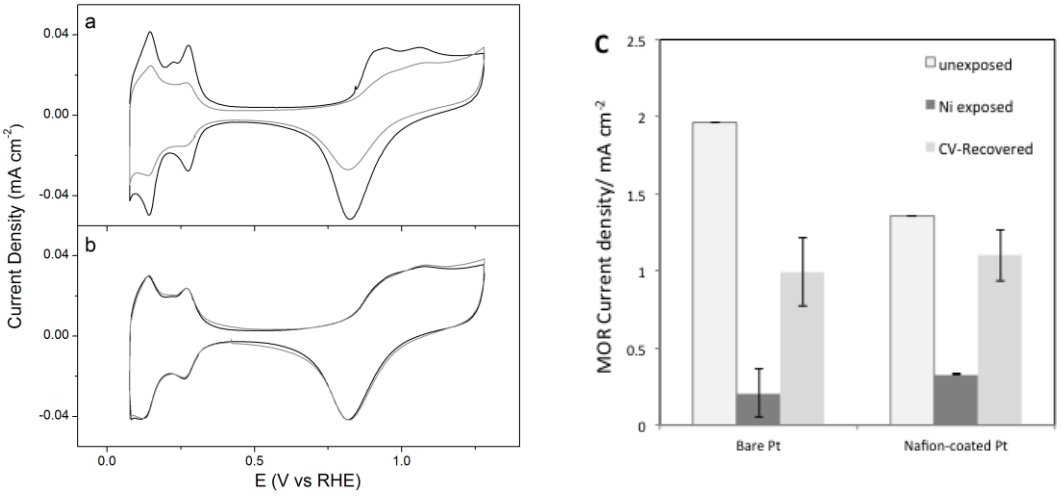

Figure 4-9: Cyclic voltammogram of: a) unexposed bare Pt electrode (black curve) and the CV-recovered of Ni exposed bare Pt electrode (gray curve)., b) unexposed Nafion-coated Pt electrode (black curve) and the CV-recovered of Ni exposed Nafion-coated Pt electrode (gray curve)., c) MOR current densities of unexposed, Ni exposed, and CV-recovered electrodes.

In order to further evaluate the activity of recovered electrodes during the MOR, the cyclic voltammetry was conducted on the CV-recovered electrodes in Ni-free 0.5 M CH_3OH + 0.5 M H_2SO_4 solution. Figure 4-9c summarizes the results of MOR peak current densities for unexposed, Ni exposed, and CV-recovered electrodes. The results show approximately 52% and 81% recovery in the MOR activity of Ni exposed bare Pt and Nafion-coated Pt electrodes, respectively.

4.4 Conclusions

In order to understand the effect of Ni solution contaminants on the Nafion-ionomer of anode electro-catalyst of DMFC, a systematic study was conducted on the Nafion-coated and bare Pt electrodes. Cyclic voltammetry was performed to evaluate voltammetric properties of unexposed and Ni exposed electrodes. The results show that the voltammetric properties (including $H_{ads/des}$ and Pt-OH formation-reduction peak currents) of bare Pt electrode exhibit a higher decrease after Ni solution exposure, as compared to the Ni exposed Nafion-coated Pt electrode. The MOR voltammetries of unexposed and Ni exposed electrodes were further obtained. A similar result was observed after Ni solution exposure of both electrodes, where only a slightly higher decrease in MOR activity of Ni exposed bare Pt electrode was obtained as compared to Ni exposed Nafion-coated Pt electrode.

EIS measurements were further conducted at different potentials (0.38 - 0.78 V) to examine the MOR mechanism on the unexposed and Ni exposed electrodes. The EIS results obtained at lower potential range (i.e., 0.38 V) showed that Ni solution

contaminants have insignificant effect on CH_3OH adsorption-dehydrogenation, as minor changes in R_{ct} values were obtained after Ni exposure of both electrodes compared to unexposed conditions. However, at more positive potential range (i.e., 0.48-0.78 V), the R_{ct} value significantly increases in the presence of Ni exposed bare Pt electrode due to sluggish H_2O dissociative-adsorption as compared to the Ni exposed Nafion-coated Pt electrode.

Based on the background voltammetry and EIS measurements, Ni solution contaminants result in a higher decrease in the voltammetric properties as well as a higher increase in R_{ct} values of the bare Pt electrode as compared to the Ni exposed Nafion-coated Pt electrode. This result indicates that Nafion-ionomer film may play as a barrier for the Ni contaminants to reach the Pt active sites. This behavior may be attributed to the negatively charged sulfonate groups of Nafion-ionomer, which can interact with the Ni cations, keeping some of these cations away from the Pt surface. This results in a lower effect of Ni contaminant on the MOR activity of Nafion-coated Pt electrode as compared to the bare Pt electrode. However, contradictory results were obtained by the MOR voltammetry measurement, where only slightly higher decrease in MOR activities of bare Pt electrode was obtained after Ni solution exposure as compared to the Ni exposed Nafion-coated Pt electrode.

The CV-recovery test revealed a near complete recovery for the Ni exposed Nafion-coated Pt electrode, while only a partial recovery was obtained for the Ni exposed bare Pt electrode.

4.5 References

[1] S. Wasmus, A. Küver, Methanol oxidation and direct methanol fuel cells: A selective review, J. Electroanal. Chem. 461 (1999) 14–31.

[2] X. Ren, M.S. Wilson, S. Gottesfeld, High performance direct methanol polymer electrolyte fuel cells, J. Electrochem. Soc. 143 (1996) L12–L15.

[3] M.K. Ravikumar, A.K. Shukla, Effect of methanol crossover in a liquid-feed polymer-electrolyte direct methanol fuel cell, J. Electrochem. Soc. 143 (1996) 2601–2606.

[4] A. Heinzel, V.M. Barragán, A review of the state-of-the-art of the methanol crossover in direct methanol fuel cells, J. Power Sources. 84 (1999) 70–74.

[5] E. Antolini, J.R.C. Salgado, E.R. Gonzalez, The stability of Pt-M (M = first row transition metal) alloy catalysts and its effect on the activity in low temperature fuel cells. A literature review and tests on a Pt-Co catalyst, J. Power Sources. 160 (2006) 957–968. doi:10.1016/j.jpowsour.2006.03.006.

[6] P. Piela, C. Eickes, E. Brosha, F. Garzon, P. Zelenay, Ruthenium Crossover in Direct Methanol Fuel Cell with Pt-Ru Black Anode, J. Electrochem. Soc. 151 (2004) A2053–A2059. doi:10.1149/1.1814472.

[7] S. Chen, H.A. Gasteiger, K. Hayakawa, T. Tada, Y. Shao-horn, Platinum-Alloy Cathode Catalyst Degradation in Proton Exchange Membrane Fuel Cells: Nanometer-Scale Compositional and Morphological Changes, J. Electrochem. Soc. 157 (2010) A82–A97. doi:10.1149/1.3258275.

[8] H.R. Colón-Mercado, B.N. Popov, Stability of platinum based alloy cathode catalysts in PEM fuel cells, J. Power Sources. 155 (2006) 253–263.

[9] N. Zamel, X. Li, Effect of contaminants on polymer electrolyte membrane fuel cells, Prog. Energy Combust. Sci. 37 (2011) 292–329. doi:10.1016/j.pecs.2010.06.003.

[10] X. Jie, Z.G. Shao, B. Yi, The effect of different valency cations on DMFC performance, Electrochem. Commun. 12 (2010) 700–702. doi:10.1016/j.elecom.2010.03.010.

[11] X. Jie, Z. Shao, J. Hou, G. Sun, B. Yi, The influence of sodium ion as a potential fuel impurity on the direct methanol fuel cells, Electrochim. Acta. 55 (2010) 4783–4788. doi:10.1016/j.electacta.2010.03.035.

[12] J.W. Guo, X.F. Xie, J.H. Wang, Y.M. Shang, Effect of current collector corrosion made from printed circuit board (PCB) on the degradation of self-breathing direct methanol fuel cell stack, Electrochim. Acta. 53 (2008) 3056–3064. doi:10.1016/j.electacta.2007.11.044.

[13] L. Ma, S. Warthesen, D.A. Shores, Evaluation of materials for bipolar plates in PEMFCs, J. New Mater. Electrochem. Syst. 3 (2000) 221–228. http://www.groupes.polymtl.ca/jnmes/modules/journal/index.php/content0647.html.

[14] A. Pozio, R.F. Silva, M. De Francesco, L. Giorgi, Nafion degradation in PEFCs from end plate iron contamination, Electrochim. Acta. 48 (2003) 1543–1549. doi:10.1016/S0013-4686(03)00026-4.

[15] Q. Jia, D.E. Ramaker, J.M. Ziegelbauer, N. Ramaswamy, A. Halder, S. Mukerjee, Fundamental aspects of ad-metal dissolution and contamination in low and medium temperature fuel cell electrocatalysis: A Cu based case study using in situ electrochemical X-ray absorption spectroscopy, J. Phys. Chem. C. 117 (2013) 4585–4596.

[16] T. Okada, G. Xie, O. Gorseth, S. Kjelstrup, N. Nakamura, T. Arimura, Ion and water transport characteristics of Nafion membranes as electrolytes, Electrochim. Acta. 43 (1998) 3741–3747.

[17] T. Okada, Y. Ayato, M. Yuasa, I. Sekine, The effect of impurity cations on the transport characteristics of perfluorosulfonated ionomer membranes, J. Phys. Chem. B. 103 (1999) 3315–3322.

[18] J.G. Goodwin, K. Hongsirikarn, S. Greenway, S. Creager, Effect of cations (Na+, Ca2+, Fe3+) on the conductivity of a Nafion membrane, J. Power Sources. 195 (2010) 7213–7220. doi:10.1016/j.jpowsour.2010.05.005.

[19] M.J. Kelly, G. Fafilek, J.O. Besenhard, H. Kronberger, G.E. Nauer, Contaminant

absorption and conductivity in polymer electrolyte membranes, J. Power Sources. 145 (2005) 249–252. doi:10.1016/j.jpowsour.2005.01.064.

[20] M. Sulek, J. Adams, S. Kaberline, M. Ricketts, J.R. Waldecker, In situ metal ion contamination and the effects on proton exchange membrane fuel cell performance, J. Power Sources. 196 (2011) 8967–8972. doi:10.1016/j.jpowsour.2011.01.086.

[21] M.J. Yang, K.Y. Park, K.B. Kim, H. Cho, H. Choi, J.Y. Park, Degradation mechanisms and mitigation strategies of metal cations in recycled fuel for direct methanol fuel cell membrane electrode assembly, J. Power Sources. 242 (2013) 646–655. doi:10.1016/j.jpowsour.2013.05.141.

[22] W. Chen, Q. Xin, G. Sun, S. Yang, Z. Zhou, Q. Mao, P. Sun, Effects of dissolved iron and chromium on the performance of direct methanol fuel cell, Electrochim. Acta. 52 (2007) 7115–7120. doi:10.1016/j.electacta.2007.05.047.

[23] H. Li, K. Tsay, H. Wang, J. Shen, S. Wu, J. Zhang, N. Jia, S. Wessel, R. Abouatallah, N. Joos, J. Schrooten, Durability of PEM fuel cell cathode in the presence of Fe3+and Al3+, J. Power Sources. 195 (2010) 8089–8093. doi:10.1016/j.jpowsour.2010.07.003.

[24] H. Li, K. Tsay, H. Wang, S. Wu, J. Zhang, N. Jia, S. Wessel, R. Abouatallah, N. Joos, J. Schrooten, Effect of Co2+on oxygen reduction reaction catalyzed by Pt catalyst, and its implications for fuel cell contamination, Electrochim. Acta. 55 (2010) 2622–2628. doi:10.1016/j.electacta.2009.12.037.

[25] J. Durst, M. Chatenet, F. Maillard, Impact of metal cations on the electrocatalytic properties of Pt/C nanoparticles at multiple phase interfaces, Phys. Chem. Chem. Phys. 14 (2012) 13000. doi:10.1039/c2cp42191g.

[26] S.M. Alia, S. Pylypenko, K.C. Neyerlin, S.S. Kocha, Platinum Nickel Nanowires as Methanol Oxidation Electrocatalysts, J. Electrochem. Soc. 162 (2015) F1299–F1304. doi:10.1149/2.0231512jes.

[27] T. Okada, Y. Ayato, H. Satou, M. Yuasa, I. Sekine, Unprecedented effect of impurity cations on the oxygen reduction kinetics at platinum electrodes covered with

perfluorinated ionomer, J. Phys. Chem. B. 15 (1999) 8490–8496. doi:10.1021/la990625e.

[28] J. Chlistunoff, B. Pivovar, Effects of ionomer morphology on oxygen reduction on Pt, J. Electrochem. Soc. 162 (2015) F890–F900. doi:10.1149/2.0661508jes.

[29] H. Li, K. Tsay, H. Wang, S. Wu, J. Zhang, N. Jia, S. Wessel, R. Abouatallah, N. Joos, J. Schrooten, Effect of Co2+ on oxygen reduction reaction catalyzed by Pt catalyst, and its implications for fuel cell contamination, Electrochim. Acta. 55 (2010) 2622–2628. doi:10.1016/j.electacta.2009.12.037.

[30] F. Büchi, M. Inaba, T.J. Schmidt, Polymer Electrolyte Fuel Cell Durability, Springer-Verlag New York, 2009. doi:10.1007/978-0-387-85536-3.

[31] D.R. Lawson, L.D. Whiteley, C.R. Martin, M.N. Szentirmay, J.I. Song, Oxygen Reduction at Nation Film-Coated Platinum Electrodes: Transport and Kinetics, J. Electrochem. Soc. 135 (1988) 2247–2253.

[32] Y. Ayato, K. Kunimatsu, M. Osawa, T. Okada, Study of Pt electrode/nafion ionomer interface in HClO4 by in situ surface-enhanced FTIR spectroscopy, J. Electrochem. Soc. 153 (2006) A203–A209. doi:10.1149/1.2137648.

[33] R. Subbaraman, D. Strmcnik, V. Stamenkovic, N.M. Markovic, Three Phase Interfaces at Electrified Metal-Solid Electrolyte Systems 1. Study of the Pt(hkl)-Nafion Interface, J. Phys. Chem. C. 114 (2010) 8414–8422. doi:10.1021/jp100814x.

[34] G. Hou, J. Parrondo, V. Ramani, J. Prakash, Kinetic and Mechanistic Investigation of Methanol Oxidation on a Smooth Polycrystalline Pt Surface, J. Electrochem. Soc. 161 (2014) F252–F258. doi:10.1149/2.045403jes.

[35] A.V. Tripković, K.D. Popović, Oxidation of methanol on platinum single crystal stepped electrodes from [110] zone in acid solution, Electrochim. Acta. 41 (1996) 2385–2394.

[36] J.M. Sieben, M.M.E. Duarte, C.E. Mayer, Methanol oxidation on carbon supported Pt–Ru catalysts prepared by electrodeposition – Evaluation of Nafion 117 film effect, Int. J. Hydrogen Energy. 35 (2010) 2018–2024. doi:10.1016/j.ijhydene.2009.12.078.

[37] B. Krishnamurthy, S. Deepalochani, K.S. Dhathathreyan, Effect of Ionomer Content in Anode and Cathode Catalyst Layers on Direct Methanol Fuel Cell Performance, Fuel Cells. 8 (2008) 404–409. doi:10.1002/fuce.200800055.

[38] J.M. Sieben, M.M.E. Duarte, C.E. Mayer, Pt–Ru-supported electrodes deposited by multiple successive cycles of potentiostatic pulses: evaluation of Nafion film effect on methanol oxidation, J. Solid State Electrochem. 14 (2010) 1555–1563. doi:10.1007/s10008-009-0972-5.

[39] R. Parsons, T. VanderNoot, The oxidation of small organic molecules. A survey of recent fuel cell related research, J. Electroanal. Chem. 257 (1988) 9–45. doi:10.1016/0022-0728(88)87028-1.

[40] T. Iwasita, Electrocatalysis of methanol oxidation, Electrochim. Acta. 47 (2002) 3663–3674. doi:10.1016/S0013-4686(02)00336-5.

[41] E.A. Batista, G.R.P. Malpass, A.J. Motheo, T. Iwasita, New insight into the pathways of methanol oxidation, Electrochem. Commun. 5 (2003) 843–846. doi:10.1016/j.elecom.2003.08.010.

[42] E. Herrero, W. Chrzanowski, A. Wieckowski, Dual path mechanism in methanol electrooxidation on a platinum electrode, J. Phys. Chem. 99 (1995) 10423–10424.

[43] M. Aramata, A., Masuda, Platinum Alloy Electrodes Bonded to Solid Polymer Electrolyte for Enhancement of Methanol Electro-oxidation and Its Reaction Mechanism, J. Electrochem. Soc. 138 (1991) 1949–1957. doi:10.1149/1.2085907.

[44] J. Otomo, X. Li, T. Kobayashi, C.-J. Wen, H. Nagamoto, H. Takahashi, AC-impedance spectroscopy of anodic reactions with adsorbed intermediates: Electro-oxidations of 2-propanol and methanol on carbon-supported Pt catalyst, J. Electroanal. Chem. 573 (2004) 99–109. doi:10.1016/j.jelechem.2004.07.002.

[45] R.E. Melnick, G.T.R. Palmore, Impedance spectroscopy of the electro-oxidation of methanol on polished polycrystalline platinum, J. Phys. Chem. B. 105 (2001) 1012–1025. doi:10.1021/jp0030847.

[46] I. Hsing, X. Wang, Y. Leng, Electrochemical impedance studies of methanol electro-oxidation on Pt/C thin film electrode, J. Electrochem. Soc. 149 (2002) A615–A621.

doi:10.1149/1.1467940.

[47] V.S. Bagotzky, Y.B. Vassiliev, O.A. Khazova, Generalized scheme of chemisorption, electrooxidation and electroreduction of simple organic compounds on platinum group metals, J. Electroanal. Chem. 81 (1977) 229–238.

[48] V.S. Bagotzky, Y.B. Vassilyev, Mechanism of electro-oxidation of methanol on the platinum electrode, Electrochim. Acta. 12 (1967) 1323–1343.

[49] H.A. Gasteiger, N. Marković, P.N. Ross Jr., E.J. Cairns, Methanol electrooxidation on well-characterized Pt-Ru alloys, J. Phys. Chem. 97 (1993) 12020–12029.

[50] X.H. Xia, T. Iwasita, F. Ge, W. Vielstich, Structural effects and reactivity in methanol oxidation on polycrystalline and single crystal platinum, Electrochim. Acta. 41 (1996) 711–718. doi:10.1016/0013-4686(95)00360-6.

[51] W. Sugimoto, K. Aoyama, T. Kawaguchi, Y. Murakami, Y. Takasu, Kinetics of CH3OH oxidation on PtRu/C studied by impedance and CO stripping voltammetry, J. Electroanal. Chem. 576 (2005) 215–221. doi:10.1016/j.jelechem.2004.10.018.

[52] D.Y. Chung, K. Lee, Y. Sung, Methanol electro-oxidation on the Pt surface: Revisiting the cyclic voltammetry interpretation, J. Phys. Chem. C. 120 (2016) 9028–9035. doi:10.1021/acs.jpcc.5b12303.

[53] J.T. Müller, P.M. Urban, W.F. Hölderich, Impedance studies on direct methanol fuel cell anodes, J. Power Sources. 84 (1999) 157–160. doi:10.1016/S0378-7753(99)00331-6.

[54] W. Tokarz, P. Piela, A. Czerwiński, Analysis of the influence of rhodium addition to platinum on its activity towards methanol electrooxidation by EIS, J. Solid State Electrochem. 14 (2010) 515–521. doi:10.1007/s10008-008-0727-8.

[55] X. Zhao, G. Sun, L. Jiang, W. Chen, Effects of Chloride Anion as a Potential Fuel Impurity on DMFC Performance, Electrochem. Solid-State Lett. 8 (2005) A149–A151. doi:10.1149/1.1854113.

[56] R.E. Melnick, G.T.R. Palmore, Time-dependent impedance of the electro-oxidation of methanol on polished polycrystalline platinum, J. Phys. Chem. B. 105 (2001) 9449–9457. doi:10.1021/jp003106p.

[57] C. Désilets, A. Lasia, Dynamic impedance study of ethanol and acetaldehyde oxidation at platinum in acid solutions, Electrochim. Acta. 78 (2012) 286–293. doi:10.1016/j.electacta.2012.05.102.

[58] F. Seland, R. Tunold, D.A. Harrington, Impedance study of formic acid oxidation on platinum electrodes, Electrochim. Acta. 53 (2008) 6851–6864. doi:10.1016/j.electacta.2007.12.021.

[59] P.K. Dahlstrøm, D.A. Harrington, F.. Seland, A study of methanol oxidation by dynamic electrochemical impedance spectroscopy, ECS Trans. 41 (2012) 35–47. doi:10.1149/1.3695100.

5. Influence of Ni Solution Contaminants on Carbon-supported Pt Electro-catalysts with different Ionomer Contents during Methanol Oxidation Reaction

Abstract

In this study, the influence of Ni solution contaminants on the electro-catalytic activities of carbon-supported platinum nanoparticle (Pt/C) catalysts with various Nafion-ionomer distributions and contents during methanol oxidation reaction (MOR) was investigated. Pt/C electrodes with various Nafion-ionomer contents in the inside and/or on the surface (respectively referred to as Nafion-incorporated and Nafion-coated Pt/C catalysts) were prepared. Cyclic voltammetry and electrochemical impedance spectroscopy (EIS) were conducted on the unexposed and Ni exposed Nafion-incorporated and Nafion-coated Pt/C electrodes. The background voltammetry results showed a higher decrease in the voltammetric properties of Nafion-incorporated Pt/C after Ni solution exposure as compared to Ni exposed Nafion-coated Pt/C electrodes. However, a similar decrease in MOR activity of all Pt/C electrodes (i.e., Nafion-incorporated and Nafion-coated) was observed after Ni solution exposure. EIS measurements were conducted at potential range of 0.58 and 0.78 V. Results showed a significant decrease in the H_2O dissociative-adsorption rate at higher potential ranges (0.68 - 0.78 V) in the presence of Ni exposed Nafion-incorporated Pt/C as compared to Ni exposed Nafion-coated Pt/C electrodes. From the results of background voltammetry and EIS measurements, it appears that the presence of Nafion-ionomer film may suppress the Ni solution poisoning effect on the Pt active sites. This behavior may be

attributed to the sulfonate groups of Nafion-ionomer film, which may interact with Ni cation contaminants and localize them away from the Pt active sites, reducing the Ni solution contaminant effect on the electro-catalytic activity of Nafion-coated Pt/C electrodes.

5.1 Introduction

The growing energy demand and environmental concern associated with the consumption of fossil fuels have led to the development of alternative sources of energy. Polymer electrolyte membrane fuel cells (PEMFCs) including direct methanol fuel cells (DMFCs) appear to be a promising source of clean energy for future energy needs. DMFC in particular is an attractive power source for portable applications owing to its high energy density, fast and convenient refueling and low emissions [1, 2]. One of the key challenges in the commercialization of fuel cells is the degradation effect of metal contaminants (originating from electro-catalyst and/or bipolar degradation [3-9]) on the overall fuel cell performance. It is well established that metal cation contaminants affect the proton conductivity of Nafion membrane of fuel cells [10–12]. Nafion is a polymer electrolyte, commonly used to conduct proton and to separate the anode and cathode compartments of fuel cells. The Nafion structure consists of a hydrophobic poly tetrafluoroethylene (PTFE) backbone with fully perfluorinated ether side chains, which are terminated by hydrophilic sulfonic groups (i.e., $–SO_3H$) providing proton conductivity [13]. As multivalent metal cation contaminants (e.g., Fe^{3+} and Cu^{2+}) have a higher affinity toward the sulfonic acid groups of Nafion as compared to monovalent protons, they can easily displace the protons present in Nafion. This may lead to a decrease in the proton conductivity and water content of Nafion membrane, which can consequently result in a degradation in the fuel cell performance [14–18].

While numerous studies have focused on the effect of metal cation

contaminants on the Nafion membrane properties, their influences on the electro-catalyst activities of fuel cells is not well understood. In a study by Li et al., the effect of Co^{2+} solution contaminants on the ORR activity of Pt catalyst was investigated [19]. The results showed a change in the ORR mechanism due to weak Co^{2+} adsorption on the Pt active sites. The effect of Co^{2+} solution contaminants on the CO electro-oxidation and ORR activities of Pt/C catalysts was investigated by Durst et al. [20]. It was shown that the formation of oxygenated species on the Pt surface is enhanced in the presence of Co^{2+} solution, resulting in an increased and decreased in the CO-oxidation and ORR activities, respectively. In this study, the effect of Co^{2+} solution contaminants was further investigated on the Pt/C electrodes with different ionomer to carbon (I/C) ratios. The result showed that the effect of Co^{2+} solution on the activity of Pt/C electrode decreased as Nafion-ionomer content increased.

There is a paucity of literature on the effect of metal solution contaminants on the anode electro-catalytic activity of DMFCs. In chapter 3, the effect of various concentrations of metal solution contaminants (i.e., Co^{2+}, Ni^{2+} and Zn^{2+}) on the MOR and ORR activities of polycrystalline Pt was investigated. The results showed a decrease in Pt electro-catalytic activity during MOR and ORR as the concentration of metal solution contaminants increased. Further in chapter 4, the effect of Ni solution contaminants on the MOR activities of Nafion-coated and bare polycrystalline Pt electrodes was investigated. The results showed a smaller Ni solution effect on the electro-catalytic activity of Nafion-coated Pt electrode as compared to bare Pt

electrode. It was suggested that the presence of Nafion-ionomer film may suppress the negative effect of metal cations on the Pt active sites. Throughout chapter 3 and chapter 4, polycrystalline Pt was used as the only tool to evaluate the influence of metal solution contaminants on the MOR and ORR activities. In order to better mimic the structure of anode electro-catalyst used in DMFC, carbon-supported platinum nanoparticle (Pt/C) catalyst was used to characterize its electro-catalytic activity in the presence of Ni solution contaminants. This study systematically investigated the effect of Ni solution contaminants on electro-catalytic activities of Pt/C catalysts with various Nafion-ionomer distributions and contents during the MOR. Pt/C electrodes were prepared either by incorporating various contents of Nafion-ionomer inside the Pt/C catalyst (referred to as Nafion-incorporated Pt/C) or by applying various contents of Nafion-ionomer on the Pt/C surface (referred to as Nafion-coated Pt/C).

5.2 Experimental Methods

5.2.1 Electrode Preparation

a) Nafion-incorporated Pt/C Electrodes

Pt/C catalyst inks were prepared by mixing 7.6 mg Pt/C (40 wt % Pt catalyst (Ketjen black-KB)) catalyst powder with 5 mL high purity water (Millipore Milli-Q, 18.2 MΩ cm) and appropriated amount of Nafion solution (Sigma-Aldrich- 5 wt.% Nafion in lower alcohols) to obtain different Nafion-ionomer to carbon (I/C) ratios of 0.5 and 2.2. The catalyst ink solution was placed in water bath and sonicated for 30 minutes. An aliquot (10 μL) of the catalyst ink was pipetted onto a glassy carbon (GC) disk electrode

(0.196 cm^2, embedded in a PTFE cylinder, Pine Instruments) to achieve 29 μgrPt cm^{-2} loading, followed by air-drying for approximately 24 hours at room temperature.

b) Nafion-coated Pt/C Electrodes

In order to obtain a well dispersed ink with a uniform coating of catalyst on the electrode substrate and to avoid the dissolution and detachment of catalyst during the experiments carried out in this work, the catalyst ink with I/C ratio of 0.5 was selected as the base catalyst to prepare Nafion-coated Pt/C electrodes. In this study, different amounts (i.e., 3 μL and 10 μL) of 5 wt% Nafion-ionomer were applied on the air-dried Pt/C electrodes with I/C 0.5, which were subsequently left to dry for approximately 24 hours at room temperature.

c) Preparation of Ni Exposed Pt/C Electrodes

In order to evaluate the effect of Ni solution contaminants on the Pt/C electrodes, the experiment was designed to allow the Ni solution to diffuse through Nafion-ionomer and Pt/C catalyst. This was done by immersing the electrochemically cleaned electrodes (described in section 5.2.3) in 0.2 M $NiSO_4$ (Alfa Aesar, 99%) containing 0.5 M H_2SO_4 (Fisher Scientific, ACS grade, 98%) for approximately 48 hours at open circuit potential.

5.2.2 Electrochemical Cell

A two-compartment electrochemical glass cell was used during the electrochemical measurements. A glassy carbon disk electrode used as a substrate to

apply the catalyst ink was employed as the working electrode. A large surface area of Pt mesh was used as the counter electrode. A saturated calomel electrode (SCE) used as the reference electrode was placed in the reference compartment, which was connected through a Luggin capillary to the main compartment. All potentials reported in this study are referred to a reversible hydrogen electrode (RHE).

5.2.3 Electrochemical Measurements

Prior to each electrochemical measurement, the Pt/C electrodes were cleaned electrochemically by scanning the potential between 0.08 and 1.28 V at a scan rate of 100 mV s^{-1} in 0.5 M H_2SO_4 for approximately 10 cycles. The number of cycles and potential window were limited in order to avoid the degradation of Pt/C catalysts. Before each electrochemical measurement, the electrolyte solution was purged with argon (purity grade 5.0) for a minimum of 30 minutes to remove dissolved oxygen.

In order to evaluate the influence of Ni solution contaminants on the voltammetric properties of various Pt/C electrodes, cyclic voltammetry measurements were conducted on the unexposed and Ni exposed Nafion-incorporated and Nafion-coated Pt/C electrodes in metal-free Ar-saturated 0.5 M H_2SO_4 solutions. The cyclic voltammograms (CVs) were recorded by scanning the potential between 0.08 and 1.28 V at a scan rate of 20 mV s^{-1}.

In order to characterize the effect of Ni solution contaminants on the MOR activities of various Pt/C electrodes, the MOR voltammetry was conducted on the unexposed and Ni exposed Pt/C electrodes in the metal-free and 0.2 M nickel sulfate

containing 0.5 M CH_3OH (Fisher Scientific, 99.9 %) + 0.5 M H_2SO_4 solution, respectively. The MOR voltammetries were conducted between 0.08 and 1 V at 20 mV s^{-1}.

To further evaluate the effect of Ni solution contaminants on the MOR mechanism on various Pt/C electrodes, the EIS measurements were conducted on the unexposed and Ni exposed Pt/C electrodes in metal-free and 0.2 M nickel sulfate containing 0.5 M H_2SO_4 + 0.5 M CH_3OH solutions, respectively. In order to conduct the EIS measurement, the Pt/C electrodes were held at a specific potential, (E= 0.58 – 0.78 V), for 30 minutes to obtain a quasi-steady state current. The impedance spectra were recorded immediately after, by sweeping the frequency from 100 kHz to 0.1 Hz under the specific constant potential with a root mean square (rms) amplitude of 10 mV.

Voltammetric measurements were carried out using a Solartron Analytical 1285 potentiostat controlled with Corrware software (v. 3.1c, Scribner Associates Inc.). The EIS measurements were conducted with a Solartron 1260 frequency response analyzer and Solartron 1285 potentiostat controlled by ZPlot software (v. 3.3c, Scribner Associates Inc.). The impedance data were fitted to an appropriate equivalent circuit using ZView impedance simulation software (Scribner Associates Inc). Throughout all experiments, the electrochemical cell was placed in a grounded Faraday cage to isolate any potential electrical noise and/or vibration affecting the electrochemical measurements.

5.3 Results and Discussion

5.3.1 Cyclic Voltammetries of Unexposed and Ni Exposed Pt/C Electrodes

In order to understand the effect of Ni solution contaminants on the voltammetric properties of Pt/C catalysts with various Nafion-ionomer distributions and contents, cyclic voltammetry was conducted on the unexposed and Ni exposed Nafion-incorporated and Nafion-coated Pt/C electrodes. Figure 5-1 (black curves) shows the CVs of unexposed Pt/C electrodes. The results show a typical characteristic behavior of Pt/C catalyst in 0.5 M H_2SO_4 solution, where hydrogen adsorption-desorption ($H_{ads/des}$) peak currents occur at lower potential (~ 0.08 - 0.28 V) followed by Pt-OH/Pt-O formation and reduction peak currents at more positive potential (~ 0.78 - 1.28 V). The electrochemical surface area (ECSA) of Pt/C catalysts was further obtained from hydrogen underpotential deposition, assuming a Coulombic charge of 210 μC cm_{Pt}^{-2}. The results are presented in Table 5-1.

CVs of unexposed Nafion-incorporated Pt/C catalysts with I/C ratios of 0.5 and 2.2 are respectively shown in Figure 5-1a and Figure 5-1b (black curves). The results show a slight increase in $H_{ads/des}$ peak currents with no onset potential shift in Pt-OH formation as the Nafion-ionomer content increased. The data presented in Table 5-1 also show an increase in the ECSA value for the Pt/C catalyst with higher Nafion-ionomer content. The smaller ECSA of the Pt/C catalyst with I/C of 0.5 may be attributed to the insufficient Nafion-ionomer content in the catalyst, resulting in a decrease in the available Pt active sites. Similar results were previously reported in the

literature, in which the ECSA of electro-catalyst increased with increasing Nafion-ionomer to an optimum content, while further increase in Nafion beyond this optimum content resulted in a decrease in the ECSA of electro-catalyst [21, 22].

CVs of unexposed Nafion-coated Pt/C catalysts with 3 and 10 μL applied Nafion-ionomer are respectively shown in Figure 5-1c and Figure 5-1d (black curves). The results show that the increase in the applied Nafion-ionomer content (i.e., at 10 μL) resulted in a decrease in $H_{ads/des}$ and Pt-OH formation/reduction peak currents. This is also confirmed by the ECSA data presented in Table 5-1, showing a decrease in ECSA value when Nafion content increased. This may be due to an increase in the Nafion thickness and/or Nafion agglomeration, which may hinder the proton access to the Pt active sites. Similar blocking impact of Nafion-ionomer on the Pt sites was previously reported in the literature, showing a decrease in the ECSA with the increase in the Nafion-ionomer content [23–25].

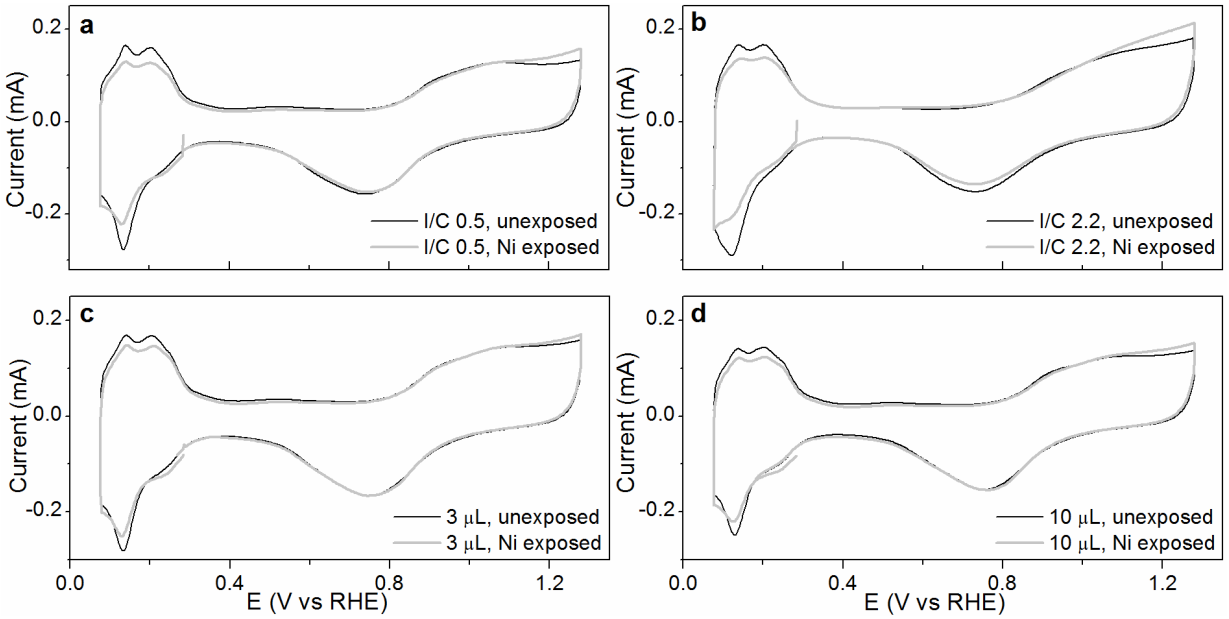

Figure 5-1: Cyclic voltammograms of unexposed (black curves) and Ni exposed (gray curves): a) Nafion-incorporated Pt/C electrodes with I/C = 0.5., b) Nafion-incorporated Pt/C electrodes with 2.2., c) Nafion-coated Pt/C electrodes with 3 µL applied Nafion-ionomer., d) Nafion-coated Pt/C electrodes with 10 µL applied Nafion-ionomer. All CVs were obtained at a scan rate of 20 mV s^{-1}.

Table 5-1. ECSA of various Pt/C electrodes

	Nafion-incorporated Pt/C electrodes				Nafion-coated Pt/C electrodes			
Electrode	I/C 0.5		I/C 2.2		3µL		10 µL	
	ECSA (m^2 gr^{-1})	Percent loss	ECSA (m^2 gr^{-1})	Percent loss	ECSA (m^2 gr^{-1})	Percent loss	ECSA (m^2 gr^{-1})	Percent loss
Unexposed electrode	101 ± 1.8	-	110 ± 1.3	-	103 ± 1.7	-	94 ± 1.2	-
Ni exposed electrode	87 ± 4.3	13.8 %	88 ± 2.5	20.0 %	98 ± 2.3	4.8 %	89 ± 2.2	5.3 %
CV-recovered electrode	94 ± 3.8	6.9 %	103 ± 4.5	6.4 %	100 ± 2.5	2.9 %	92 ± 1.6	2.1 %

Figure 5-1 (gray curves) shows the CVs of Ni exposed Nafion-incorporated and Nafion-coated Pt/C electrodes. The overall voltammogram results of all Ni exposed Pt/C electrodes show a decrease in $H_{ads/des}$ peak currents with no onset potential shift in Pt-OH formation, as compared to the unexposed condition. The percent loss in the ECSA values after Ni solution exposure of all Pt/C electrodes are presented in Table 5-1. The results show a higher decrease in the ECSA of Nafion-incorporated Pt/C electrodes after Ni solution exposure (approximately 13.8 to 20 %) as compared to the Ni exposed Nafion-coated Pt/C electrodes (approximately 4.8 to 5.3 %). Based on these results, it appears that the presence of Nafion-ionomer film (in case of the Nafion-coated Pt/C electrodes) may partially prevent the negative effect of Ni solution contaminants on the Pt active sites. A similar result was previously reported in chapter 4. The results showed a significant decrease in the voltammetric properties of bare Pt electrode after Ni solution exposure as compared to the Ni exposed Nafion-coated Pt electrode.

The recovery of various Pt/C catalysts after Ni solution exposure was further examined by conducting cyclic voltammetry (i.e., CV-recovery) on Ni exposed Pt/C electrodes at potential range of 0.08 – 1.28 V in Ni-free 0.5 M H_2SO_4 for 8 cycles. The results are presented in Table 5-1. A slightly higher recovery was obtained for the Ni exposed Nafion-coated Pt/C electrodes as compared to the Ni exposed Nafion-incorporated Pt/C electrodes. This may be due to the presence of Nafion film, which may help to diminish the Pt dissolution. Based on these results, it appears that the Pt dissolution and/or decrease in durability of Pt/C catalysts may slightly influence the

overall electro-catalytic activity of Ni exposed Pt/C electrodes.

5.3.2 MOR Voltammetries of Unexposed and Ni Exposed Pt/C Electrodes

To further understand the effect of Ni solution contaminants on the MOR activity of Pt/C catalysts with various Nafion-ionomer distributions and contents, the MOR voltammetry was conducted on the unexposed and Ni exposed Nafion-incorporated and Nafion-coated Pt/C electrodes. Figure 5-2 (black curves) shows a typical MOR voltammogram for all unexposed Pt/C electrodes, in which the MOR onset potential appears at ~ 0.5 - 0.6 V, followed by a fully developed oxidation peak at approximately 0.86 V. The results further show a decrease in the MOR anodic peak current density as the Nafion-ionomer content increased in both unexposed Nafion-incorporated and Nafion-coated Pt/C electrodes. The increase in Nafion-ionomer content may result in a sluggish CH_3OH diffusion to and CO_2 removal from the Pt active sites [2,22, 26, 27]. Moreover, Figure 5-2c (black curve) shows an increase in the MOR anodic peak current density for the unexposed Nafion-coated Pt/C electrode with 3 μL applied Nafion-ionomer, as compared to the base Pt/C electrode (shown in Figure 5-2a, black curve). The increase in the MOR activity may be attributed to the partial penetration of Nafion-ionomer film into the base Pt/C catalyst, which may enhance CH_3OH transport to the Pt active sites [28].

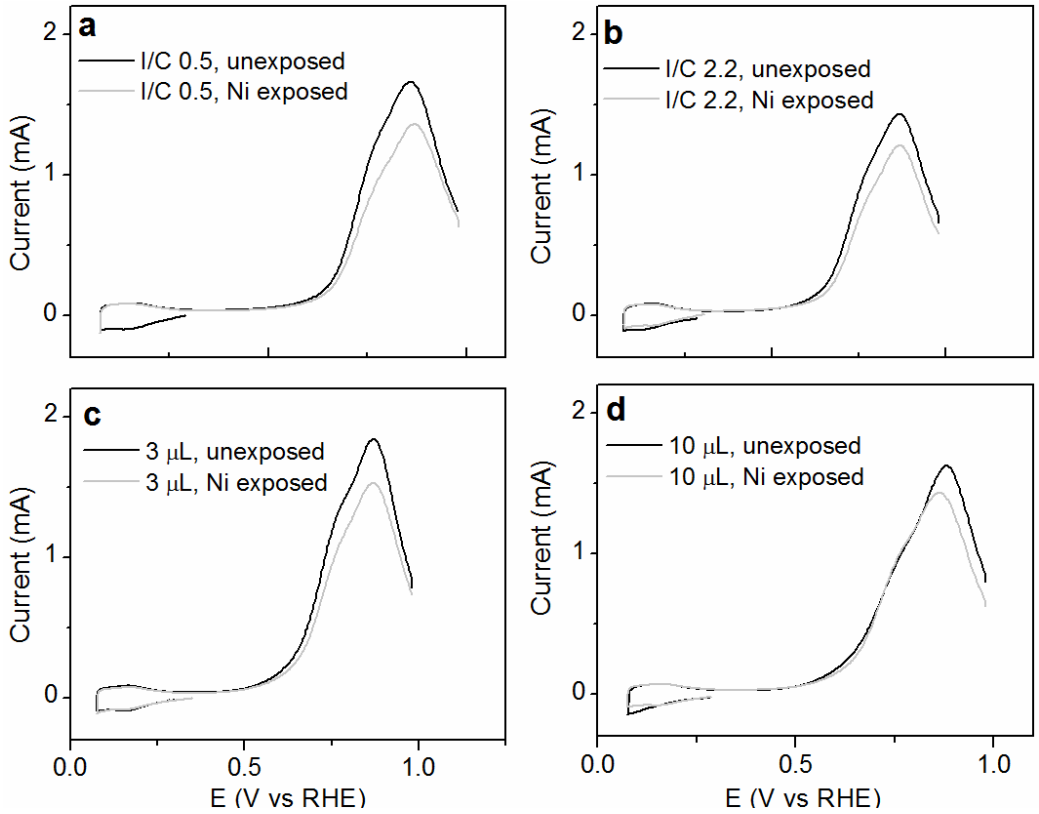

Figure 5-2: MOR voltammograms of unexposed (black curves) and Ni exposed (gray curves): a) Nafion-incorporated Pt/C electrode with I/C = 0.5., b) Nafion-incorporated Pt/C electrode with I/C = 2.2., c) Nafion-coated Pt/C electrode with 3 μL applied Nafion-ionomer., d) Nafion-coated Pt/C electrode with 10 μL applied Nafion-ionomer. All CVs were obtained at a scan rate of 20 mV s^{-1}.

Figure 5-2 (gray curves) shows the MOR voltammograms of Ni exposed Nafion-incorporated and Nafion-coated Pt/C electrodes. The results show a relatively similar decrease in the MOR anodic peak current density (approximately 12 to 18%) after Ni solution exposure of all Pt/C electrodes as compared to the unexposed condition. These results are inconsistent with the results obtained during the background voltammetry measurements (presented in section 5.3.1), where Ni solution contaminants showed a stronger negative effect on the voltammetric properties of Nafion-incorporated Pt/C electrodes as compared to Nafion-coated Pt/C electrodes.

5.3.3 Electrochemical Impedance Spectroscopy (EIS) of CH_3OH Oxidation Reaction

As it is known, EIS can separate multistep electrochemical reactions over a wide frequency range. The EIS analysis of MOR (referred to as Nyquist plot) shows different behavior at different applied potentials [29-32]. In this study, the EIS was used to analyze the effect of Ni solution contaminants on the intrinsic properties of Pt/C catalysts with various Nafion-ionomer distributions and contents during the MOR. The EIS measurements were conducted within potential ranges of 0.58 and 0.78 V. Equivalent circuit models presented in Figure 5-3 are further used to analyze Nyquist plots obtained at different applied potentials. The following sections present the EIS results for unexposed and Ni exposed Nafion-incorporated and Nafion-coated Pt/C electrodes at different applied potentials.

(a) (b)

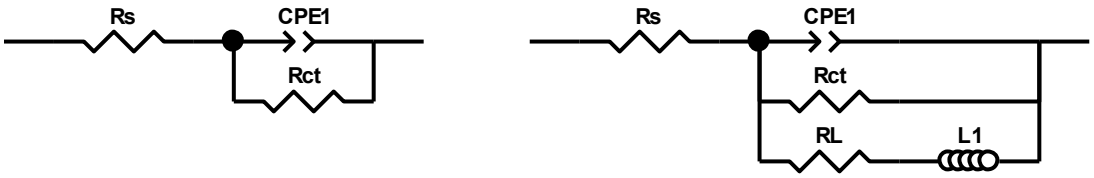

Figure 5-3: Equivalent circuits used to fit the Nyquist plots of CH_3OH oxidation reaction on Pt/C electrodes.

EIS at 0.58 V_{RHE}:

Figure 5-4 shows the Nyquits plots of unexposed and Ni exposed Nafion-incorporated and Nafion-coated Pt/C electrodes at E = 0.58 V. A large arc in the first quadrant of the Nyquist plot was observed for all cases. This behavior may be associated with the slow CH_3OH adsorption-dehydrogenation, which can result in the formation of adsorbed CO (CO_{ads}), subsequently blocking the Pt active sites from further CH_3OH adsorption [29,30,33]. As shown in Figure 5-4 (gray circle), a similar arc behavior can be observed for all Ni exposed Pt/C electrodes as compared to the unexposed condition. The results show an increase in the arc diameter after Ni solution exposure of Nafion-incorporated Pt/C electrodes as Nafion-ionomer content increased, while this change is insignificant for the Ni exposed Nafion-coated Pt/C electrodes.

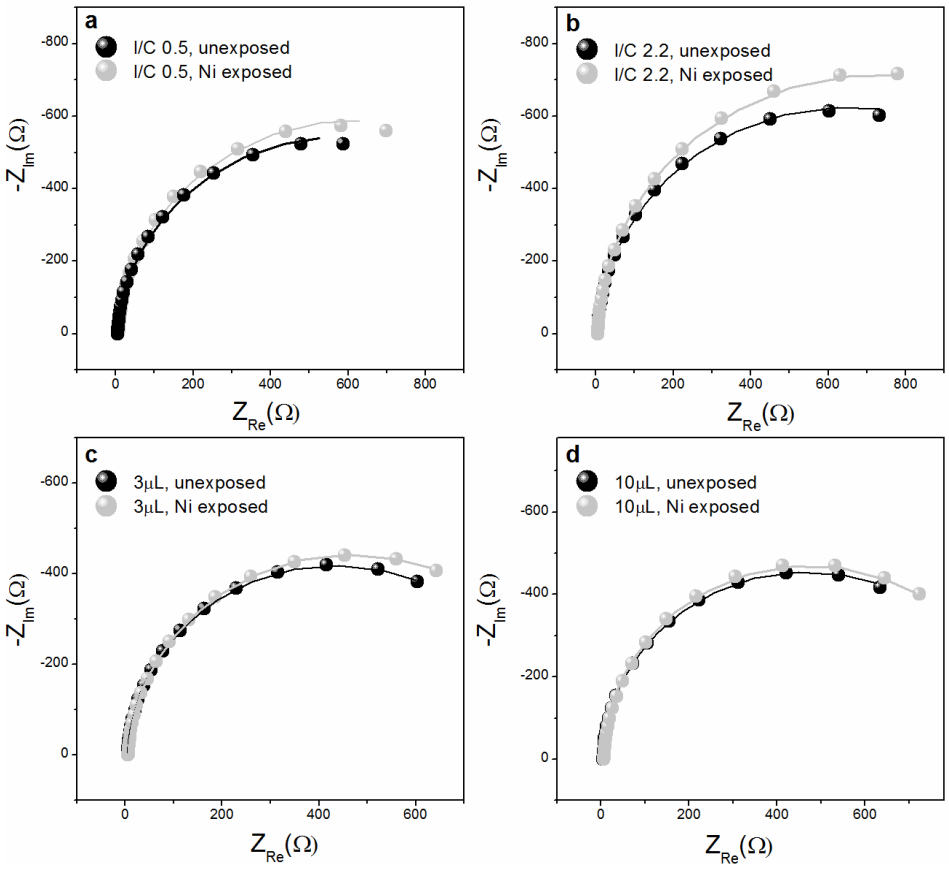

Figure 5-4: Nyquist plots of unexposed (black circle) and Ni exposed (gray circle): a) Nafion-incorporated Pt/C electrode with I/C = 0.5., b) Nafion-incorporated Pt/C electrode with I/C = 2.2., c) Nafion-coated Pt/C electrode with 3 μL applied Nafion-ionomer., d) Nafion-coated Pt/C electrode with 10 μL applied Nafion-ionomer. The EIS was obtained at 0.58 V.

In order to analyze the Nyquist plots at this potential, the equivalent circuit shown in Figure 5-3a is used to fit the data. In this circuit, the R_s is the solution resistance, which represents the sum of electrolyte and Nafion-ionomer resistance. A pure double layer capacitance is replaced with constant phase element (CPE) and R_{ct} represents the charge transfer resistance of CH_3OH adsorption-dehydrogenation [30]. The fitted parameters of equivalent circuit are summarized in Table 5-2. As presented, the R_{ct} values of the unexposed Nafion-coated Pt/C electrodes are smaller as compared

to the unexposed Nafion-incorporated Pt/C electrodes. This behavior may be due to the partial Nafion-ionomer film penetration into porous structure of Pt/C catalyst layer, which may facile CH_3OH transport to the Pt active sites. As expected from Nyquist plots and confirmed by fitted data presented in Table 5-2, the R_{ct} value of Ni exposed Nafion-incorporated Pt/C increases with increasing Nafion-ionomer content from I/C = 0.5 to 2.2, as compared to the unexposed condition. However, the increase in R_{ct} value is insignificant for the Ni exposed Nafion-coated Pt/C electrodes. Based on these observations, it appears that Nafion-ionomer film may inhibit the negative influence of Ni solution contaminants on the Pt active sites, resulting in insignificant change on the CH_3OH adsorption-dehydrogenation.

Table 5-2. Fitting parameters obtained from the Nyquist plot at E = 0.58 V shown in Figure 5-4.

Sample		R_s (Ω)	CPE1-T (F)	CPE1-P (F)	R_{ct} (Ω)
Nafion-incorporated Pt/C	I/C 0.5, unexposed	5.2	0.0015	0.97	1146
	I/C 0.5, Ni exposed	5.3	0.0012	0.97	1235
	I/C 2.2, unexposed	5.1	0.0011	0.98	1209
	I/C 2.2, Ni exposed	5.3	0.00099	0.99	1370
Nafion-coated Pt/C	3 µL, unexposed	5.2	0.0012	0.98	860
	3 µL, Ni exposed	5.7	0.0012	0.97	924
	10 µL, unexposed	5.2	0.0012	0.98	925
	10 µL, Ni exposed	5.9	0.00097	1.00	935

EIS at 0.68 V_{RHE}:

Figure 5-5 shows the Nyquist plots of unexposed and Ni exposed Nafion-incorporated and Nafion-coated Pt/C electrodes at E= 0.68 V. The results show a similar arc behavior for the Nyquist plots of all unexposed and Ni exposed Pt/C electrodes, in which a capacitive arc appears at high frequency followed by an inductive semicircle in the fourth quadrant at low frequency. The inductive behavior is a well-known characteristic for the reactions involving a strong adsorbed intermediate (i.e., strong CO_{ads} coverage) [34, 35]. As the applied potential increases, the oxidation removal of CO_{ads} by OH_{ads} (formed through H_2O dissociative-adsorption) becomes more accelerated, resulting in more Pt active sites available for the subsequent CH_3OH adsorption-dehydrogenation and formation of CO_{ads}. As the strong CO_{ads} coverage responds slowly to the alternating applied potential, it may lead to a delay between potential perturbation and the resulting alternative current, which may result in the appearance of pseudo-inductive behavior at low frequency [32].

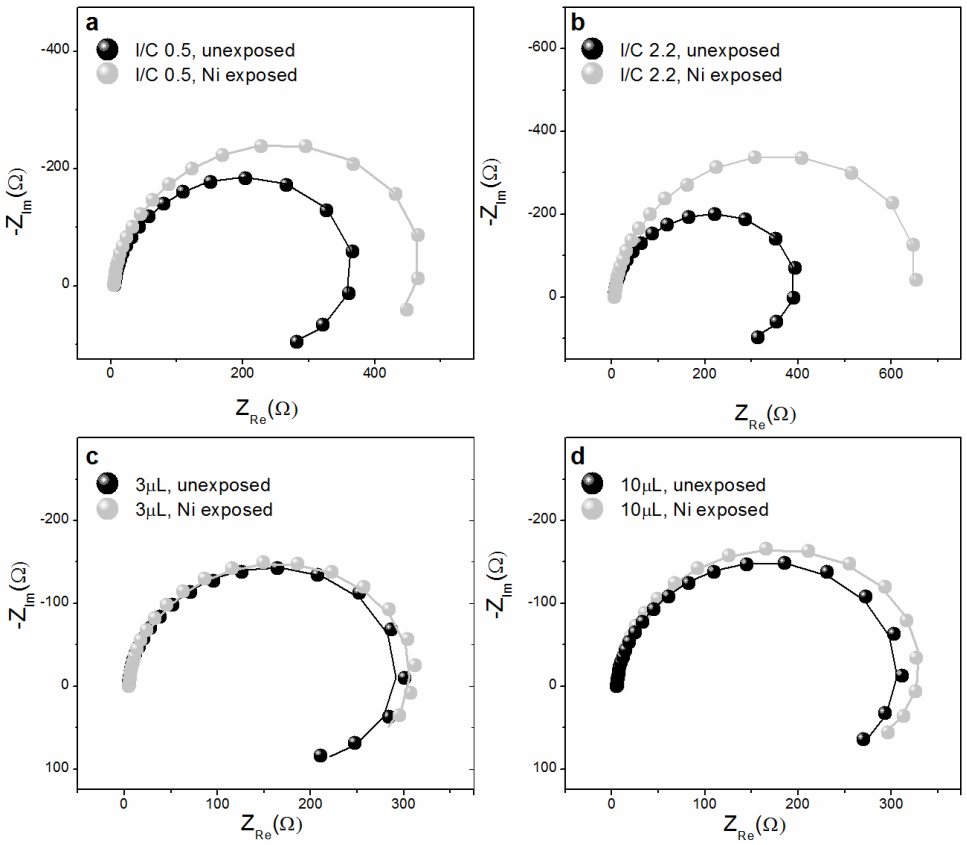

Figure 5-5: Nyquist plots of unexposed (black circle) and Ni exposed (gray circle): a) Nafion-incorporated Pt/C electrode with I/C = 0.5., b) Nafion-incorporated Pt/C electrode with I/C = 2.2., c) Nafion-coated Pt/C electrode with 3 µL applied Nafion-ionomer., d) Nafion-coated Pt/C electrode with 10 µL applied Nafion-ionomer. The EIS was obtained at 0.68 V.

After Ni solution exposure, the Nyquist plots of Ni exposed Nafion-incorporated Pt/C electrodes (shown in Figure 5-5a and Figure 5-5b, gray circles) show a significant increase in the arc diameter as compared to the unexposed condition. However, this increase in the arc diameter is insignificant for the Nyquist plots of Ni exposed Nafion-coated Pt/C electrodes (shown in Figure 5-5c and Figure 5-5d, gray circles) as compared to the unexposed Nafion-coated Pt/C electrodes. To further analyze the Nyquist plots at this potential, the equivalent circuit shown in Figure 5-3b is used to fit the data. In this circuit, the R_{ct} is the charge transfer resistance, L represents the inductance and R_L is

the inductance resistance, which is used to adjust the phase-delay due to the CO_{ads} coverage relaxation process [34,36]. Results are presented in Table 5-3. As shown, the R_{ct} values are smaller in the presence of unexposed Nafion-coated Pt/C electrodes as compared to the unexposed Nafion-incorporated Pt/C electrodes. This result is consistent with the data obtained at lower potential range (i.e., 0.58 V). As expected from the Nyquist plot, the R_{ct} values significantly increase after Ni solution exposure of Nafion-incorporated Pt/C electrodes, while minor changes were observed for the Ni exposed Nafion-coated Pt/C electrodes. This behavior may indicate a decrease in the oxidative removal rate of CO_{ads}, due to the sluggish formation of OH_{ads} through H_2O dissociative-adsorption after Ni solution exposure of Nafion-incorporated Pt/C electrodes. The insignificant change in R_{ct} values after Ni solution exposure of Nafion-coated Pt/C electrode may be attributed to the presence of a continuous network of Nafion-ionomer film on the electrode surface, which may be formed due to the insufficient penetration of Nafion-ionomer through the thickness of Pt/C catalyst layer. This Nafion-ionomer film may play as a barrier to protect the Pt active sites from the negative impact of Ni solution contaminants. A similar trend was previously reported in chapter 4, where a smaller negative effect of Ni solution contaminants on the Nafion-coated Pt electrode was observed as compared to the bare Pt electrode.

Table 5-3. Fitting parameters obtained from the Nyquist plot at E = 0.68 V shown in Figure 5-5.

Sample		R_s (Ω)	CPE1-T (F)	CPE1-P (F)	R_{ct}(Ω)	R_L(Ω)	L(H)
Nafion-incorporated Pt/C	I/C 0.5, unexposed	5.5	0.00142	0.93	442	185	648
	I/C 0.5, Ni exposed	5.7	0.00119	0.94	544	354	1437
	I/C 2.2, unexposed	5.2	0.00131	0.93	482	218	750
	I/C 2.2, Ni exposed	6.0	0.00103	0.95	776	541	2412
Nafion-coated Pt/C	3 µL, unexposed	5.1	0.00128	0.94	323	129	587
	3 µL, Ni exposed	5.5	0.00106	0.95	326	216	1244
	10 µL, unexposed	5.6	0.00138	0.95	330	136	873
	10 µL, Ni exposed	5.9	0.00099	0.96	353	249	1067

EIS at 0.78 V_{RHE}:

Figure 5-6 shows the Nyquist plots of unexposed and Ni exposed Nafion-incorporated and Nafion-coated Pt/C electrodes at E= 0.78 V. The results show that the Nyquist plot appeared at the second and third quadrants at high and low frequency, respectively. The negative impedance observed in the Nyquist plot is described as hidden negative impedance, as the voltammogram has a positive slope at this potential [37,38]. As the potential increases, the reaction rates of CH_3OH dehydrogenation and CO_{ads} oxidation becomes faster, hence the formation and removal of the reaction intermediate (CO_{ads}) approach to each other. At more positive potential, the formation of OH_{ads} through H_2O dissociative-adsorption becomes faster, which may accelerate the CO_{ads} oxidation rate and inhibit further CH_3OH adsorption-dehydrogenation. Based on previous study, the appearance of negative impedance at high frequency is associated with the rapid OH_{ads} formation on the Pt active sites [39]. Sweeping the frequency to a lower range leads to the slow CO_{ads} coverage formation, resulting in a positive impedance. However, the positive impedance at lower frequency cannot be observed in this study, as the lowest frequency used is 0.1 Hz.

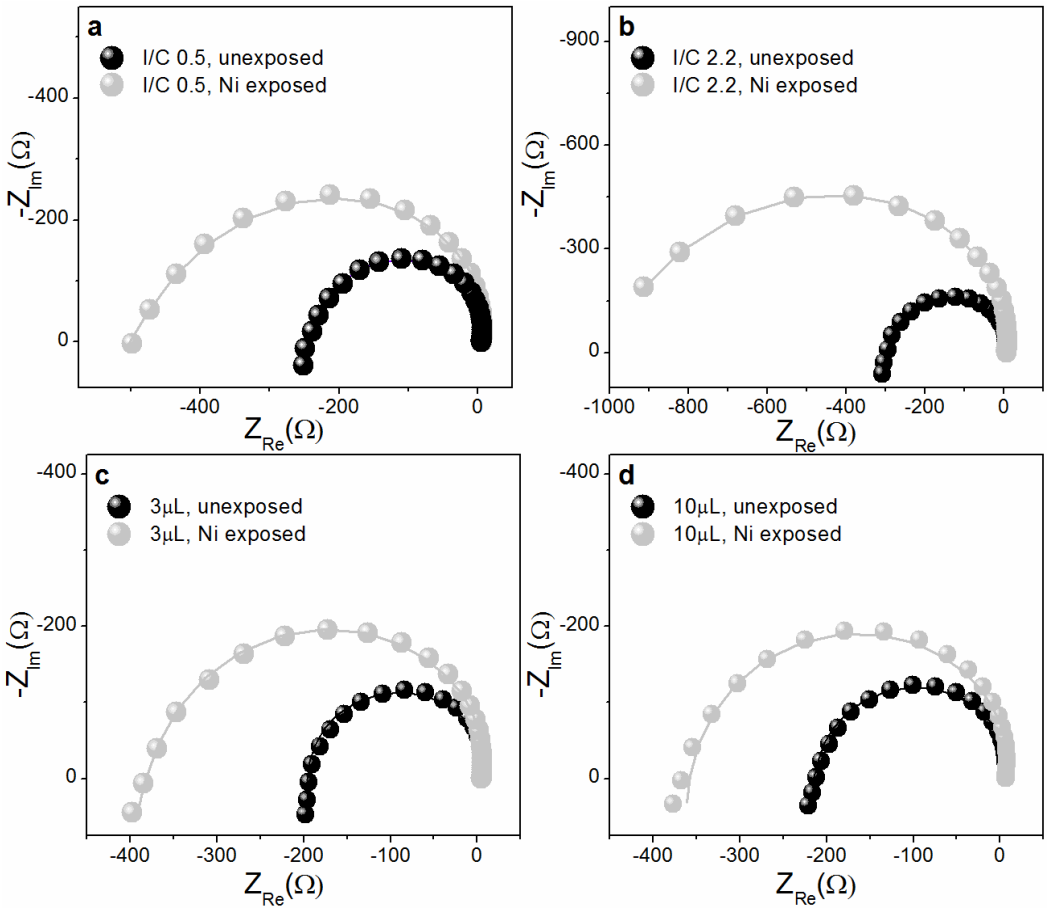

Figure 5-6: Nyquist plots of unexposed (black circle) and Ni exposed (gray circle): a) Nafion-incorporated Pt/C electrode with I/C = 0.5., b) Nafion-incorporated Pt/C electrode with I/C = 2.2., c) Nafion-coated Pt/C electrode with 3 μL applied Nafion-ionomer., d) Nafion-coated Pt/C electrode with 10 μL applied Nafion-ionomer. The EIS was obtained at 0.78 V.

As shown in Figure 5-6 (gray circle), an increase in arc diameter can be observed for the Nyquist plots of Ni exposed Nafion-incorporated and Nafion-coated Pt/C electrodes as compared to the unexposed condition. However, this increase in arc diameter is more significant for the Ni exposed Nafion-incorporated Pt/C electrodes as compared to the Ni exposed Nafion-coated Pt/C electrodes.

To further analyze the Nyquist plots at this potential, the equivalent circuit shown in Figure 5-3b is used to fit the data. The corresponding fitted data are summarized and presented in Table 5-4. As expected from the sudden change in the Nyquist plots behavior at this potential, the results show a negative R_{ct} value for the unexposed and Ni exposed Pt/C electrodes. The results also show a significant increase in the R_{ct} values after Ni solution exposure of Nafion-incorporated Pt/C electrodes as compared to Ni exposed Nafion-coated Pt/C electrodes. This indicates that Ni solution contaminants can significantly lower the H_2O dissociative-adsorption rate, resulting in the lower OH_{ads} formation on the Nafion-incorporated Pt/C electrodes.

Based on the EIS results presented in this section, it appears that R_{ct} values are smaller in the presence of unexposed Nafion-coated Pt/C electrodes as compared to the Nafion-incorporated Pt/C electrodes. This behavior may be associated with the partial penetration of Nafion-ionomer film in the Pt/C catalyst, resulting in a facile CH_3OH transport to the Pt active sites. The EIS results also reveal that the R_{ct} values significantly increased after Ni solution exposure of Nafion-incorporated Pt/C electrodes as compared to the Ni exposed Nafion-coated Pt/C electrodes. This result

indicates that the presence of Nafion-ionomer film may partially diminish the negative effect of Ni solution contaminants on the Nafion-coated Pt/C electrodes. This behavior may be associated with the sulfonate group of Nafion-ionomer film, which may attract the Ni cations and localize them away from the Pt active sites, eventually suppressing the poisoning effect of Ni solution contaminants on the electro-catalytic activities of Nafion-coated Pt/C electrodes.

Table 5-4. Fitting parameters obtained from the Nyquist plot at E = 0.78 V shown in Figure 5-6.

Sample		R_s (Ω)	CPE1-T (F)	CPE1-P (F)	R_{ct} (Ω)	R_L(Ω)	L(H)
Nafion-incorporated Pt/C	I/C 0.5, unexposed	4.7	0.00143	0.89	-216	218	907
	I/C 0.5, Ni exposed	5.2	0.00128	0.89	-377	462	1442
	I/C 2.2, unexposed	4.9	0.00116	0.92	-276	178	1110
	I/C 2.2, Ni exposed	5.5	0.00097	0.94	-802	879	4203
Nafion-coated Pt/C	3 µL, unexposed	5.4	0.00141	0.88	-185	97	764
	3 µL, Ni exposed	5.5	0.00117	0.90	-286	288	1302
	10 µL, unexposed	6.0	0.00116	0.90	-204	163	1047
	10 µL, Ni exposed	6.2	0.00105	0.91	-254	175	1255

5.4 Conclusions

In order to understand of the effect of Ni solution contaminants on the anode electro-catalyst of DMFC, a systematic study was conducted on Nafion-incorporated and Nafion-coated Pt/C electrodes with different Nafion-ionomer contents. Cyclic voltammetry was conducted in order to evaluate the voltammetric properties of various unexposed and Ni exposed Pt/C electrodes. The results showed a higher decrease in the voltammetric properties (including ECSA) of Nafion-incorporated Pt/C after Ni solution exposure, as compared to Ni exposed Nafion-coated Pt/C electrodes. The MOR voltammetries of unexposed and Ni exposed Pt/C electrodes were further obtained. The results showed a similar decrease in the MOR activity of all Pt/C electrodes after Ni solution exposure as compared to the unexposed condition.

The EIS measurement was further conducted at potential range of 0.58 - 0.78 V to examine the effect of Ni solution contaminants on the intrinsic properties of Nafion-incorporated and Nafion-coated Pt/C electrodes during the MOR. The EIS results obtained at lower potential (E = 0.57 V) showed an increase in the R_{ct} value of Ni exposed Nafion-incorporated Pt/C as Nafion-ionomer content increased (from I/C = 0.5 to 2.2), indicating a decrease in CH_3OH adsorption-dehydrogenation, as compared to the Ni exposed Nafion-coated Pt/C electrodes. At more positive potentials (E = 0.68 - 0.78 V), the results showed a significant increase in R_{ct} values in the presence of Ni exposed Nafion-incorporated Pt/C electrodes, indicating a decrease in H_2O dissociative-adsorption rate, while this change in R_{ct} values is smaller for the Nafion-coated Pt/C

electrodes after Ni solution exposure.

Based on the background voltammetry and EIS measurements, the results showed a smaller poisoning effect of Ni solution contaminants on the Nafion-coated Pt/C as compared to the Nafion-incorporated Pt/C electrodes. This behavior may indicate that the presence of Nafion-ionomer film can play as a barrier for the Ni solution contaminants, partially inhibiting the negative effect of Ni contaminants on the Pt active sites. This may be attributed to the interaction of Ni cations with negatively charged sulfonate sites of Nafion-ionomer film, which may repel the cations away from the Pt active sites. This may result in a smaller Ni poisoning effect on the activity of Nafion-coated Pt/C electrodes as compared to Nafion-incorporated Pt/C electrodes. Contradictory results were observed in the MOR voltammetry performed as part of this study, which showed a similar decrease in MOR activities after Ni solution exposure of Nafion-incorporated and Nafion-coated Pt/C electrodes.

5.5 References

[1] S.K. Kamarudin, F. Achmad, W.R.W. Daud, Overview on the application of direct methanol fuel cell (DMFC) for portable electronic devices, Int. J. Hydrogen Energy. 34 (2009) 6902–6916. doi:10.1016/j.ijhydene.2009.06.013.

[2] X. Zhao, X. Fan, S. Wang, S. Yang, B. Yi, Q. Xin, G. Sun, Determination of ionic resistance and optimal composition in the anodic catalyst layers of DMFC using AC impedance, Int. J. Hydrogen Energy. 30 (2005) 1003–1010. doi:10.1016/j.ijhydene.2005.01.006.

[3] J.W. Guo, X.F. Xie, J.H. Wang, Y.M. Shang, Effect of current collector corrosion made from printed circuit board (PCB) on the degradation of self-breathing direct methanol fuel cell stack, Electrochim. Acta. 53 (2008) 3056–3064. doi:10.1016/j.electacta.2007.11.044.

[4] J. Wind, R. Späh, W. Kaiser, G. Böhm, Metallic bipolar plates for PEM fuel cells, J. Power Sources. 105 (2002) 256–260. doi:10.1016/S0378-7753(01)00950-8.

[5] L. Dubau, J. Durst, F. Maillard, L. Guétaz, M. Chatenet, J. André, E. Rossinot, Further insights into the durability of Pt3Co/C electrocatalysts: Formation of “hollow” Pt nanoparticles induced by the Kirkendall effect, Electrochim. Acta. 56 (2011) 10658–10667. doi:10.1016/j.electacta.2011.03.073.

[6] E. Antolini, J.R.C. Salgado, E.R. Gonzalez, The stability of Pt-M (M = first row transition metal) alloy catalysts and its effect on the activity in low temperature fuel cells. A literature review and tests on a Pt-Co catalyst, J. Power Sources. 160 (2006) 957–968. doi:10.1016/j.jpowsour.2006.03.006.

[7] F. Maillard, L. Dubau, J. Durst, M. Chatenet, J. André, E. Rossinot, Durability of Pt3Co/C nanoparticles in a proton-exchange membrane fuel cell: Direct evidence of bulk Co segregation to the surface, Electrochem. Commun. 12 (2010) 1161–1164. doi:10.1016/j.elecom.2010.06.007.

[8] E.A. Cho, U.S. Jeon, S.A. Hong, I.H. Oh, S.G. Kang, Performance of a 1 kW-class PEMFC stack using TiN-coated 316 stainless steel bipolar plates, J. Power Sources.

142 (2005) 177–183. doi:10.1016/j.jpowsour.2004.10.032.

[9] H. Tawfik, Y. Hung, D. Mahajan, Metal bipolar plates for PEM fuel cell-A review, J. Power Sources. 163 (2007) 755–767. doi:10.1016/j.jpowsour.2006.09.088.

[10] T. Okada, Y. Ayato, M. Yuasa, I. Sekine, The Effect of Impurity Cations on the Transport Characteristics of Perfluorosulfonated Ionomer Membranes, J. Phys. Chem. B. 103 (1999) 3315–3322. doi:10.1021/jp983762d.

[11] H.L. Yeager, A. Steck, Cation and Water Diffusion in Nation Ion Exchange Membranes : Influence of Polymer Structure, J. Electrochem. Soc. 128 (1981) 1880–1884. doi:10.1149/1.2127757.

[12] M. Sulek, J. Adams, S. Kaberline, M. Ricketts, J.R. Waldecker, In situ metal ion contamination and the effects on proton exchange membrane fuel cell performance, J. Power Sources. 196 (2011) 8967–8972. doi:10.1016/j.jpowsour.2011.01.086.

[13] K.A. Mauritz, R.B. Moore, State of understanding of Nafion, Chem. Rev. 104 (2004) 4535–4585. doi:10.1021/cr0207123.

[14] J.G. Goodwin Jr., K. Hongsirikarn, S. Greenway, S. Creager, Effect of cations (Na+, Ca2+, Fe3+) on the conductivity of a Nafion membrane, J. Power Sources. 195 (2010) 7213–7220. doi:10.1016/j.jpowsour.2010.05.005.

[15] T. Okada, H. Satou, M. Okuno, M. Yuasa, Ion and water transport characteristics of perfluorosulfonated ionomer membranes with H+ and alkali metal cations, J. Phys. Chem. B. 106 (2002) 1267–1273. doi:10.1021/jp013195l.

[16] Y. Legras, M.a, Hirata, Q.T. Nguyen, D. Langevin, M. Métayer, Sorption and diffusion behaviors of water in Nafion 117 membranes with different counter ions, Desalination. 147 (2002) 351–357. doi:10.1016/S0011-9164(02)00608-2.

[17] H.L. Yeager, A. Steck, Cation and water diffusion in nafion ion exchange membranes: Influence of polymer structure, J. Electrochem. Soc. 128 (1981) 1880–1884. doi:10.1149/1.2127757.

[18] S. Shi, A.Z. Weber, A. Kusoglu, STRUCTURE-TRANSPORT RELATIONSHIP OF PERFLUOROSULFONIC-ACID MEMBRANES IN DIFFERENT CATIONIC FORMS,

Electrochim. Acta. 220 (2016) 517–528.

[19] H. Li, K. Tsay, H. Wang, S. Wu, J. Zhang, N. Jia, S. Wessel, R. Abouatallah, N. Joos, J. Schrooten, Effect of Co2+on oxygen reduction reaction catalyzed by Pt catalyst, and its implications for fuel cell contamination, Electrochim. Acta. 55 (2010) 2622–2628. doi:10.1016/j.electacta.2009.12.037.

[20] J. Durst, M. Chatenet, F. Maillard, Impact of metal cations on the electrocatalytic properties of Pt/C nanoparticles at multiple phase interfaces, Phys. Chem. Chem. Phys. 14 (2012) 13000–13009. doi:10.1039/c2cp42191g.

[21] M.A. Abdelkareem, T. Tsujiguchi, N. Nakagawa, Effect of black catalyst ionomer content on the performance of passive DMFC, J. Power Sources. 195 (2010) 6287–6293. doi:10.1016/j.jpowsour.2010.04.070.

[22] J.H. Kim, H.Y. Ha, I.H. Oh, S.A. Hong, H.N. Kim, H.I. Lee, Electrochemical studies of DMFC anodes with different ionomer content, Electrochim. Acta. 50 (2004) 801–806. doi:10.1016/j.electacta.2004.02.069.

[23] A.M. Gomez-marin, A. Berna, J.M. Feliu, Spectroelectrochemical Studies of the Pt (111)/ Nafion Interface Cast Electrode, J. Phys. Chem. C. 114 (2010) 20130.

[24] S. Gottesfeld, S., Raistrick, I.D., Srinivasan, Oxygen Reduction Kinetics on a Platinum RDE Coated with a Recast Nafion Film, J. Electrochem. Soc. 134 (1987) 1455–1462. doi:10.1149/1.2100689.

[25] J. Chlistunoff, B. Pivovar, Effects of Ionomer Morphology on Oxygen Reduction on Pt, J. Electrochem. Soc. 162 (2015) F890–F900. doi:10.1149/2.0661508jes.

[26] B. Krishnamurthy, S. Deepalochani, K.S. Dhathathreyan, Effect of ionomer content in anode and cathode catalyst layers on direct methanol fuel cell performance, Fuel Cells. 8 (2008) 404–409. doi:10.1002/fuce.200800055.

[27] J.M. Sieben, M.M.E. Duarte, C.E. Mayer, Pt-Ru-supported electrodes deposited by multiple successive cycles of potentiostatic pulses: Evaluation of Nafion film effect on methanol oxidation, J. Solid State Electrochem. 14 (2010) 1555–1563. doi:10.1007/s10008-009-0972-5.

[28] Y.-S. Wu, R.-G. Wu, T.-K. Yeh, C.-H. Tsai, Y.-C. Su, F.-G. Tseng, Thickness Control

over Ionomer Coatings on Nano Patterned Three-Phase Zones for a Highly Efficient Electrode, J. Electrochem. Soc. 159 (2012) F242–F248. doi:10.1149/2.041207jes.

[29] W. Sugimoto, K. Aoyama, T. Kawaguchi, Y. Murakami, Y. Takasu, Kinetics of CH3OH oxidation on PtRu/C studied by impedance and CO stripping voltammetry, J. Electroanal. Chem. 576 (2005) 215–221. doi:10.1016/j.jelechem.2004.10.018.

[30] I.-M. Hsing, X. Wang, Y.-J. Leng, Electrochemical Impedance Studies of Methanol Electro-oxidation on Pt/C Thin Film Electrode, J. Electrochem. Soc. 149 (2002) A615–A621. doi:10.1149/1.1467940.

[31] D. Chakraborty, I. Chorkendorff, T. Johannessen, Electrochemical impedance spectroscopy study of methanol oxidation on nanoparticulate PtRu direct methanol fuel cell anodes: Kinetics and performance evaluation, J. Power Sources. 162 (2006) 1010–1022. doi:10.1016/j.jpowsour.2006.08.010.

[32] J.T. Müller, P.M. Urban, W.F. Hölderich, Impedance studies on direct methanol fuel cell anodes, J. Power Sources. 84 (1999) 157–160. doi:10.1016/S0378-7753(99)00331-6.

[33] X.H. Xia, T. Iwasita, F. Ge, W. Vielstich, Structural effects and reactivity in methanol oxidation on polycrystalline and single crystal platinum, Electrochim. Acta. 41 (1996) 711–718. doi:10.1016/0013-4686(95)00360-6.

[34] D.A. Harrington, B.E. Conway, ac Impedance of Faradaic reactions involving electrosorbed intermediates-I. Kinetic theory, Electrochim. Acta. 32 (1987) 1703–1712. doi:10.1016/0013-4686(87)80005-1.

[35] R.D. Armstrong, M. Henderson, Impedance plane display of a reaction with an adsorbed intermediate, J. Electroanal. Chem. 39 (1972) 81–90. doi:10.1016/S0022-0728(72)80477-7.

[36] Y.C. Liu, X.P. Qiu, W.T. Zhu, G.S. Wu, Impedance studies on mesocarbon microbeads supported Pt-Ru catalytic anode, J. Power Sources. 114 (2003) 10–14. doi:10.1016/S0378-7753(02)00527-X.

[37] F. Seland, R. Tunold, D.A. Harrington, Impedance study of formic acid oxidation on

platinum electrodes, Electrochim. Acta. 53 (2008) 6851–6864. doi:10.1016/j.electacta.2007.12.021.

[38] M.T.M. Koper, Non-linear phenomena in electrochemical systems, J. Chem. Soc. - Faraday Trans. 94 (1998) 1369–1378.

[39] R.E. Melnick, G.T.R. Palmore, Time-dependent impedance of the electro-oxidation of methanol on polished polycrystalline platinum, J. Phys. Chem. B. 105 (2001) 9449–9457. doi:10.1021/jp003106p.

6. Conclusions and Future Directions

6.1 Conclusions

Presented in this thesis is a systemic approach for characterizing the effect of metal solution contaminants on the electro-catalysts activities of DMFCs. First, the effect of metal solution contaminants (i.e., Co, Ni and Zn with sulfate and nitrate as counter-anions) on the polycrystalline Pt catalytic activities during the MOR and ORR was investigated. Secondly, the effect of Ni solution contaminants on the MOR activity of Nafion-coated Pt electrode as compared to the bare Pt electrode was investigated, in order to better understand the effect of metal solution contaminants on the Nafion-ionomer properties of anode electro-catalysts. Finally, the effect of Ni solution contaminants on the MOR activity of Nafion-incorporated and Nafion-coated Pt/C electrodes was evaluated to understand the effect of contaminants on the anode electro-catalyst with various Nafion-ionomer distributions and contents.

In chapter 3, the effect of various concentrations (i.e., $2x10^{-x}$ M (x=1-7)) of metal salt solutions (i.e., Co, Ni and Zn with sulfate and nitrate as counter-anions) and their corresponding counter-anions on the voltammetric properties and electro-catalytic activities of polycrystalline Pt during the MOR and ORR were investigated. The cyclic voltammetry measurements showed that the presence of 0.2 M metal sulfate (Co, Ni and Zn) and $Zn(NO_3)_2$ solutions resulted in the UPD of metal at lower potential ranges (~ 0.3 V >). However, scanning the potential to more positive range showed no significant change in the voltammetric properties of polycrystalline Pt as compared to the

voltammogram of Pt in the metal-free solutions. Furthermore, the cyclic voltammetry of polycrystalline Pt obtained in the presence of 0.2 M $Co(NO_3)_2$ and $Ni(NO_3)_2$ solutions showed a partial UPD of metal due to the concurrent reduction of nitrate counter-anions at lower potential ranges (~ 0.3 V >). The effect of various concentrations of metal solutions on the MOR activities of Pt and Pt_xRu_y was further investigated in chapter 3. Results showed a decrease in MOR peak current density as the concentration of metal solution increased. The MOR voltammetry was also obtained in the metal-free 0.4 M HNO_3 solution to better characterize the effect of counter-anion on the MOR activity of polycrystalline Pt. Results showed that a combined effect of adsorbed counter-anions and hydrated metal cations (located at OHP) may be responsible for the decrease in MOR activity of Pt. Finally, the effect of various concentrations of metal salt solutions on the ORR activity of Pt was investigated using RDE technique. Furthermore, the effect of counter-anions (from metal sulfate and metal nitrate) on the ORR activity of Pt was investigated. The results showed a combined effect of adsorbed counter-anions and metal cations may result in a decrease in ORR activity of Pt.

In chapter 4, the effect of Ni solution contaminants on the MOR activity and mechanism of Nafion-coated and bare Pt catalysts was systematically investigated using cyclic voltammetry and EIS measurements. The voltammetric properties of these electrodes were evaluated after Ni solution exposure. Results showed a significant decrease in $H_{ads/des}$ peak currents at lower potential range (< 0.3 V) and Pt-OH/Pt-O formation reduction peak current at more positive potential range (> 0.8 V) after Ni

exposure of bare Pt. However, a negligible effect of Ni solution was observed on the voltammetric properties of Nafion-coated Pt electrode. Furthermore, MOR voltammetry was conducted on the unexposed and Ni exposed Nafion-coated and bare Pt electrodes. The results showed a decrease in MOR activity of both Ni exposed electrodes. However, a slightly higher decrease was observed in the MOR activity of bare Pt electrode after Ni exposure as compared to Ni exposed Nafion-coated Pt electrode. The EIS measurement was conducted at various potential ranges (0.38 – 0.78 V) on the unexposed and Ni exposed Nafion-coated and bare Pt electrodes. The results showed an increase in R_{ct} values at various potential ranges in the presence of unexposed Nafion-coated Pt electrode as compared to the unexposed bare Pt electrode. This result indicates that the hydrophobic properties of Nafion-ionomer film may result in a decrease in methanol adsorption-dehydrogenation and H_2O dissociative-adsorption rate (subsequently leading to a decrease in the oxidative removal rate of CO_{ads}). After Ni solution exposure, the results showed a significant increase in the R_{ct} values of bare Pt electrode at more positive potential, E > 0.48 V. This result indicates that Ni solution contaminants have a significant poisoning effect on the Pt active sites, resulting in a decrease in H_2O dissociative-adsorption rate. Based on the cyclic voltammetry and EIS results, it appears that the presence of Nafion-ionomer film can play as a barrier for the Ni solution contaminants. This behavior may be attributed to the high affinity of the negatively charged sulfonate group of Nafion-ionomer towards higher valance cations, which can interact with the Ni cations, keeping some of these cations away from the Pt surface. Further, the recovery potential of Ni exposed electrode was investigated in this study.

The results showed a near complete recovery in the MOR activity of Ni exposed Nafion-coated Pt electrode, while only a partial recovery was obtained for the Ni exposed bare Pt electrode.

In chapter 5, the effect of Ni solution contaminants on Nafion-incorporated and Nafion-coated Pt/C electrodes with various Nafion-ionomer contents was investigated. In this study, Pt/C catalysts were selected to closely simulate the common anode electro-catalyst used in DMFC. Cyclic voltammetry and EIS measurements were utilized to conduct this study. According to the cyclic voltammetry measurements, a higher decrease in the voltammetric properties of Nafion-incorporated Pt/C electrodes was observed after Ni solution exposure as compared to Ni exposed Nafion-coated Pt/C electrodes. The MOR voltammetry was further conducted on the unexposed and Ni exposed Pt/C electrodes. The results showed a similar decrease in MOR activity of all Pt/C catalysts after Ni solution exposure. The EIS measurements were conducted on unexposed and Ni exposed Pt/C electrodes at various potential ranges (0.58 – 0.78 V). The EIS results showed an increase in the R_{ct} value at lower potential range (0.58 V) after Ni exposure of Nafion-incorporated Pt/C electrodes, indicating a decrease in CH_3OH adsorption-dehydrogenation rate. At higher potential ranges (0.68 - 0.78 V), a significant increase in the R_{ct} values of Ni exposed Nafion-incorporated Pt/C was observed as compared to Ni exposed Nafion-coated Pt/C electrodes. This result may be associated with the decrease in the oxygenated species formation on the Nafion-incorporated Pt/C after Ni solution exposure, due to a decrease in H_2O dissociative-

adsorption rate. According to these results, it appears that Nafion-ionomer film may protect the Pt active site from the negative effect of Ni solution contaminants, resulting in a lower Ni contaminant effect on the electro-catalytic activity of Nafion-coated Pt/C electrodes.

6.2 Future Directions

Based on the results obtained through this study, our recommended future research is presented in the current section.

As shown in chapter 3, a combined effect of counter anions and metal cations appeared to be responsible for the decrease in MOR and ORR activities of Pt. In order to have a better understanding of the Pt interface in the presence of metal solution contaminants, well-defined Pt single crystal surfaces can be used to characterize the specific adsorption of counter-anions in the presence of metal cations. This understanding can be further expanded by characterizing a three-phase interface of single crystalline Pt interface with Nafion-ionomer in the presence of metal solution contaminants.

Through chapter 4, the effect of high concentrations of Ni solution contaminants on the Nafion-coated Pt electrode with 12 μm Nafion-ionomer film thickness was investigated. This study can be further expanded by analyzing the effect of various concentrations of metal solutions on the Nafion-coated Pt electrode with different Nafion-ionomer film thicknesses for a longer Ni solution exposure. This approach can help to have a better understanding regarding the role of Nafion-ionomer in the

presence of metal solution contaminants.

Through chapter 4, the recovery test of Ni exposed bare Pt electrodes was conducted as part of the research. The results showed a partial recovery obtained for the Ni exposed bare Pt. In order to have a better understanding of the recovery potential of Ni exposed bare Pt electrodes, the effect of potential window and cycle number during cyclic voltammetry and/or the effect of applying various constant potentials can be further considered.

In this study, the effect of divalent cations (Ni^{2+}) was investigated on the Nafion-ionomer (in case of Nafion-coated Pt, Nafion-incorporated and Nafion-coated Pt/C electrodes). Therefore, multi and monovalnet metal cations may also be used as a source of metal contaminants, in order to evaluate of the effect of metal cations with higher and lower valence on the activity of these electrodes.

Through chapter 4 and chapter 5, the results showed that the role of Nafion-ionomer content is critical in the presence of metal cation contaminants. Therefore, characterizing the effect of metal solution contaminants on the anode and cathode electro-catalytic activities of DMFCs with different Nafion-ionomer contents may provide valuable information for minimizing the detrimental effect of metal contaminants on the fuel cell performance.

Appendix

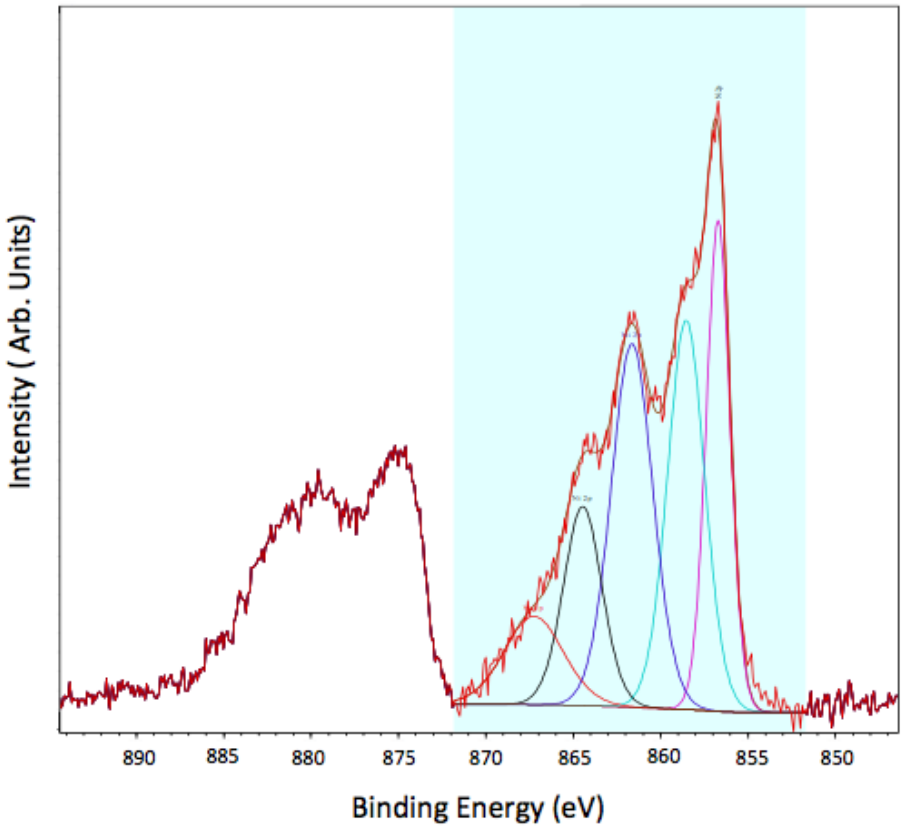

Figure A1: Ni $2p_{3/2}$ X-ray photoelectron spectra of Ni exposed Pt electrode.

As described in section 4.3.1, the XPS results of Ni exposed Pt electrode only reveals the presence of $NiSO_4$ on Pt surface.